AD-A278 501

DTIC
ELECTE
APR 2 5 1994
S G D

RESONANCE CAPTURE IN UNBALANCED DUAL-SPIN SPACECRAFT

THESIS

Raymond Tsui
First Lieutenant, USAF

AFIT/GA/ENY/94M-3

Approved for public release;
Distribution

DEPARTMENT OF THE AIR FORCE
AIR UNIVERSITY
AIR FORCE INSTITUTE OF TECHNOLOGY

DTIC QUALITY INSPECTED 3

Wright-Patterson Air Force Base, Ohio

AFIT/GA/ENY/94M-3

DTIC
ELECTE
APR 2 5 1994
S G D

RESONANCE CAPTURE IN UNBALANCED DUAL-SPIN SPACECRAFT

THESIS

Raymond Tsui
First Lieutenant, USAF

AFIT/GA/ENY/94M-3

Approved for public release; distribution unlimited

154P8 94-12339

94 4 22 013

AFIT/GA/ENY/94M-3

RESONANCE CAPTURE IN UNBALANCED DUAL-SPIN SPACECRAFT

THESIS

Presented to the Faculty of the Graduate School of Engineering

of the Air Force Institute of Technology

Air University

In Partial Fulfillment of the

Requirements for the Degree of

Master of Science in Astronautical Engineering

Raymond Tsui, B.S.

First Lieutenant, USAF

Accesion For	
NTIS CRA&I	☒
DTIC TAB	☐
Unannounced	☐
Justification	
By	
Distribution /	
Availability Codes	
Dist	Avail and / or Special
A-1	

March, 1994

Approved for public release; distribution unlimited

Acknowledgements

The numerical analysis in this thesis was done using *MATLAB*. The Mathworks, Inc., creators of this tool for scientists and engineers, have been kind enough to allow me to print my modified version of *MATLAB*'s ODE45 subroutine, which I call MYODE45, in Appendix D.

I also owe a great deal of gratitude to the following people, all of whom have helped me in one way or another complete this thesis and succeed in my graduate studies. First, I would like to thank Colonel Bob Bartlow, commander of the 654th Civil Engineering Squadron, Tinker Air Force Base, Oklahoma, for allowing me to come to AFIT after less than two years on duty as a Civil Engineering officer. He has always supported his officers in their career endeavors and has clearly done so in my case at some personal sacrifice. Second, I'd like to thank First Lieutenant Cristián Puebla of the Chiléan Air Force, who translated Wittenburg's paper for me from German to English. Without his help, Chapter 3 of this thesis could not have been written. But more importantly, his friendship has made my assignment at AFIT much more enjoyable, and it will continue to grow beyond the foreseeable future. Next, I owe countless thanks to Captain Chris Hall, a fellow Cornell graduate as well as my thesis advisor. Captain Hall goes beyond the call of duty when it comes to making sure his advisees understand their problems. Not only has he set aside a great deal of time each week to work with each of us on a one-to-one basis, but he has ***always*** been available for help on a "walk-in" basis. Finally, I'd like to thank my family for their continuous long-distance support while I studied at AFIT. The love and encouragement which my parents and my brothers bestowed upon me was without a doubt the key to my success. For this I am eternally grateful.

Raymond Tsui

Table of Contents

	Page
Acknowledgements	ii
List of Figures	vii
List of Tables	ix
Abstract	x
I. Introduction	1
1.1 Dual-Spin Stabilization	1
1.2 Problem Statement	4
1.3 Literature Review	4
1.3.1 Earlier Analyses	4
1.3.2 Spinup Problems: Trap States	6
1.4 Outline of the Thesis	8
II. The Equations of Motion	10
2.1 Modelling the System	10
2.1.1 Assumptions	10
2.1.2 Frames of Reference	12
2.2 Deriving the Governing Equations	13
2.2.1 The Principal Frame	14
2.2.2 The Pseudo-Principal Frame	18
2.3 Dimensionless Equations of Motion	21
2.4 Rotational Kinetic Energy	24

Page

III. Special Case: Zero Motor Torque ($\varepsilon = 0$) 29

3.1 The First Change of Variables: $x_2 \Longrightarrow \varphi$ 31

3.2 The Second Change of Variables: $\varphi \Longrightarrow z$ 36

IV. Graphical Representations of Spinup Dynamics (5:Ch. 4) 41

4.1 Momentum Spheres 41

4.2 The μy Plane 46

4.2.1 Geometric Influence on the Shape of the μy Plane 47

4.2.2 Determination of the Equilibrium Trajectories . . 50

4.2.3 Stability of the Equilibrium Trajectories 54

V. Spinup 58

5.1 Kinsey's Model 59

5.1.1 PPL According to Kinsey (13, 14) 60

5.1.2 Kinsey's Model Translated into the μy Plane . . . 60

5.2 Redefinition of Resonance Capture 63

5.2.1 Effects of the Motor Torque ε 70

5.2.2 Effects of Initial Phase 74

5.3 Probability of Capture 79

5.3.1 Probabilities of Capture Across a Single Momentum Sphere 81

5.3.2 Probabilities of Capture Throughout the μy Plane 88

VI. Conclusion and Recommendations 95

6.1 Summary and Conclusions 95

6.2 Recommendations for Further Research 97

Page

Appendix A. Converting From $\mathcal{F}^e$ to $\mathcal{F}^p$ 99

A.1 Direction Cosine Matrix, $\mathbf{Q}$ 99

A.1.1 Description 99

A.1.2 Matrix Form 99

A.2 Direction of the Rotor Spin Axis, $\boldsymbol{\alpha}$ 99

A.2.1 Vector Form 99

A.2.2 Inverse Transformation 100

A.3 Angular Velocity, $\boldsymbol{\nu}$ 100

A.3.1 Vector Form 100

A.3.2 Inverse Transformation 100

A.4 Angular Momentum, $\mathbf{m}$ 101

A.4.1 Vector Form 101

A.4.2 Inverse Transformation 101

A.5 The Inertia-Like Matrix, $\mathbf{J}$ 101

A.5.1 Description 101

A.5.2 Matrix Form 101

A.5.3 Inverse Transformation 102

Appendix B. Translation of Kinsey's Parameters (13) 103

B.1 Definitions 103

B.1.1 Kinsey's Dimensional Parameters 103

B.1.2 Kinsey's Dimensionless Geometric Parameters . . 104

B.1.3 Kinsey's Dimensionless Angular Velocity Components 104

B.1.4 Kinsey's Dimensionless Initial Conditions 104

B.2 Step 1: Redimensionalizing Kinsey's Equations 105

B.3 Step 2: Parameter Translation and Rotation to $\mathcal{F}^e$ 106

B.3.1 Spacecraft Moment of Inertia Tensor, $\mathbf{I}$ 106

Page

B.3.2 Rotor Inertial Angular Velocity, ω_R 107

B.3.3 Direction of the Rotor's Axis of Symmetry, **a** . . . 107

B.3.4 Relative Velocity Between the Platform and Rotor, ω_s 107

B.3.5 Angular Momentum Vector, **h** 107

B.3.6 Motor Torque, g_a 108

Appendix C. The All-Spun Initial Condition 109

Appendix D. Computer Code 111

D.1 CAPPROB.M 111

D.2 EOM.M 113

D.3 FILTERCOMP.M 114

D.4 FINDPROB.M 115

D.5 IFPR.M 117

D.6 INITIALCOND.M 119

D.7 INITIALCONDX2NOT0.M 120

D.8 INTEGRATE.M 121

D.9 KINSEY.M 123

D.10 MODEQ.M 125

D.11 MYODE45.M 131

D.12 NOTORQEOM.M 134

D.13 PHASEINT.M 135

D.14 PROBCAP.M 136

D.15 SPHERE.M 137

Bibliography 139

List of Figures

Figure		Page
1.	The Unbalanced Gyrostat	11
2.	Angular Momentum Vectors Relative to the Balanced-Body and Principal Frames	17
3.	Momentum Sphere for a Gyrostat Having $\mu = 0.1, \varepsilon = 0$	43
4.	Momentum Sphere for a Gyrostat Having $\mu = 0.4, \varepsilon = 0$	44
5.	Momentum Sphere for a Gyrostat Having $\mu = 0.7, \varepsilon = 0$	45
6.	The μy Plane for the Oblate-Prolate Gyrostat	47
7.	The μy Plane for the Oblate-Intermediate Gyrostat	49
8.	The μy Plane for the Intermediate-Prolate Gyrostat	49
9.	The μy Plane for the Axial Gyrostat	51
10.	Application of Poincaré Stability Criteria Along the Dual-Spin Equilibrium Trajectories	56
11.	Application of Poincaré Stability Criteria Along the Flat Spin Equilibrium Trajectories	56
12.	Application of Poincaré Stability Criteria Along the Unstable Equilibrium Trajectories	57
13.	Capture and Escape as Defined by Kinsey	61
14.	The μy Plane for Kinsey's Gyrostat	63
15.	Closeup of the μy Plane for Kinsey's Gyrostat (Inset 1)	64
16.	Closeup of the μy Plane for Kinsey's Gyrostat (Inset 2)	64
17.	Momentum Sphere at the End of Spinup	67
18.	Conditions Which May Lead to Capture	69
19.	Capture and Escape of Two Geometrically Identical Spacecraft with Different Motor Torques	71
20.	Capture and Escape of Two Identical Spacecraft Having Kinsey's Geometric Parameters and Different Motor Torques	73

Figure		Page
21.	Nutation Angles for Capture and Escape of Kinsey's Gyrostat . . .	74
22.	Capture and Escape Resulting From Two Different Initial Values of μ and y	76
23.	Capture and Escape Resulting From Two Different Initial Positions on the Momentum Sphere at the Same Values of μ and y	76
24.	Constant Energy Curve Defined By $\mu = 0.7$ and $y = -1.0576$ Projected in the x_2x_3 Plane	77
25.	Capture and Escape for Initial Conditions Along the Constant Energy Curve Defined By $\mu = 0.7, y = -1.0576$, and $\varepsilon = -0.01$	80
26.	Sections of the Constant Energy Curve Corresponding to Capture and Escape	80
27.	Capture and Escape for Initial Conditions Along the Constant Energy Curve Defined By $\mu = 0.7, y = -0.8638$, and the Given Torques . . .	81
28.	Three Distinct Regions of the μy Plane	82
29.	Region A	83
30.	Region B	84
31.	Region C	85
32.	Probability of Capture Versus Initial Energy at $\mu_0 = 0.7$.	86
33.	Probabilities of Capture of Two Identical Spacecraft Having Different Motor Torques	87
34.	Probabilities of Capture in the Domain of $\mathbf{O}_\mu$ ($\varepsilon = -0.01$ and $\mu = 0.4$)	89
35.	Probabilities of Capture in the Domain of $\mathbf{F}_{1\mu}$ ($\varepsilon = -0.01$ and $\mu = 0.4$)	89
36.	Probabilities of Capture in the Domain of $\mathbf{F}_{2\mu}$ ($\varepsilon = -0.01$ and $\mu = 0.4$)	90
37.	Probabilities of Capture in the Domain of $\mathbf{O}_\mu$ ($\varepsilon = -0.01$ and $\mu = 0.1$)	91
38.	Probabilities of Capture in the Domain of $\mathbf{P}_\mu$ ($\varepsilon = -0.01$ and $\mu = 0.1$)	91
39.	Probabilities of Capture in the Domain of $\mathbf{F}_{1\mu}$ ($\varepsilon = -0.01$ and $\mu = 0.1$)	92
40.	Probabilities of Capture in the Domain of $\mathbf{F}_{2\mu}$ ($\varepsilon = -0.01$ and $\mu = 0.1$)	92
41.	Probabilities of Capture for Initial Conditions Throughout the μy Plane	93
42.	Probabilities of Capture in a Highly Asymmetric Gyrostat	93

List of Tables

Table		Page
1.	Expressions for $x_1(\varphi)$ and $x_3(\varphi)$ for Each Possible Case	32
2.	Second Change of Fast Variables	36
3.	Classification of Spacecraft Geometry in Terms of the Inertia-Like Parameters	48
4.	Classification of Spacecraft Geometry in Terms of the Dimensionless Parameters	50
5.	Translation of Kinsey's Geometric Parameters and Initial Conditions	62
6.	Translation of Kinsey's Dimensionless Motor Torques	62

Abstract

This study examines the spinup dynamics of dual-spin spacecraft having an imbalanced rotor. Of particular interest is a phenomenon called "resonance capture" during which the spinup motor torque induces uncontrolled growth of nutation. A captured spacecraft tumbles end-over-end, while an escaped spacecraft experiences little nutation growth. The conditions which lead to both states are analyzed. A set of criteria based on the spacecraft's kinetic energy at the end of spinup is used to determine whether or not it has been captured. To calculate the final energies against which these criteria are compared, a set of nondimensional equations of motion are numerically integrated. Using computer simulations, the magnitude of the motor torque is shown to affect the probability of capture. For prolate spinup, larger torques are desirable, whereas for oblate spinup, smaller torques are preferred. This probability is also influenced by the initial spin configuration and is determined here as a function of the initial energies. For a given motor torque, some initial energies lead to guaranteed capture and others to guaranteed escape. This information is combined to form a "map" which allows designers to find the best initial spinup conditions for a given spacecraft.

RESONANCE CAPTURE IN UNBALANCED DUAL-SPIN SPACECRAFT

I. Introduction

1.1 Dual-Spin Stabilization

The orientation of artificial satellites is one of the most crucial factors in the successful performance of their mission. They are often required to maintain a fixed attitude relative to inertial space. One of the earliest methods developed for fixing satellite orientation is ***spin stabilization.*** Because the environmental torques acting on the spinning spacecraft are small, its angular momentum will remain essentially unchanged over an extended period of time. By ensuring that the proper spin axis is aligned parallel to the spacecraft's angular momentum vector, the satellite will not deviate appreciably from this attitude, even in the presence of small external torques.

Spacecraft attitude dynamics became an important subject immediately after the launch of the United States' first satellite, *Explorer I.* The designers of this prolate (rod-like) spacecraft understood from the classical work of Poinsot that stabilization of the satellite in inertial space would be achieved by spinning it about either its major or minor axis of inertia. Stability in this case refers to ***directional stability:*** if, in the presence of small disturbances, the direction of the body-fixed axis aligned with the spacecraft angular momentum vector undergoes an arbitrarily small deviation, its spin is directionally stable (11:121). Unbeknownst to these engineers, however, the presence of energy dissipation plays an important role in the stability of the spin configuration. Dissipative characteristics are inherent in all spacecraft, taking the form of extremely nonlinear processes such as material deformation, antenna whip,

and fuel slosh. Under their influence, the rotational kinetic energy of the spacecraft is gradually lost as heat. In short, Poinsot's results only apply to an ideal, perfectly rigid rotating body. Since that time, it has become a well-known fact that stability of a single rotating dissipative body can only occur about its major inertia axis because this corresponds to the state of minimum rotational kinetic energy. Because *Explorer I* was prolate, it violated this *major-axis rule* and was thereby forced to conform to it. The spacecraft's major axis aligned itself along the direction of its angular momentum causing it to tumble in a flat-spin.

From this experience, later spin-stabilized spacecraft were purposefully designed as squat cylinders so that axial rotation would correspond to spin about the major inertia axis. This type of geometry is described as disc-like, or oblate. Although stability is ensured with the oblate spacecraft, its geometry severely affects the design of the launch vehicle used to deliver it into orbit. The girth of the payload shroud which encloses the satellite must be greater than that of the rest of the rocket. This leads to complications such as increased drag.

Another problem arising from the spin-stabilized spacecraft is the intermittent coverage afforded to specific "fixed" objects in space due to its incessant rotation. Early communications satellites could not remain focused on the Earth, so they were required to carry omnidirectional antennas. These antennas are unable to transmit or receive signals as well as directional ones, which are aimed at a particular location. For the same reason, spin stabilized satellites are not ideal for carrying scientific payloads intended to observe the sun, stars, or other fixed celestial objects. This directional issue was resolved with the development of the *gyrostat* or *dual-spin satellite*. These terms apply to spacecraft which have an inertially-fixed or slowly rotating *platform* in conjunction with a *rotor* that spins to provide attitude stability. All directional-dependent equipment are mounted on the non-spinning or slowly-spinning platform. Gyrostats come in two basic forms characterized by the relative placement of the platform and rotor. One form is designed with the rotor mounted

inside the platform, while the other has it attached externally. The first of these is called a ***bias momentum satellite***, and the second is simply recognized as a gyrostat. This thesis focuses on the dynamics of the latter. The first "dual-spinner" was Ball Brothers' Orbiting Solar Observatory (OSO-1), which carried instrumentation on a stationary platform that continuously faced the sun (16).

A gyrostat is usually deployed in an "all-spun" condition in which the platform and rotor are locked so that the satellite spins as a single rigid body. The maneuver during which it enters its dual-spin state is known as ***spinup*** or ***despin***, the former referring to the motor's effect on the rotor and the latter to its effect on the platform. Since both terms describe the same maneuver, they are used interchangeably throughout this study. During spinup, a motor induces relative spin between the platform and rotor. If the process is successful, the platform will be despun so that most or all of the spacecraft's angular momentum is stored in the spinning rotor.

In the 1960s, Tony Iorillo, an engineer working for the Hughes Aircraft Company, and Vernon Landon, an engineer at RCA, independently discovered another advantage of the dual-spin configuration (16, 10:3). They found that this type of spacecraft can violate the major-axis rule. The implications were significant: it was no longer necessary to build oblate satellites. From the major-axis rule, as given in (11:445), it is clear that oblate dual-spinners always satisfy the condition for stability. With a little more insight, it can be seen that prolate spacecraft ***may*** do so as well. For this to be true, the stable damping of the platform must overcome the unstable damping of the rotor. In this context, "damping" refers to the rate of energy dissipation in each body. This revolutionary concept was later validated in 1969 with the successful launch of the first prolate dual-spin satellite, *TACSAT I*. Today, most commercial communications satellites are dual-spinners (10:4).

Energy dissipation is not the only factor which causes a gyrostat to tumble. Even a hypothetically rigid spacecraft in an ideal torque-free environment will do so under certain conditions which are inherent to the spacecraft itself. If this occurs

during the spinup maneuver, the gyrostat is said to undergo *resonance capture*. This can occur in oblate as well as prolate spacecraft.

1.2 Problem Statement

An unbalanced gyrostat has an axisymmetric, unbalanced rotor coupled to an axisymmetric, balanced platform. Our goal is to study resonance capture for this particular geometry using the energy technique developed by Hall (6). The probability of capture is determined from these results and is used to construct a tool which enables the spacecraft designer to find ideal initial spinup conditions.

1.3 Literature Review

1.3.1 Earlier Analyses. The dynamics of the gyrostat have been studied extensively in the past. The classical model has a balanced axisymmetric rotor coupled to a platform that may be neither balanced nor axisymmetric. Because there are two bodies involved, we sometimes refer to this as a *system*. Both bodies are rigid so that energy dissipation is negligible, as are all external torques which may affect the dynamics. They are connected by a rigid shaft about which relative spin may occur, driven by either a constant-velocity or constant-torque motor. The shaft is aligned along the rotor's axis of symmetry so that the moment of inertia tensor of the system is constant. This greatly simplifies the analysis. With these assumptions, the governing equations become relatively straightforward. A solution to these equations has already been determined for the unperturbed axial gyrostat. In this context, "unperturbed" refers to the condition in which no torque exists between the platform and rotor, and "axial" describes a gyrostat whose platform is balanced. In this special case, the equations of motion are integrable making possible a closed-form analytical solution.

One of the earliest solutions to the axial gyrostat problem was found by Masaitis in 1961 (17). His model consists of an axisymmetric and an asymmetric body

free to rotate about a frictionless shaft which coincides with one of the principal directions of the system. The governing equations, based on those of Euler, are written in terms of the system angular velocities. Masaitis derived these for the platform and rotor independently, thereby arriving at six coupled expressions. He then reduced their number from six to four by making use of the system constraints. Three of these are coupled, nonlinear ordinary differential equations, while the fourth is a simple first order differential equation which can be solved independently of the others. Masaitis was able to rearrange the three coupled equations into two integrable forms. He achieved this by obtaining quadratic expressions for two of the three angular velocity components in terms of the third, thereby decoupling the equations. He then solved these equations in terms of elliptic functions.

Other dynamicists have continued to build upon Masaitis's work. Cochran *et al.* (3), for example, were able to develop governing equations in terms of angular momentum rather than angular velocity – another variation of Euler's equations. Following a procedure similar to Masaitis, they were not only able to express the angular momenta in terms of elliptic functions, but they also found such expressions for the Euler angles as well.

Hall (5, 8) also derived Euler's equations in terms of angular momentum, but he did so in *dimensionless* form so that his equations appear much simpler than those of his predecessors. He then found the analytical solutions to these equations which determine the unperturbed motion of the axial gyrostat, again based on the classical elliptic functions. When the motion is slightly perturbed, Hall noted that the equations of motion are no longer integrable. By using the *method of averaging*, he was able to find *approximate* solutions to the perturbed motion relevant to spinup. He also developed a very convenient means by which spinup dynamics can be observed by looking at the change of system kinetic energy versus the rotor's inertial angular momentum. Hall later extended this method to the biaxial gyrostat (7), but he did not show how to obtain an analytical solution to this particular system.

Kinsey *et al.* (13, 14) also examined the dynamics of spinup, but they used a different spacecraft geometry. Their model consists of a balanced axisymmetric *platform* connected to an unbalanced axisymmetric *rotor*. The difference between their model and the classical gyrostat exists only in nomenclature, however, because they merely reversed the roles of the platform and rotor (5:70). Hence, their analysis is based on despinning the platform rather than spinning up the rotor. Kinsey's governing equations, like those of Masaitis, are developed for both bodies independently relative to inertial space and are written in terms of angular velocity. Their solution is approximated via a "near-identity transformation." This is a form of the method of averaging.

Wittenburg's (22) analysis is not limited to the axial gyrostat. He developed solution techniques for three different cases. These are based on different rotor axis orientations. Case I assumes the rotor is parallel to one of the principal axes of the gyrostat. Case II is slightly more general; the rotor axis no longer coincides with any particular principal direction, but it is constrained to lie within a principal plane. Finally, in Case III, the rotor is arbitrarily oriented. The first of these corresponds to the axial gyrostat. As noted above, these solutions have been well-documented. The second case is analogous to Kinsey's problem and is the model that we are currently examining. Case III is beyond the scope of this thesis.

1.3.2 Spinup Problems: Trap States. Scher and Farrenkopf (20) have identified two "trap states" which may occur during spinup. These are conditions in which the final spin configuration of the spacecraft has deviated significantly from the intended dual-spin state. The *minimum energy trap* occurs after the maneuver is completed. Viscous damping in the bearing causes the relative spin between the rotor and platform to diminish. Over an extended period of time, it eventually ceases so that the spacecraft becomes a single spinning body. During this process, energy is dissipated. As a consequence of the major-axis rule, prolate spacecraft will enter

a flat-spin. Scher and Farrenkopf have shown that recovery from this condition is possible by pulsing the spinup motor at one of the natural frequencies of the system.

The second trap state they identified is the *resonance trap*, denoted by Kinsey as *precession phase lock* and referred to in this study as *resonance capture*, or simply *capture*. This may occur as spinup proceeds. In our analysis, a dual-spin satellite which avoids this trap is said to have *escaped*. To be a candidate for resonance capture, a gyrostat which has a balanced, axisymmetric platform must have a rotor that possesses one of the following three geometric properties: asymmetric and balanced, axisymmetric and unbalanced, or asymmetric and unbalanced (6). A spacecraft experiencing resonance capture undergoes a large growth in nutation. This phenomenon has been studied by Kinsey *et al.* for the case pertaining to the axisymmetric and unbalanced rotor. Their conclusions are based on the size of the nutation angle and the magnitude of the inertial angular velocities of both the platform and rotor at the conclusion of spinup. They observe that resonance capture will result for a system having an inadequate spinup motor torque (one that is too small) when the inertial angular velocity of the unbalanced rotor approaches the inertial free precession rate of the spacecraft. Kinsey's analysis is discussed in greater detail in Chapter 5.

Hall, on the other hand, examined resonance capture for gyrostats having an asymmetric and balanced rotor in (6) and gave a partial treatment of this phenomenon for the asymmetric, unbalanced rotor case in (7). In (6), he established a set of criteria for capture in terms of the system *energy*. He showed that nutation growth begins when trajectories of the perturbed system cross the instantaneous separatrices of the unperturbed system and is actually independent of the inertial free precession rate.

An intriguing technique based on adiabatic invariant theory was developed by Henrard in 1980 (9) to estimate the *probability of capture*. Henrard's equations of motion are expressed as a generalized Hamiltonian function analogous to the simple

pendulum. His method allows one to determine the likelihood that capture will occur for a simple harmonic oscillator given a particular set of initial conditions.

1.4 Outline of the Thesis

Our analysis begins in Chapter 2 with the development of the system model and the governing equations. This is done in two different reference frames to illustrate the effect that the coordinate system has on the complexity of the equations. Appendix A illustrates the means with which to convert from one frame to the other. These equations are then nondimensionalized to simplify the analysis. Using these dimensionless parameters, some important first integral relations are developed which play an important role in the analysis of spinup.

In Chapter 3 an attempt is made to find the exact solution of the unperturbed system of equations. Using a variation of Wittenburg's technique, it is shown that an analytical solution exists, but that it is extremely difficult to express. As a result, the only practical ways to solve the spinup problem are to find approximate solutions or to numerically integrate the equations of motion. We choose the latter method.

The fourth chapter shows two graphical techniques to analyze spinup. One method is to generate a series of momentum spheres, and the other is to observe how the rotational kinetic energy varies with the inertial angular momentum of the balanced body over time. The latter method was originally developed in (5) for the axial gyrostat and is adapted here for this new geometry.

In Chapter 5, Kinsey's model is reexamined using the techniques developed in this thesis. With the procedure outlined in Appendix B, his dimensionless parameters are translated into our own. From the analysis of Kinsey's model it becomes clear that the definitions held by Kinsey and Hall for resonance capture are incompatible. As a result, more precise definitions for both views are offered.

The probability of capture for different initial conditions is defined in Chapter 5 as well. These conditions include, but are not limited to, the all-spun state, whose

expression is derived in Appendix C. This probability forms the basis of an innovative method for which spacecraft designers can choose the best initial spinup conditions.

Finally, in Chapter 6 the procedure and results are briefly summarized, and recommendations are made for possible continuing research on the subject. The *MATLAB* code used throughout the analysis is provided in Appendix D.

II. The Equations of Motion

The gyrostat's behavior is governed by its equations of motion. Throughout the literature it is clear that these may take numerous forms. Their complexity depends on the assumptions made while modelling the system, the reference frame in which they are expressed, and the way in which the parameters are defined. The assumptions are an integral part of the analysis. They are used to turn an otherwise intractable problem, wrought with extensive nonlinearities and random happenstances, into one which can be examined with relative ease. But simplifying assumptions alone do not ensure minimum complexity. Proper selection of the reference frame allows us to bypass certain terms in our expressions, and well-defined dimensionless parameters can compact large groups of terms into smaller ones. All of these concepts are used in this chapter to construct the governing equations for the unbalanced spacecraft.

2.1 Modelling the System

2.1.1 Assumptions. The spacecraft is modelled after Kinsey's gyrostat (14, 13:20), as shown in Figure 1. It consists of two bodies, a platform ($\mathcal{P}$) and rotor ($\mathcal{R}$), capable of relative spin about an axis which joins them. The platform is axisymmetric, and the relative spin axis is aligned with its axis of symmetry. For this reason it is dynamically balanced. The rotor is also axisymmetric, but unlike the platform, it is unbalanced. This particular geometry is defined here as an *unbalanced gyrostat.* During spinup, the motor torque is constant and bearing friction is negligible. Also, the entire spacecraft is considered to be perfectly rigid. As a result, energy dissipation is ignored. Finally, the spacecraft is assumed to rotate in a torque-free environment.

In the classical gyrostat, the platform and rotor designations are reversed. The term "spinup" describes the effect of the motor torque on the inertial angular

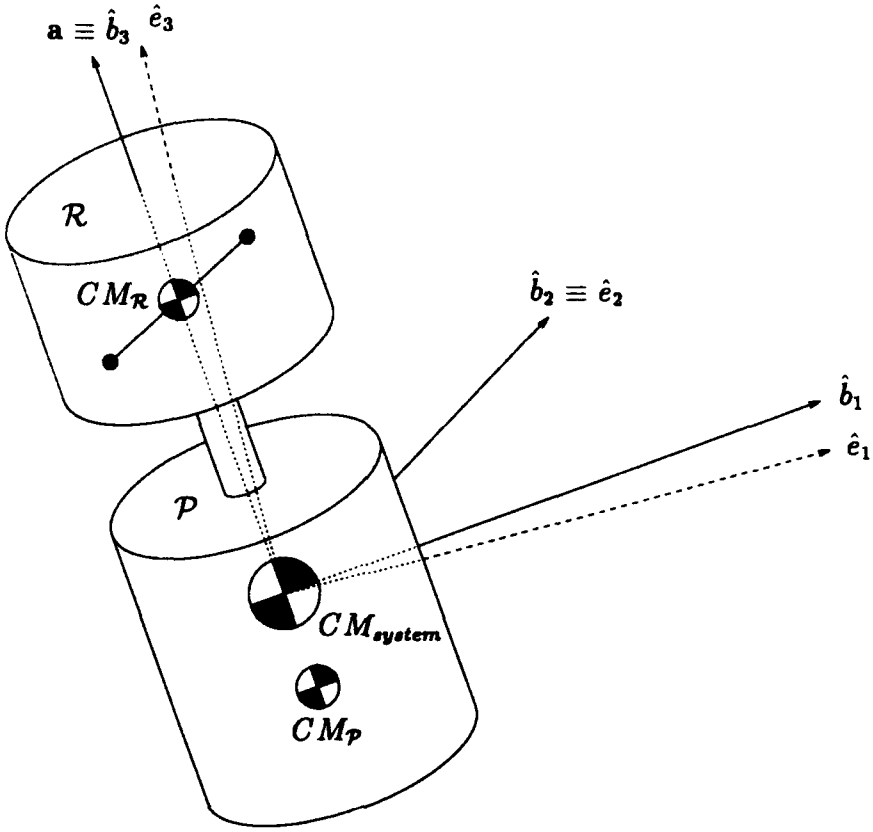

Figure 1. The Unbalanced Gyrostat. The rotor imbalance is denoted by the point masses.

velocity of the balanced body, normally the *rotor*. Strictly speaking, because we have exchanged the names of these components, this term is no longer applicable because it implies that this angular velocity will increase with time. The opposite holds true in our case; the balanced body is required to slow down. As a result, this maneuver would be more accurately described as "platform despin," or just "despin." In the former case, the motor torque is positive while in the latter, it is negative. This is the only difference between the two. If neither body were specified, both spinup and despin would be indistinguishable. For this reason, rather than become embroiled in semantics, we refer to both cases interchangeably throughout this thesis.

2.1.2 Frames of Reference. There are an infinite number of reference frames about which the equations of motion may be expressed, but only three of these are potentially sensible choices. All three are body-fixed frames with origins at the center of mass of the spacecraft. Because no external forces or moments act on the system, they may be considered inertially-fixed. The first of these is defined here as the ***balanced-body frame***. It is actually the principal frame of the platform itself, but it is fixed to the rotor. The second frame that we consider is the ***principal frame of the spacecraft***. Due to the presence of the imbalance, these two frames do not coincide. Finally, we look at a third frame which at first glance appears to have no physical significance. As we show later in the chapter, this non-intuitive coordinate system is actually our frame of choice. It is denoted here as the ***pseudo-principal*** frame. As dictated by convention, all frames are "right-handed" and orthogonal, and they can easily be "rotated" from one to another via Euler angle transformations. In this thesis, each reference frame is written as follows: $\mathcal{F}^a$ refers to frame a with unit vectors $\{\hat{a}_1, \hat{a}_2, \hat{a}_3\}$. Hence, the balanced-body frame is $\mathcal{F}^b$, the principal frame is $\mathcal{F}^e$, and the pseudo-principal frame is $\mathcal{F}^p$.

In the balanced-body frame, the $\hat{b}_3$ axis is aligned with the rotor, whose direction is given by the vector $\mathbf{a}$, while the $\hat{b}_1$ and $\hat{b}_2$ axes coincide with the transverse axes of the platform. Hence, $\hat{b}_3 \equiv \mathbf{a}$. This is shown in Figure 1.

The principal frame, $\mathcal{F}^e$, is obtained from $\mathcal{F}^b$ by a simple "2" rotation. This is also shown in Figure 1. In the axial gyrostat, both of these are coincident. For this special case it is most convenient to express the equations of motion in the principal frame because the products of inertia disappear, leaving a diagonal inertia tensor which reduces the complexity of the governing equations. However, as we shall see, these equations expressed in $\mathcal{F}^e$ for our particular model are still too abstruse due to the dynamic imbalance of the rotor. As a result, we abandon the principal frame in favor of $\mathcal{F}^p$, which is not shown in the figure. This frame presents us with the simplest form for our equations of motion. It allows us to account for the dynamic

imbalance of the rotor while preserving the diagonality of an "inertia-like" matrix. The term "pseudo-principal" is used because $\mathcal{F}^p$ is not actually the true principal frame of the spacecraft. This is explained in more detail later in the chapter.

Kinsey formulated the governing equations with respect to $\mathcal{F}^b$. In this frame, the moment of inertia tensor for the unbalanced gyrostat has the following form:

$$\mathbf{I}^b = \begin{bmatrix} I_{11} & 0 & I_{13} \\ 0 & I_{11} & 0 \\ I_{13} & 0 & I_{33} \end{bmatrix}.$$

The products of inertia, I_{13}, represent the dynamic imbalance of the rotor. These complicate the governing equations by introducing certain terms which would disappear with the selection of a better coordinate system, as shown later in this chapter. Rather than doing this, however, Kinsey simplified them with yet another assumption (one which we are able to avoid): the magnitude of the rotor imbalance is very small. In so doing, the equations become less involved since the high order imbalance terms are neglected. But at the same time, the applicability of Kinsey's equations are restricted to ***slightly*** unbalanced spacecraft only. By following the methods of Hughes (11) and Hall (5, 7, 8) and using $\mathcal{F}^p$ as our frame of choice, we avoid these problems altogether in our particular formulation. Unlike Kinsey, we do not restrict the magnitude of the imbalance. As a result, our equations of motion are applicable to more general unbalanced spacecraft.

2.2 Deriving the Governing Equations

The rotational motion of the system is governed by a set of four scalar differential equations. Three of these arise from Euler's equations, which are only adequate to describe the motion of a ***single*** rotating rigid body, while the fourth accounts for the dual-spin nature of the system. Since we are only interested in studying the attitude dynamics of the spacecraft, translational motion is irrelevant. As mentioned

above, (13) and (14) derive these expressions with respect to $\mathcal{F}^b$. We develop ours in terms of both $\mathcal{F}^e$ and $\mathcal{F}^p$. Our purpose here is to justify our selection of the pseudo-principal frame over the other two.

2.2.1 The Principal Frame. Euler's equations state that the sum of all external torques acting on a spinning rigid body is equal to the rate of change of its angular momentum. In vector form, this is given as:

$$\mathbf{M}^e = \dot{\mathbf{h}}^e + \boldsymbol{\omega}_R^{e\times}\mathbf{h}^e \tag{1}$$

where, according to Hughes (11:67):

$$\mathbf{h}^e = \mathbf{I}^e\boldsymbol{\omega}_R^e + I_s\omega_s\mathbf{a}^e. \tag{2}$$

The variables and parameters in both expressions are defined as follows:

$\mathbf{M}^e$ $\equiv$ sum of all external torques acting on the system expressed in $\mathcal{F}^e$

$\mathbf{h}^e$ $\equiv$ system angular momentum expressed in $\mathcal{F}^e$

$\mathbf{I}^e$ $\equiv$ system inertia tensor expressed in $\mathcal{F}^e$

$\boldsymbol{\omega}_R^e$ $\equiv$ rotor inertial angular velocity expressed in $\mathcal{F}^e$

$\mathbf{a}^e$ $\equiv$ unit vector denoting direction of platform/rotor spin axis expressed in $\mathcal{F}^e$

I_s $\equiv$ platform moment of inertia about $\mathbf{a}^e$

ω_s $\equiv$ platform angular velocity relative to the rotor about $\mathbf{a}^e$.

Since the vector $\mathbf{a}^e$ lies in the $\hat{e}_1\hat{e}_3$ plane, it has the following form:

$$\mathbf{a}^e = \begin{bmatrix} a_1 \\ 0 \\ a_3 \end{bmatrix}.$$

This parameter determines the *degree of rotor imbalance*. Furthermore, the term $\boldsymbol{\omega}_R^{e\times}$ is a skew-symmetric matrix formed by the components of $\boldsymbol{\omega}_R^e$. It looks like the following:

$$\boldsymbol{\omega}_R^{e\times} = \begin{bmatrix} 0 & -\omega_3 & \omega_2 \\ \omega_3 & 0 & -\omega_1 \\ -\omega_2 & \omega_1 & 0 \end{bmatrix}.$$

When this is post-multiplied by a column vector $\mathbf{v}$, the cross-product $\boldsymbol{\omega}_R^e \times \mathbf{v}$ is obtained.

Because we neglect the effect of the external torques ($\mathbf{M}^e = \mathbf{0}$), Equation (1) may be rewritten in terms of $\dot{\mathbf{h}}^e$, giving a system of three coupled, nonlinear ordinary differential equations.

$$\dot{\mathbf{h}}^e = -\boldsymbol{\omega}_R^{e\times}\mathbf{h}^e \tag{3}$$

From this point the superscript e is dropped from the notation. It is implicitly understood, unless otherwise indicated, that all vectors and matrices are expressed in $\mathcal{F}^e$.

The fourth expression required to complete the set of governing equations is based on the rate of change of the platform's inertial angular momentum due to the spinup motor torque. This angular momentum is defined as follows:

$$\mathbf{h}_P = \mathbf{I}_P\boldsymbol{\omega}_P \tag{4}$$

where

$$\begin{aligned} \mathbf{I}_P &\equiv \text{inertia tensor of the platform expressed in } \mathcal{F}^e \\ \boldsymbol{\omega}_P &\equiv \text{platform inertial angular velocity expressed in } \mathcal{F}^e. \end{aligned}$$

Another important expression needed here is the relative spin rate between the platform and rotor:

$$\boldsymbol{\omega}_s \equiv \boldsymbol{\omega}_P - \boldsymbol{\omega}_R = \omega_s \mathbf{a}. \tag{5}$$

We are mainly interested in the component of $\mathbf{h}_P$ along the relative spin axis since this is the only component affected by the spinup motor torque, g_a. We denote this as $\mathbf{h}_a$. Because the direction of $\mathbf{h}_a$ is known (it points along the vector $\mathbf{a}$), all we need is its magnitude:

$$h_a = \mathbf{a}^T \mathbf{h}_P.$$

Substitution from (4) gives

$$h_a = \mathbf{a}^T \mathbf{I}_P \boldsymbol{\omega}_P. \tag{6}$$

We now apply some elementary algebra to Equation (5). First, we solve for $\boldsymbol{\omega}_P$ in terms of the other variables. Afterwards, we insert this result into (6) to get

$$h_a = \mathbf{a}^T \mathbf{I}_P (\boldsymbol{\omega}_R + \omega_s \mathbf{a}). \tag{7}$$

Because $\mathbf{a}$ coincides with the symmetry axis of the platform, $\mathbf{a}^T \mathbf{I}_P = I_s \mathbf{a}^T$, transforming (7) into

$$h_a = I_s \mathbf{a}^T \boldsymbol{\omega}_R + I_s \omega_s. \tag{8}$$

Its time rate of change is therefore

$$\dot{h}_a = I_s \mathbf{a}^T \dot{\boldsymbol{\omega}}_R + I_s \dot{\omega}_s$$

or simply

$$\dot{h}_a = g_a \tag{9}$$

since this change is the sole effect of the motor torque. Figure 2 shows both $\mathbf{h}$ and $\mathbf{h}_a$ as they appear relative $\mathcal{F}^b$ and $\mathcal{F}^e$. The nutation angle, η, is also shown. This

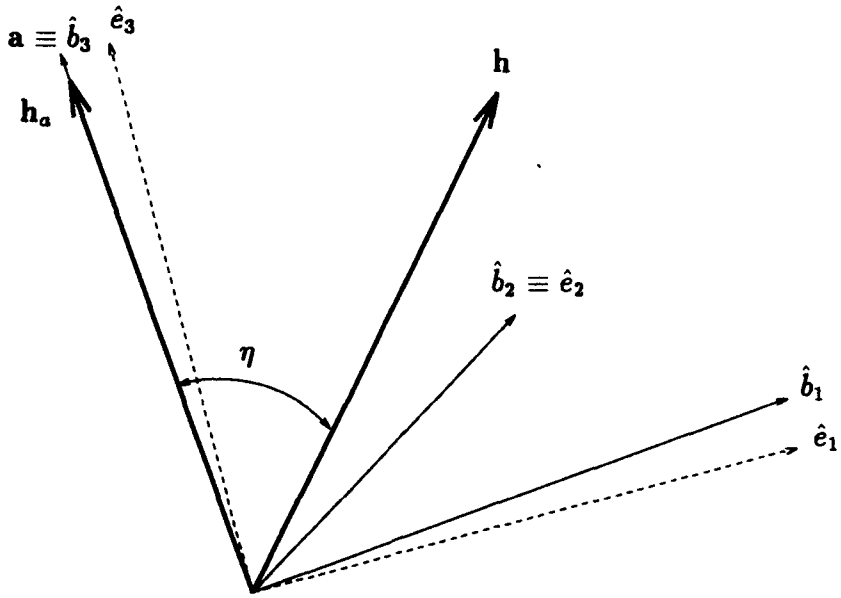

Figure 2. Angular Momentum Vectors Relative to the Balanced-Body and Principal Frames

variable is defined as the angle between the rotor spin axis and the system angular momentum vector.

Together, Equations (3) and (9) are the governing equations expressed in the principal frame. To emphasize this point, we write them below as a single set of equations:

$$\begin{aligned} \dot{\mathbf{h}} &= -\boldsymbol{\omega}_R^{\times}\mathbf{h} \\ \dot{h}_a &= g_a. \end{aligned} \tag{10}$$

As innocuous as these appear, their explicit scalar forms are actually quite cumbersome. They are obtained through rather tedious algebra and are summarized

below:

$$\dot{h}_1 = \frac{h_2(h_3 - h_{a3})}{I_3 - I_s a_3^2} + \frac{h_2 I_s a_1 a_3[(h_1 - h_{a1})(I_3 - I_s a_3^2) + I_s a_1 a_3(h_3 - h_{a3})]}{(I_3 - I_s a_3^2)[(I_1 - I_s a_1^2)(I_3 - I_s a_3^2) - (I_s a_1 a_3)^2]} - \frac{h_2 h_3}{I_2} \tag{11}$$

$$\dot{h}_2 = \frac{h_3[(h_1 - h_{a1})(I_3 - I_s a_3^2) + I_s a_1 a_3(h_3 - h_{a3})]}{(I_1 - I_s a_1^2)(I_3 - I_s a_3^2) - (I_s a_1 a_3)^2} - \frac{h_1(h_3 - h_{a3})}{I_3 - I_s a_3^2} - \frac{h_1 I_s a_1 a_3[(h_1 - h_{a1})(I_3 - I_s a_3^2) + I_s a_1 a_3(h_3 - h_{a3})]}{(I_3 - I_s a_3^2)[(I_1 - I_s a_1^2)(I_3 - I_s a_3^2) - (I_s a_1 a_3)^2]} \tag{12}$$

$$\dot{h}_3 = \frac{h_1 h_2}{I_2} - \frac{h_2[(h_1 - h_{a1})(I_3 - I_s a_3^2) + I_s a_1 a_3(h_3 - h_{a3})]}{(I_1 - I_s a_1^2)(I_3 - I_s a_3^2) - (I_s a_1 a_3)^2} \tag{13}$$

$$\dot{h}_a = g_a \tag{14}$$

where

$$h_1, h_2, h_3 \equiv \text{components of } \mathbf{h} \text{ in the three principal directions}$$

$$h_{a1}, h_{a3} \equiv \text{components of } \mathbf{h}_a \text{ along } \hat{e}_1 \text{ and } \hat{e}_3\text{, respectively.}$$

Rather than proceed from here with our analysis, we need to find a more manageable set of equations. By deriving them in the pseudo-principal frame, $\mathcal{F}^p$, we can achieve this goal. Furthermore, by defining a simple set of dimensionless parameters, we are able to reduce them to an even easier form with which to work.

2.2.2 The Pseudo-Principal Frame. The complexity in $\mathcal{F}^e$ results from the rotor's imbalance. Although this coordinate system is the principal frame of the entire spacecraft, the inertia tensor of the rotor alone is not diagonal. It is therefore not aligned with any of the principal directions. To remove its complicating effect from the derivation, we need to find a suitable expression for the spacecraft geometry in which the imbalance is "absorbed" into the system's overall moments of inertia. The frame in which this resulting *inertia-like* matrix is diagonal is defined here as the pseudo-principal frame. To do this, the model must first be transformed into

an *apparent gyrostat* as defined in (11:158). Instead of writing the inertia tensor of the spacecraft in its own principal frame, as given by $\mathbf{I}$, we need to diagonalize the quantity $\mathbf{I} - I_s\mathbf{a}\mathbf{a}^T$, the result of which we denote as $\mathbf{J}$. The rotation matrix $\mathbf{Q}$ which gives this transformation therefore enables us to write the variables and parameters from the principal frame in terms of $\mathcal{F}^p$. Thus, we define the following terms:

$$\mathbf{J} \equiv \mathbf{Q}(\mathbf{I} - I_s\mathbf{a}\mathbf{a}^T)\mathbf{Q}^T \tag{15}$$

$$\mathbf{m} \equiv \mathbf{Q}\mathbf{h} \tag{16}$$

$$\boldsymbol{\nu} \equiv \mathbf{Q}\boldsymbol{\omega}_R \tag{17}$$

$$\boldsymbol{\alpha} \equiv \mathbf{Q}\mathbf{a}. \tag{18}$$

Their explicit forms are summarized in Appendix A. Note that $\mathbf{J}$ has the following form:

$$\mathbf{J} = \begin{bmatrix} J_1 & 0 & 0 \\ 0 & J_2 & 0 \\ 0 & 0 & J_3 \end{bmatrix}. \tag{19}$$

From this it is clear that $\mathcal{F}^p$ is the principal frame of the apparent gyrostat.

We are now ready to develop the equations of motion in terms of this new coordinate system. As before, we obtain Euler's equations in terms of the angular momentum $\mathbf{m}$. Then we decompose this vector into three separate scalar expressions. The rotor angular momentum h_a is the same here as in $\mathcal{F}^e$; being a scalar quantity, it is invariant regardless of the coordinate system in which it is derived. Just as in references (5:28) and (8), we shall define dimensional time to be $\tilde{t}$, and the first time derivative to be $d()/d\tilde{t}$.

We begin by considering Equation (2) once again, rewritten below.

$$\mathbf{h} = \mathbf{I}\boldsymbol{\omega}_R + I_s\omega_s\mathbf{a}.$$

Solving for $I_s\omega_s$ from (8), we substitute this expression into the above to get

$$\mathbf{h} = \mathbf{I}\boldsymbol{\omega}_R + h_a\mathbf{a} - I_s\mathbf{a}^T\boldsymbol{\omega}_R\mathbf{a}$$

or, equivalently

$$\mathbf{h} = (\mathbf{I} - I_s\mathbf{a}\mathbf{a}^T)\boldsymbol{\omega}_R + h_a\mathbf{a}.$$

Next, solving for $\boldsymbol{\omega}_R$ gives:

$$\boldsymbol{\omega}_R = (\mathbf{I} - I_s\mathbf{a}\mathbf{a}^T)^{-1}(\mathbf{h} - h_a\mathbf{a}).$$

Here we apply the transformations given by Equations (15) - (18), leaving us with

$$\boldsymbol{\nu} = \mathbf{J}^{-1}(\mathbf{m} - h_a\boldsymbol{\alpha}). \tag{20}$$

This relation becomes useful after we find the pseudo-principal expression for Euler's equations. Following a procedure completely analogous to the derivation of Equations (10) in $\mathcal{F}^e$, these are written as

$$\begin{aligned} \frac{d\mathbf{m}}{d\bar{t}} &= -\boldsymbol{\nu}^\times\mathbf{m} \\ \frac{dh_a}{d\bar{t}} &= g_a. \end{aligned} \tag{21}$$

Substitution of (20) into (21) gives the final form of the vector equations:

$$\begin{aligned} \frac{d\mathbf{m}}{d\bar{t}} &= -\mathbf{J}^{-1}(\mathbf{m} - h_a\boldsymbol{\alpha})^\times\mathbf{m} \\ \frac{dh_a}{d\bar{t}} &= g_a. \end{aligned} \tag{22}$$

These expressions are easy to decompose. Recall that $\mathbf{J}$ is a diagonal matrix given by Equation (19). We may express the other pseudo-principal variables and

parameters in terms of their components as well:

$$\mathbf{m} = \begin{bmatrix} m_1 \\ m_2 \\ m_3 \end{bmatrix}, \quad \boldsymbol{\nu} = \begin{bmatrix} \nu_1 \\ \nu_2 \\ \nu_3 \end{bmatrix}, \text{ and } \quad \boldsymbol{\alpha} = \begin{bmatrix} \alpha_1 \\ 0 \\ \alpha_3 \end{bmatrix}.$$

By substituting these into (22), we are left with the following scalar equations of motion:

$$\frac{dm_1}{d\bar{t}} = m_2 m_3 \left(\frac{J_2 - J_3}{J_2 J_3} \right) - \frac{m_2 h_a \alpha_3}{J_3} \tag{23}$$

$$\frac{dm_2}{d\bar{t}} = m_1 m_3 \left(\frac{J_3 - J_1}{J_1 J_3} \right) + \frac{m_1 h_a \alpha_3}{J_3} - \frac{m_3 h_a \alpha_1}{J_1} \tag{24}$$

$$\frac{dm_3}{d\bar{t}} = m_1 m_2 \left(\frac{J_1 - J_2}{J_1 J_2} \right) + \frac{m_2 h_a \alpha_1}{J_1} \tag{25}$$

$$\frac{dh_a}{d\bar{t}} = g_a. \tag{26}$$

Note their relative simplicity compared to their $\mathcal{F}^e$ counterparts [Equations (11) - (14)]. An important consequence is the ease with which they can be nondimensionalized. Analyzing our model gyrostat in dimensionless form further simplifies the equations, as we show below.

2.3 Dimensionless Equations of Motion

Nondimensional analysis permits us to examine the spacecraft's dynamics from a general standpoint. The use of dimensionless parameters lets us view the behavior of a *whole series of similar systems* from a single set of governing equations. This fact, in addition to the analytical simplicity it provides, serve as justification for the extra effort involved in finding the nondimensional forms. The most important step in this procedure is to define the parameters. It is best to do so in a way that preserves their physical significance. Our technique is an extension of that used in references (5, 7, 8).

First we nondimensionalize the inertia-like terms J_n ($n = 1, 2, 3$), as shown in Equation (19). This is made possible with the following definition:

$$J_3' \equiv J_3 + I_s \alpha_3^2. \ .$$

J_3 is the parameter by which all the inertia-like terms are scaled. Note that this definition is not arbitrary. Its physical significance becomes apparent when compared to Equation (85) in Appendix A. As can be seen, J_3' is the bottom diagonal term of $\mathbf{I} = \mathbf{Q}^T[\mathbf{J} + I_s \boldsymbol{\alpha}\boldsymbol{\alpha}^T]\mathbf{Q}$. We could make a similar definition involving J_1, i.e. $J_1' \equiv J_1 + I_s \alpha_1^2$, but both definitions taken together are unnecessary; one of them is redundant since all inertia-like terms must be scaled by a common factor. In this analysis we ignore the latter. The dimensionless counterparts of the J_n are thus defined as follows:

$$i_1 = 1 - \frac{J_3}{J_1} \implies J_1 = \frac{J_3}{1 - i_1} \tag{27}$$

$$i_2 = 1 - \frac{J_3}{J_2} \implies J_2 = \frac{J_3}{1 - i_2} \tag{28}$$

$$i_3 = 1 - \frac{J_3}{J_3'} \implies J_3' = \frac{J_3}{1 - i_3} \implies i_3 = \frac{I_s \alpha_3^2}{J_3'}. \tag{29}$$

Next, keeping in mind that $m = |\mathbf{m}|$, the dimensionless momentum components are defined as:

$$x_1 = m_1/m \tag{30}$$

$$x_2 = m_2/m \tag{31}$$

$$x_3 = m_3/m \tag{32}$$

Since external torques are neglected, angular momentum is conserved. Hence,

$$m = \sqrt{m_1^2 + m_2^2 + m_3^2} \equiv \text{constant}.$$

Substitution of the corresponding nondimensional parameters translates this to

$$x_1^2 + x_2^2 + x_3^2 = 1.$$

This fundamental constant is useful in our analysis. It is a *first integral.*

We still have one dimensionless angular momentum variable to define. This is related to the inertial angular momentum of the platform, h_a:

$$\mu = \frac{h_a}{m}. \tag{33}$$

Finally, the expressions

$$t = \frac{m\bar{t}}{J_3} \tag{34}$$

$$\varepsilon = \frac{g_a J_3}{m^2} \tag{35}$$

are the nondimensional counterparts of time and despin motor torque, respectively.

We now have all the tools necessary to build our model. Given Equation (23)

$$\frac{dm_1}{d\bar{t}} = m_2 m_3 \left(\frac{J_2 - J_3}{J_2 J_3}\right) - \frac{m_2 h_a \alpha_3}{J_3}$$

we replace J_2 with its alternate form from (28) so that the expression simplifies to

$$\frac{dm_1}{d\bar{t}} = m_2 m_3 \frac{i_2}{J_3} - \frac{m_2 h_a \alpha_3}{J_3}.$$

By making use of Equation (34), the left hand side undergoes the following transformation:

$$\frac{dm_1}{d\bar{t}} \Rightarrow \frac{m}{J_3}\frac{dm_1}{dt} \equiv \frac{m}{J_3}\dot{m}_1.$$

Dividing both sides of the equality by m^2 and then multiplying by J_3 eliminates the remaining dimensional terms from the expression. The dimensionless equation in

the pseudo-principal $\hat{p}_1$ direction is therefore

$$\dot{x}_1 = (i_2 x_3 - \mu\alpha_3)x_2. \tag{36}$$

The other three equations result from similar manipulations of Equations (24) - (26). Their final forms are summarized below:

$$\begin{aligned} \dot{x}_2 &= -i_1 x_1 x_3 + \mu[\alpha_3 x_1 - \alpha_1(1 - i_1)x_3] && (37) \\ \dot{x}_3 &= [(i_1 - i_2)x_1 + (1 - i_1)\mu\alpha_1]x_2 && (38) \\ \dot{\mu} &= \varepsilon && (39) \end{aligned}$$

Equations (36) - (39) bear some similarity to the governing equations of the biaxial gyrostat (7). The main difference between both models is the fact that the biaxial gyrostat has two balanced axisymmetric rotors which act analogously to our single balanced platform. Thus, the biaxial system has two explicit, independent rotor angular momentum terms, defined in reference (7) as μ_1 and μ_2. Close examination of our governing equations reveals two "rotor terms" as well. These are the components of μ in the pseudo-principal $\hat{p}_1$ and $\hat{p}_3$ directions, i.e. $\mu\alpha_1$ and $\mu\alpha_3$. Hence, we may conclude that the unbalanced dual-spin spacecraft is merely a special case of a biaxial gyrostat whose rotor speeds are directly proportional to one another. This analogy is easily extended to the more general ***triaxial gyrostat*** where the rotor is arbitrarily positioned.

2.4 Rotational Kinetic Energy

A special dynamic case to consider is that of unperturbed motion, or equivalently, zero motor torque ($\varepsilon = 0$). When this occurs, the equations of motion are integrable, allowing us to find closed-form analytical solutions to (36) - (39). This procedure is examined in great detail in the next chapter. We mention this special case here in order to introduce a useful variable related to the system kinetic energy.

From Equation (39), we see that zero motor torque corresponds to the condition

$$\mu = \text{constant}. \tag{40}$$

Because μ is an invariant quantity, (40) is a first integral. Recall that when the equations of motion were initially derived, another first integral had been introduced in the guise of conservation of angular momentum:

$$x_1^2 + x_2^2 + x_3^2 = 1. \tag{41}$$

In addition to these, there is yet a third constant of motion. Since we are considering the zero motor torque case as well as neglecting energy dissipation, there are neither external moments nor internal axial shaft torques acting on the system. Therefore, kinetic energy T does not change. Conservation of energy provides us with another useful first integral. It is derived here in both dimensional and nondimensional form.

From Hughes (ignoring the translational kinetic energy terms):

$$T = \frac{1}{2}\boldsymbol{\omega}_R{}^T \mathbf{I}\boldsymbol{\omega}_R + \frac{1}{2}I_s\omega_s^2 + I_s\omega_s\mathbf{a}^T\boldsymbol{\omega}_R. \tag{42}$$

Note that this is written in $\mathcal{F}^e$. We can easily translate it to $\mathcal{F}^p$ using the transformations given by (15) - (18). Hence,

$$T = \frac{1}{2}\boldsymbol{\nu}^T\left(\mathbf{J} + I_s\boldsymbol{\alpha}\boldsymbol{\alpha}^T\right)\boldsymbol{\nu} + \frac{1}{2}I_s\omega_s^2 + I_s\omega_s\boldsymbol{\alpha}^T\boldsymbol{\nu}. \tag{43}$$

Since $\boldsymbol{\alpha} = [\alpha_1\ 0\ \alpha_3]^T$, the dyad $\boldsymbol{\alpha}\boldsymbol{\alpha}^T$ looks like

$$\boldsymbol{\alpha}\boldsymbol{\alpha}^T = \begin{bmatrix} \alpha_1^2 & 0 & \alpha_1\alpha_3 \\ 0 & 0 & 0 \\ \alpha_1\alpha_3 & 0 & \alpha_3^2 \end{bmatrix}.$$

Substitution of this and other relevant parameters into Equation (43) gives

$$T = \frac{1}{2}[\nu_1\ \nu_2\ \nu_3]\begin{bmatrix} J_1 + I_s\alpha_1^2 & 0 & I_s\alpha_1\alpha_3 \\ 0 & J_2 & 0 \\ I_s\alpha_1\alpha_3 & 0 & J_3 + I_s\alpha_3^2 \end{bmatrix}\begin{bmatrix} \nu_1 \\ \nu_2 \\ \nu_3 \end{bmatrix} + \frac{1}{2}I_s\omega_s^2 + I_s\omega_s\,[\alpha_1\ 0\ \alpha_3]\begin{bmatrix} \nu_1 \\ \nu_2 \\ \nu_3 \end{bmatrix}.$$

Matrix multiplication reduces it to its more convenient scalar form:

$$T = \frac{1}{2}[J_1\nu_1^2 + J_2\nu 2^2 + J_3\nu_3^2 + I_s(\alpha_1\nu_1 + \alpha_3\nu_3 + \omega_s)^2].$$

The last term inside the square brackets can be simplified to h_a^2/I_s. This comes from application of the appropriate Euler transformations to Equation (8). Thus we get

$$T = \frac{1}{2}\left(J_1\nu_1^2 + J_2\nu_2^2 + J_3\nu_3^2 + \frac{h_a^2}{I_s}\right). \tag{44}$$

It would be convenient to express T in terms of the angular momentum components, (m_1, m_2, m_3), rather than angular velocity, (ν_1, ν_2, ν_3). Doing so permits us to rewrite it in terms of our predefined nondimensional parameters. Equation (20) helps us in this endeavor. It provides us with

$$\begin{aligned} \nu_1 &= \frac{m_1 - h_a\alpha_1}{J_1} \\ \nu_2 &= \frac{m_2}{J_2} \\ \nu_3 &= \frac{m_3 - h_a\alpha_3}{J_3}. \end{aligned}$$

Substituting these into (44) results in

$$T = \frac{1}{2}\left[\frac{(m_1 - h_a\alpha_1)^2}{J_1} + \frac{m_2^2}{J_2} + \frac{(m_3 - h_a\alpha_3)^2}{J_3} + \frac{h_a^2}{I_s}\right] = \text{constant}. \tag{45}$$

Our next step is to nondimensionalize this expression. Note that if we ignore the last term in the equation, we are still left with a constant which we define as

$$T_0 = \frac{1}{2}\left[\frac{(m_1 - h_a\alpha_1)^2}{J_1} + \frac{m_2^2}{J_2} + \frac{(m_3 - h_a\alpha_3)^2}{J_3}\right] \tag{46}$$

such that $T = T_0 + h_a^2/(2I_s)$. Hughes refers to T_0 as an "energy-like quantity" because it lacks the term we ignored.

Multiplying both sides of Equation (46) by J_3/m_2 produces

$$\hat{T} \equiv \frac{T_0 J_3}{m_2} = \frac{1}{2}[(x_1 - \mu\alpha_1)^2(1 - i_1) + x_2^2(1 - i_2) + (x_3 - \mu\alpha_3)^2]. \tag{47}$$

We now have a dimensionless expression for kinetic energy. Although this looks like a simple equation, it is not in a convenient form to analyze rotor spinup ($\epsilon \neq 0$); as shown in Chapters 4 and 5, this quantity plays an important role in the discussion. With this in mind, we need to find a way to simplify it further.

A new variable y is defined to satisfy this need. It results from the manipulation of $\hat{T}$ in such a way to preserve its invariant nature. This can be done if y is defined as a combination of $\hat{T}$ and the other first integrals,

$$y = f(\hat{T}, \mu, \mu^2, x_1^2 + x_2^2 + x_3^2).$$

Written explicitly in terms of arbitrary multiples of these expressions, we have

$$y = k_1\hat{T} + k_2\mu + k_3\mu^2 + k_4(x_1^2 + x_2^2 + x_3^2)$$

where k_1, k_2, k_3 and k_4 are constants which must be determined. The problem we now face is how this is done. By expanding (47) and collecting terms, this becomes

more obvious.

$$\hat{T} = \frac{1}{2}\{(x_1^2 + x_2^2 + x_3^2) + 2\mu[x_1\alpha_1(i_1 - 1) - x_3\alpha_3] + \mu^2[\alpha_1^2(1 - i_1) + \alpha_3^2] - (i_1x_1^2 + i_2x_2^2)\}$$

First, arbitrarily setting $k_1 = 2$ eliminates the factor of 1/2 altogether. Next, by choosing $k_3 = -[\alpha_1^2(1 - i_1) + \alpha_3^2]$ and $k_4 = -1$, the first and third terms in $\hat{T}$ disappear. Finally, since the coefficient of μ in this equation is not constant, the second term cannot be eliminated. Therefore, the best choice for k_2 is zero. By making these choices, the final form of the energy-like first integral is

$$y = 2\mu[(i_1 - 1)\alpha_1x_1 - \alpha_3x_3] - (i_1x_1^2 + i_2x_2^2). \tag{48}$$

In the perturbed system ($\varepsilon \neq 0$), μ is no longer constant. As a result, energy is not conserved so that y varies with time. Its first time derivative is given by the chain rule

$$\dot{y} = \frac{\partial y}{\partial \mu}\dot{\mu} + \frac{\partial y}{\partial x_1}\dot{x}_1 + \frac{\partial y}{\partial x_2}\dot{x}_2 + \frac{\partial y}{\partial x_3}\dot{x}_3$$

into which Equations (36) - (39) are substituted. This gives:

$$\dot{y} = 2\varepsilon[(i_1 - 1)\alpha_1x_1 - \alpha_3x_3]. \tag{49}$$

We now have all the tools necessary to study the gyrostat's dynamic behavior during spinup. For rigid body dynamics, this does not generally require examination of the system kinetic energy. Kinetic energy is normally important when dissipation is considered. Despite this fact, we show in Chapters 4 and 5 that it actually simplifies our analysis. Before doing so, however, we examine the special case of unperturbed motion in the next chapter. An attempt is made to obtain the solution of the equations of motion in terms of Jacobi's elliptic functions.

III. Special Case: Zero Motor Torque ($\varepsilon = 0$)

In the previous chapter we found the dimensionless equations which govern the behavior of the gyrostat. For convenience, they are summarized below:

$$\dot{x}_1 = (i_2 x_3 - \mu\alpha_3)x_2 \tag{50}$$

$$\dot{x}_2 = -i_1 x_1 x_3 + \mu[\alpha_3 x_1 - \alpha_1(1 - i_1)x_3] \tag{51}$$

$$\dot{x}_3 = [(i_1 - i_2)x_1 + (1 - i_1)\mu\alpha_1]x_2 \tag{52}$$

$$\dot{\mu} = \varepsilon \tag{53}$$

$$\dot{y} = 2\varepsilon[(i_1 - 1)\alpha_1 x_1 - \alpha_3 x_3] \tag{54}$$

These equations are analytically soluble only when the motion of the system is unperturbed ($\varepsilon = 0$), implying that μ, and therefore h_a, must be constant. This is the subject of the present chapter. Specifically, we attempt to develop their exact analytical solution in terms of *Jacobi's elliptic functions* using a variation of the technique developed by Wittenburg (22).

When the system is perturbed as in spinup, the equations are no longer integrable. This means that an exact analytical solution cannot be found. However, for small perturbations, i.e. small values of ε, their solutions can be approximated from those of the unperturbed system. This has been done for the axial gyrostat. An unfortunate consequence of the rotor imbalance in our particular model is that even these *unperturbed* solutions cannot easily be expressed. Theoretically they do exist, but there is no known practical form in which they may be written. As a result, an analytical approximation of the *perturbed* solutions is not readily obtainable. Therefore, our entire spinup analysis is based solely on numerical integration of the governing equations. Despite this fact, we press on with our analytical solution only to show *how* they can be found.

Although we employ Wittenburg's technique for our model, there are three important differences to bear in mind. First, Wittenburg used dimensional variables and parameters whereas we use the nondimensional ones introduced in Chapter 2. Second, Wittenburg solved the equations in terms of angular velocity. Since ours are based on angular momentum, we need to modify the technique to take this into account as well. Third, Wittenburg studied the specific case for which ω_s, rather than h_a, is constant. Hughes (11:158-161) shows that both of these cases are analytically similar. The main thrust of this exercise is to reduce the three $\dot{x}_n$ $(n = 1, 2, 3)$ equations into a *single* expression. Since $\varepsilon = 0$, this is a separable first order differential equation from which a closed form solution can theoretically be obtained.

The tools needed for this exercise consist of Equations (50) – (52) and the first integrals arising from momentum and energy conservation:

$$x_1^2 + x_2^2 + x_3^2 = 1 \tag{55}$$

$$2\mu[(i_1 - 1)\alpha_1 x_1 - \alpha_3 x_3] - (i_1 x_1^2 + i_2 x_2^2) = y. \tag{56}$$

Adding a multiple of (55) to (56) simplifies both by eliminating a common term and producing a compact form of the two. Inspection of both equations leads us to conclude that the easiest term to eliminate is x_2^2. Multiplying (55) by i_2, and then adding it to (56) gives:

$$\underbrace{(i_2 - i_1)x_1^2 - 2\mu\alpha_1(1 - i_1)x_1}_{A} + \underbrace{i_2 x_3^2 - 2\mu\alpha_3 x_3}_{B} = i_2 + y.$$

This expression must be rearranged in order to facilitate future changes of variables. This is done by adding and subtracting

$$(i_2 - i_1)\left[\frac{\mu\alpha_1(1 - i_1)}{i_2 - i_1}\right]^2$$

to the polynomial denoted by A, while adding and subtracting

$$i_2\left[\frac{\mu\alpha_3}{i_2}\right]^2$$

to that denoted by B. This unusual algebraic manipulation changes our compact first integral into

$$(i_2-i_1)\left[x_1-\frac{\mu\alpha_1(1-i_1)}{i_2-i_1}\right]^2+i_2\left[x_3-\frac{\mu\alpha_3}{i_2}\right]^2-\frac{[\mu\alpha_1(1-i_1)]^2}{i_2-i_1}-\frac{(\mu\alpha_3)^2}{i_2}=i_2+y.$$

If we define a *constant* function of μ as follows:

$$D^*(\mu)=i_2+\frac{[\mu\alpha_1(1-i_1)]^2}{i_2-i_1}+\frac{(\mu\alpha_3)^2}{i_2}$$

(constant since $\varepsilon=0$), the combined first integral reduces to

$$(i_2-i_1)\left[x_1-\frac{\mu\alpha_1(1-i_1)}{i_2-i_1}\right]^2+i_2\left[x_3-\frac{\mu\alpha_3}{i_2}\right]^2=D^*(\mu)+y. \tag{57}$$

3.1 The First Change of Variables: $x_2 \Longrightarrow \varphi$

Having found Equation (57), we now introduce our first set of variable substitutions. Letting

$$f_1=\frac{D^*(\mu)+y}{i_2-i_1}\quad\text{and}\quad f_3=\frac{D^*(\mu)+y}{i_2},$$

Equation (57) takes the following form:

$$\frac{\{x_1-[\mu\alpha_1(1-i_1)]/(i_2-i_1)\}^2}{f_1}+\frac{[x_3-\mu\alpha_3/i_2]^2}{f_3}=1. \tag{58}$$

The appearance of this equation hints vaguely at a familiar trigonometric identity. In fact, this is Wittenburg's intent. As we now show, not only do we make use of the trigonometric functions sine and cosine, but their hyperbolic counterparts as well.

Case	f_1	f_3	$x_1(\varphi)$	$x_3(\varphi)$
I	>0	>0	$[\mu\alpha_1(1-i_1)]/(i_2-i_1)+\sqrt{f_1}\cos\varphi$	$\mu\alpha_3/i_2+\sqrt{f_3}\sin\varphi$
II	>0	<0	$[\mu\alpha_1(1-i_1)]/(i_2-i_1)+\sqrt{f_1}\cosh\varphi$	$\mu\alpha_3/i_2+\sqrt{-f_3}\sinh\varphi$
III	<0	>0	$[\mu\alpha_1(1-i_1)]/(i_2-i_1)+\sqrt{-f_1}\sinh\varphi$	$\mu\alpha_3/i_2+\sqrt{f_3}\cosh\varphi$
IV	$=0$	$=0$	—	—

Table 1. Expressions for $x_1(\varphi)$ and $x_3(\varphi)$ for Each Possible Case

Note that there are four distinct cases to consider based on the signs of f_1 and f_3. At this point we introduce a new variable, φ. For each case, we rewrite x_1, x_2, and x_3 in terms of this new parameter. These are summarized in Table 1. In each case, conservation of angular momentum allows us to write $x_2(\varphi)$ in terms of the other dimensionless angular momenta:

$$x_2(\varphi) = \pm\sqrt{1 - x_1^2(\varphi) - x_3^2(\varphi)}. \tag{59}$$

Also note that, at first glance, Case IV presents us with a dilemma. It implies that $D^*(\mu) = -y$ so that $x_1(\varphi)$ and $x_3(\varphi)$ must have indeterminate values. In fact, we need not concern ourselves with this particular situation because it corresponds to a singular equilibrium point on the surface of a momentum sphere. This concept is explained in more detail in the next chapter. Also, note that there is no case in which both f_1 and f_3 are less than 0. This is impossible since Equation (58) would not be satisfied.

At this point the governing equations can be expressed in terms of the single variable φ. Clearly, φ must be a function of time. Since there are three distinct cases for which this parameter can be determined, we must derive three distinct expressions for $\varphi(t)$. In so doing, we deviate slightly from the method outlined in reference (22). Whereas Wittenburg based all subsequent calculations on the differentiation of the energy equation, we shall do the same using our expression for momentum conservation. We choose this route because Equation (55) bears greater

similarity to Wittenburg's energy equation than does Equation (56). His expression is shown here for comparison

$$I_1\omega_1^2 + I_2\omega_2^2 + I_3\omega_3^2 = 2T.$$

With this in mind, we proceed with our search for $\varphi = \varphi(t)$ by considering Cases I - III individually. The following derivation applies specifically to Case I. We simply state the final results of the other two since they are obtained in exactly the same manner, using the appropriate substitutions where needed from Table 1.

Differentiation of Equation (55) with respect to time gives:

$$2x_1\dot{x}_1 + 2x_2\dot{x}_2 + 2x_3\dot{x}_3 = 0$$

which we rearrange to get

$$x_2\dot{x}_2 = -x_1\dot{x}_1 - x_3\dot{x}_3. \tag{60}$$

From Table 1, $\dot{x}_1$ and $\dot{x}_3$ are written as

$$\begin{aligned} \dot{x}_1(\varphi) &= -\dot{\varphi}\sqrt{f_1}\sin\varphi \\ \dot{x}_3(\varphi) &= \dot{\varphi}\sqrt{f_3}\cos\varphi. \end{aligned}$$

These transform (60) into:

$$x_2\dot{x}_2 = -\dot{\varphi}(x_1\sqrt{f_1}\sin\varphi - x_3\sqrt{f_3}\cos\varphi). \tag{61}$$

Table 1 also provides a means with which to eliminate the explicit appearance of $\sin\varphi$ and $\cos\varphi$ from the equation. We can see that

$$\sin\varphi = \frac{x_3 - \mu\alpha_3/i_2}{\sqrt{f_3}}$$

$$\cos\varphi = \frac{x_1 - [\mu\alpha_1(1-i_1)]/(i_2-i_1)}{\sqrt{f_1}},$$

so that

$$x_2\dot{x}_2 = \dot{\varphi}\left[x_1\sqrt{\frac{f_1}{f_3}}\left(x_3 - \frac{\mu\alpha_3}{i_2}\right) - x_3\sqrt{\frac{f_3}{f_1}}\left(x_1 - \frac{\mu\alpha_1(1-i_1)}{i_2-i_1}\right)\right].$$

At this point we have a single expression for our first three governing equations in terms of x_1, x_2, x_3, $\dot{x}_2$, and $\dot{\varphi}$. Using the definitions of f_1 and f_3, we can also expand the ratios of f_1/f_3 and f_3/f_1 in terms of the system's inertia parameters. This gives

$$\begin{aligned} x_2\dot{x}_2 &= \dot{\varphi}\left\{x_1\frac{1}{i_2}\sqrt{\frac{i_2}{i_2-i_1}}(i_2x_3 - \mu\alpha_3) - x_3\frac{1}{i_2-i_1}\sqrt{\frac{i_2-i_1}{i_2}}[(i_2-i_1)x_1 - \mu\alpha_1(1-i_1)]\right\} \\ &= \dot{\varphi}\sqrt{\frac{1}{i_2(i_2-i_1)}}\{x_1(i_2x_3 - \mu\alpha_3) - x_3[(i_2-i_1)x_1 - \mu\alpha_1(1-i_1)]\} \\ &= \dot{\varphi}\sqrt{\frac{1}{i_2(i_2-i_1)}}[i_1x_1x_3 - \mu\alpha_3x_1 + \mu\alpha_1(1-i_1)x_3]. \end{aligned} \tag{62}$$

We have reached a significant point in the derivation, for if we compare the term in the square brackets in Equation (62) to our original equations of motion, we find that it is equivalent to $-\dot{x}_2$! Hence, this seemingly complex expression can be condensed into a very simple form:

$$x_2 = -\dot{\varphi}\sqrt{\frac{1}{i_2(i_2-i_1)}}. \tag{63}$$

Furthermore, substitution of Equation (59) gives

$$\pm\sqrt{1 - x_1^2 - x_3^2} = -\dot{\varphi}\sqrt{\frac{1}{i_2(i_2-i_1)}}.$$

We can ignore the negative sign in front of $\dot{\varphi}$ and substitute for x_1 and x_3 from Table 1 to get an expression solely in terms of φ and $\dot{\varphi}$:

$$\pm\sqrt{1 - \left[\frac{\mu\alpha_1(1-i_1)}{i_2-i_1} + \sqrt{f_1}\cos\varphi\right]^2 - \left[\frac{\mu\alpha_3}{i_2} + \sqrt{f_3}\sin\varphi\right]^2} = \dot{\varphi}\sqrt{\frac{1}{i_2(i_2-i_1)}}.$$

Finally, noting that this result is separable, we can rewrite it as

$$\pm\sqrt{i_2(i_2-i_1)}\int dt = \int \frac{d\varphi}{\sqrt{1-\left[\frac{\mu\alpha_1(1-i_1)}{i_2-i_1}+\sqrt{f_1}\cos\varphi\right]^2-\left[\frac{\mu\alpha_3}{i_2}+\sqrt{f_3}\sin\varphi\right]^2}}. \quad (64)$$

This is only possible when the motor torque is zero. If this were not the case, then μ is *not* constant over time.

Cases II and III yield similar results. By following the same procedure, we get for Case II:

$$\pm\sqrt{i_2(i_2-i_1)}\int dt = \int \frac{d\varphi}{\sqrt{1-\left[\frac{\mu\alpha_1(1-i_1)}{i_2-i_1}+\sqrt{f_1}\cosh\varphi\right]^2-\left[\frac{\mu\alpha_3}{i_2}+\sqrt{-f_3}\sinh\varphi\right]^2}}. \quad (65)$$

and for Case III:

$$\pm\sqrt{i_2(i_2-i_1)}\int dt = \int \frac{d\varphi}{\sqrt{1-\left[\frac{\mu\alpha_1(1-i_1)}{i_2-i_1}+\sqrt{-f_1}\sinh\varphi\right]^2-\left[\frac{\mu\alpha_3}{i_2}+\sqrt{f_3}\cosh\varphi\right]^2}}. \quad (66)$$

The right hand sides of Equations (64) - (66) are *elliptic integrals.* In general, an elliptic integral has the form $\int R\left[t,\sqrt{P(t)}\right]dt$, where R is a rational function and $P(t)$ is a third or fourth degree polynomial having unique (nonrepeated) roots (2:1). Legendre had shown that there are three canonical forms of this general expression denoted by the terms "elliptic integral of the first, second, and third kind." According to Byrd and Friedman (2), our expressions fall under the first category.

Having found the elliptic integral solution, we have shown that our model is analytically similar to the axial gyrostat. However, our work is not yet complete. Recall that our ultimate goal is to obtain an explicit, closed-form expression for our "fast" variable φ (which is a transformation of our *real* fast variable of interest, x_2). Equations (64) - (66) are essentially of the form $t = F(\varphi)$. Thus, we must invert them to get $\varphi = F^{-1}(t)$. But (64) - (66) are not in a form convenient for

further analysis. Fortunately, Wittenburg developed a procedure to "normalize" these equations into simple polynomials. As explained later in the chapter, the final form of the solution depends on their roots, as other authors have shown (3, 5, 8, 17). Its main drawback, however, is that another change of variables is needed. Hence, the evolution of the fast variable takes the following form:

$$x_2 \Longrightarrow \varphi \Longrightarrow z$$

As we did above, all work is shown explicitly for Case I while the results of the other two are simply stated.

3.2 *The Second Change of Variables:* $\varphi \Longrightarrow z$

The new incarnation of the fast variable $z = z(\varphi)$ takes either form in Table 2:

Case	$z(\varphi)$
I	$\tan(\varphi/2)$
II and III	$\tanh(\varphi/2)$

Table 2. Second Change of Fast Variables

In order to make use of this new expression, we expand the right hand side of Equation (64) so that it becomes:

$$\int (c_1 \sin^2\varphi + c_2 \cos^2\varphi + c_3 + 2c_4 \sin\varphi + 2c_5 \cos\varphi)^{-1/2} d\varphi. \tag{67}$$

where

$$\begin{aligned} c_1 &= -f_3 \\ c_2 &= -f_1 \\ c_3 &= 1 - \left[\frac{\mu\alpha_1(1-i_1)}{i_2 - i_1}\right]^2 - \left(\frac{\mu\alpha_3}{i_2}\right)^2 \end{aligned}$$

$$
\begin{aligned}
c_4 &= -\frac{\mu\alpha_3\sqrt{f_3}}{i_2} \\
c_5 &= -\frac{\mu\alpha_1(1-i_1)\sqrt{f_1}}{i_2-i_1}
\end{aligned}
$$

We then substitute the appropriate change of variables from Table 2. By making use of the following trigonometric identities:

for Case I:

$$\sin 2\theta = \frac{2\tan\theta}{1+\tan^2\theta} \text{ and } \cos 2\theta = \frac{1-\tan^2\theta}{1+\tan^2\theta}$$

and, for Cases II and III, which we include for completeness:

$$\sinh 2\theta = \frac{2\tanh\theta}{1-\tanh^2\theta} \text{ and } \cosh 2\theta = \frac{1+\tanh^2\theta}{1-\tanh^2\theta}$$

(67) is transformed into

$$2\int\left[c_1\left(\frac{4z^4}{1+2z^2+z^4}\right)+c_2\left(\frac{1-2z^2+z^4}{1+2z^2+z^4}\right)+c_3+c_4\left(\frac{4z}{1+z^2}\right)+2c_5\left(\frac{1-z^2}{1+z^2}\right)\right]^{-1/2}\frac{dz}{1+z^2}$$

or, in normalized polynomial form:

$$2\int\frac{dz}{\sqrt{(c_2+c_3+2c_5)+(4c_4)z+2(2c_1-c_2+c_3)z^2+(4c_4)z^3+(c_2+c_3-2c_5)z^4}} \tag{68}$$

Although Wittenburg leaves the solution in integral form, we shall take a step backward and express it as a differential equation. Doing so reminds us that it is still an equation of motion. Supplanting the right hand side of (64) with its normalized transformation, then rearranging appropriately gives

$$\dot{z} = \pm\frac{1}{2}\sqrt{i_2(i_1-i_2)}\sqrt{(c_2+c_3+2c_5)+(4c_4)z+2(2c_1-c_2+c_3)z^2+(4c_4)z^3+(c_2+c_3-2c_5)z^4} \tag{69}$$

Through a similar procedure, the normalized differential equations for Cases II and III are both represented by

$$\dot{z} = \pm\frac{1}{2}\sqrt{i_2(i_1 - i_2)}\sqrt{(a_2 + a_3 + 2a_5) + (4a_4)z + 2(2a_1 + a_2 - a3)z^2 - (4a_4)z^3 + (a_2 + a_3 - 2a_5)z^4}. \tag{70}$$

The difference between the latter two cases is in the value of the coefficients. For Case II:

$$\begin{aligned}
a_1 &= f_3 \\
a_2 &= -f_1 \\
a_3 &= 1 - \left[\frac{\mu\alpha_1(1 - i_1)}{i_2 - i_1}\right]^2 - \left(\frac{\mu\alpha_3}{i_2}\right)^2 \\
a_4 &= -\frac{\mu\alpha_3\sqrt{-f_3}}{i_2} \\
a_5 &= -\frac{\mu\alpha_1(1 - i_1)\sqrt{f_1}}{i_2 - i_1}
\end{aligned}$$

whereas for Case III:

$$\begin{aligned}
a_1 &= f_1 \\
a_2 &= -f_3 \\
a_3 &= 1 - \left[\frac{\mu\alpha_1(1 - i_1)}{i_2 - i_1}\right]^2 - \left(\frac{\mu\alpha_3}{i_2}\right)^2 \\
a_4 &= -\frac{\mu\alpha_1(1 - i_1)\sqrt{-f_1}}{i_2 - i_1} \\
a_5 &= -\frac{\mu\alpha_3\sqrt{f_3}}{i_2}.
\end{aligned}$$

At this point we have reduced the number of governing equations from five to three. Two of these are the slow equations expressed by (53) and (54) since they are clearly of $\mathcal{O}(\varepsilon)$. The third is fast, embodied by either of two differential equations which are indirect functions of the dimensionless angular momenta (x_1, x_2, and x_3).

These case-dependent equations are given by (69) and (70) as well as the appropriate form of their respective coefficients.

Since $\varepsilon = 0$, both expressions are separable. Thus, they may be rewritten in the following form:

$$\int dt = 2\int \frac{dz}{\sqrt{i_2(i_2 - i_1)}\sqrt{p_0 + p_1 z + p_2 z^2 + p_3 z^3 + p_4 z^4}} \tag{71}$$

Equation (71) is an expression for time in the form $t = F(z)$. The analytical solution of the fast variable must therefore be obtained by inverting the expression to get $z = F^{-1}(t)$. The final form of z depends on the roots of the quartic polynomial on the right hand side of (71). The act of finding these roots, however, is by no means an easy task. This has already been done for the axial gyrostat, whose solution is relatively simple since its quartic polynomial is factorable into two quadratics. In our case, we are not so fortunate because our polynomial is not as simple. Even though *Mathematica* is able to find a closed form expression for each root, they are all large enough to fill several pages. Despite this difficulty, the mere fact that the roots can be found *proves* that an exact analytical solution does exist.

Assuming we are able to find the roots, our next step is to rewrite Equation (71) in one of the standard forms defined in (2:95). Since this equation contains the integral of the square root of a quartic, it has the following general form:

$$t = \int_{z_0}^{z} \frac{d\xi}{\sqrt{a_0(\xi + r_1)(\xi + r_2)(\xi + r_3)(\xi + r_4)}}.$$

Inverting this expression to get the explicit solution for z now depends on whether the roots r_n $(n = 1, 2, 3, 4)$ are real or complex. In general, the final solution looks like either of the following:

$$z(u; k) = \beta \left\{ \frac{1 - \alpha_1^2 \mathrm{sn}^2(u; k)}{1 - \alpha^2 \mathrm{sn}^2(u; k)} \right\}$$

or

$$z(u;k) = \beta \left\{ \frac{1 - \alpha_1 \mathrm{cn}(u;k)}{1 - \alpha \mathrm{cn}(u;k)} \right\}.$$

Both expressions are derived for the axial gyrostat in reference (5:Ch. 5). Although our model is not the same as Hall's, the general form of these expressions are identical (with the exception of the value of the constants) since they arise from the same standard forms in reference (2). Once the analytical solution for z is known, it becomes a matter of changing the variables back to the original x_2.

As can be seen, Wittenburg's procedure is extremely complicated and is generally impractical for the case of the unbalanced gyrostat. Assuming that a powerful computer is available, it is easier to numerically integrate the equations of motion. Despite our failure to analytically solve these equations, there are still some positive outcomes from our effort. First, we have shown that an exact analytical solution theoretically does exist. Second, our failure justifies the approximate analytical solution found in references (13) and (14), which uses a form of the method of averaging involving a near-identity transformation.

IV. Graphical Representations of Spinup Dynamics (5:Ch. 4)

In Chapter 2 we develop the equations which govern the motion of our model. Now we apply them to the spinup problem. During this maneuver, the behavior of the gyrostat depends on its geometry, initial spin configuration (given by the initial conditions), and the magnitude of the motor torque. In this chapter, we analyze the effects of the geometry. Specifically, we develop a graphical tool which shows how the physical parameters of the gyrostat, given by the moments of inertia and the magnitude of the rotor imbalance, circumscribe all of the possible ways in which spinup can occur. We show here that there are certain motions which are stable over time and others which are not. All of this can be shown in the two-dimensional plane of the slowly-varying parameters, μ and y. We relegate all discussion of the effects of the motor torque and the initial conditions to the next chapter.

4.1 Momentum Spheres

Because all external torques are neglected in this model, angular momentum is conserved. Hence, $x_1^2 + x_2^2 + x_3^2 = 1$, which clearly shows that solutions to the equations of motion are confined to the surface of a *unit momentum sphere*. If there is no component of torque acting along the rigid shaft connecting the platform and rotor ($\varepsilon = 0$), these solutions form closed curves of constant energy analogous to *polhodes* on the classical momentum ellipsoids. As previously discussed, the constant energy curves are given by

$$y = 2\mu[(i_1 - 1)\alpha_1 x_1 - \alpha_3 x_3] - (i_1 x_1^2 + i_2 x_2^2).$$

Several examples are shown in Figures 3 – 5 along with simplified sketches to better visualize their topology. Because these sketches are two dimensional representations of three dimensional objects, they are formed by "piercing" the spheres at the points denoted by $\mathbf{O}_\mu$ and then "dilating these holes" until the spheres are flattened. These

diagrams are drawn at different values of μ for the same set of geometric parameters.

There are either two, four, or six equilibrium points on the momentum sphere for any given value of μ. This variable defines the topology of the momentum sphere. Figures 3 – 5 depict specific situations for all three cases. Two of the equilibria correspond to the desired oblate and prolate dual-spin conditions ($\mathbf{O}_\mu$ and $\mathbf{P}_\mu$, respectively) and two correspond to the two possible flat-spin configurations ($\mathbf{F}_{1\mu}$ and $\mathbf{F}_{2\mu}$) which may result from resonance capture, a phenomenon that is examined in the next chapter. All four are stable equilibria and are characterized by the *centers* in Figures 3 – 5. The two remaining equilibria are both unstable *saddles* ($\mathbf{U}_\mu$). The notation used here is similar to that developed in references (5) and (8).

As the value of μ is incremented, the equilibria on the corresponding series of momentum spheres appear to shift position. For very small values of μ, all six are present (Figure 3). As this parameter increases from zero, the two unstable equilibria converge. Eventually, a critical value of μ is reached, μ_{pf}, at which both $\mathbf{U}_\mu$ collide. Since $\mathbf{P}_\mu$ is situated directly between them, all three equilibria coalesce into a single saddle point. On a bifurcation diagram, this event looks like a pitchfork and is therefore known as a ***pitchfork bifurcation.*** Afterwards only four equilibria remain (Figure 4). As μ assumes higher values, both $\mathbf{F}_{1\mu}$ and $\mathbf{F}_{2\mu}$ approach the new saddle. In general, $\mathbf{F}_{1\mu}$ is closer to $\mathbf{P}_\mu$ than is its flat-spin counterpart, so when the second critical value of μ is reached, μ_{sn}, $\mathbf{F}_{1\mu}$ and $\mathbf{P}_\mu$ annihilate leaving only two stable equilibria (see Figure 5). This event is called a ***saddle-node bifurcation.***

The momentum sphere illustrates the behavior of the spacecraft's angular momentum vector for a given set of geometric parameters: i_n $(n = 1, 2, 3), \alpha_1$, and α_3. The platform's inertial angular momentum μ determines the topology of the sphere, y denotes the particular constant energy curve of the unperturbed motion, and (x_1, x_2, x_3) pinpoint the system's exact position on this curve. During spinup, μ varies with time. As a result, y is no longer constant so that the curves are no longer closed.

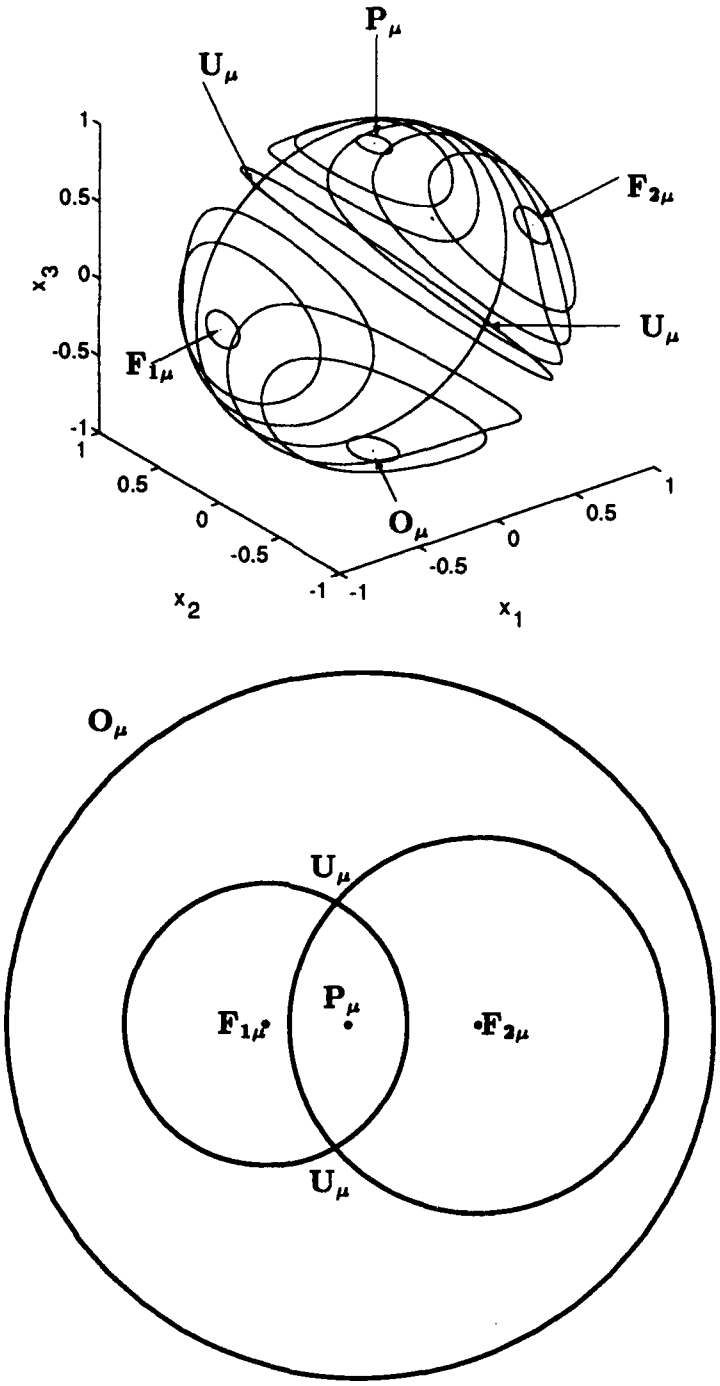

Figure 3. Momentum Sphere for a Gyrostat Having $\mu = 0.1, \varepsilon = 0$, and the Following Geometric Parameters: $i_1 = 0.7, i_2 = 0.3, i_3 = 0.8, \alpha_1 = 0.5, \alpha_3 = 0.866$

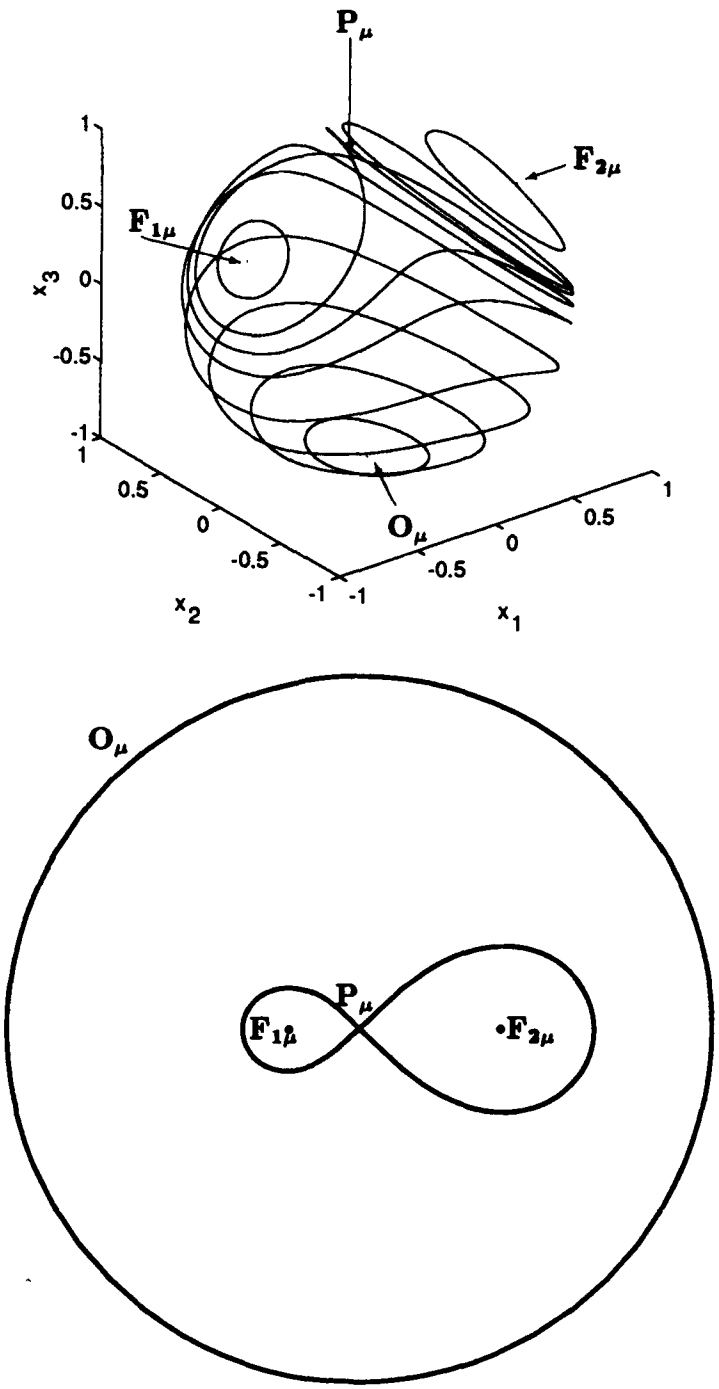

Figure 4. Momentum Sphere for a Gyrostat Having $\mu = 0.4, \varepsilon = 0$, and the Following Geometric Parameters: $i_1 = 0.7, i_2 = 0.3, i_3 = 0.8, \alpha_1 = 0.5, \alpha_3 = 0.866$

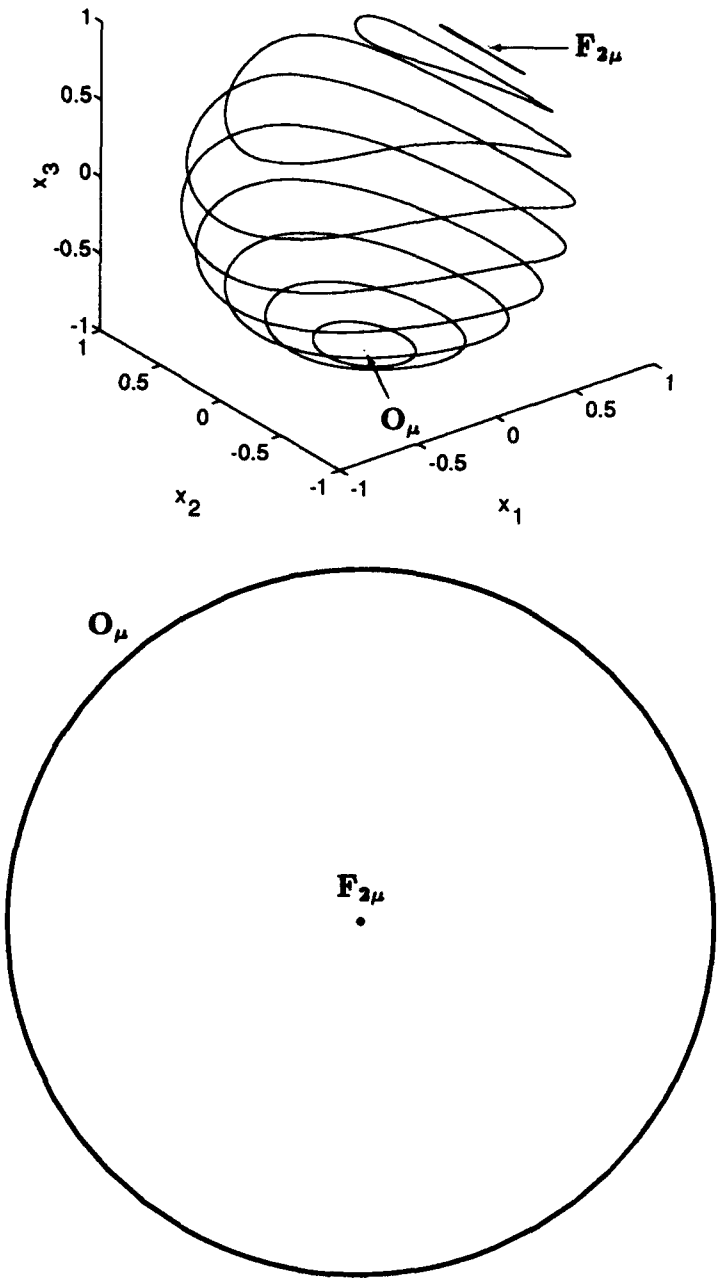

Figure 5. Momentum Sphere for a Gyrostat Having $\mu = 0.7, \varepsilon = 0$, and the Following Geometric Parameters: $i_1 = 0.7, i_2 = 0.3, i_3 = 0.8, \alpha_1 = 0.5, \alpha_3 = 0.866$

Recall that in this case, the rate of change of the gyrostat's rotational kinetic energy is expressed in dimensionless form as

$$\dot{y} = 2\varepsilon[(i_1 - 1)\alpha_1 x_1 - \alpha_3 x_3].$$

Thus, in order to observe the spacecraft's attitude during this maneuver, a series of instantaneous spheres must be generated at sufficiently small intervals of μ, and the corresponding instantaneous angular momentum positions must be plotted on their surfaces. This method is extremely resource-intensive. As such, it is best implemented on more powerful computers. Fortunately, there is a simpler way to visualize spinup first proposed by Hall in 1992 (5). Rather than create a whole series of three dimensional momentum spheres, all we need to do is look at a *single* plane defined by μ and y.

4.2 The μy Plane

The μy plane is a bifurcation diagram which shows the evolution of the stable and unstable equilibria on the momentum sphere for different values of μ. Figure 6 shows a typical example. Later we see that this is only one of three general forms; the shape of the plane depends on the relative sizes of the geometric parameters. By convention, the solid lines represent all of the possible energy states of the stable equilibria while the dashed lines are indicative of those of the saddles and separatrices over the entire range of μ. One particular sphere can be mapped to a corresponding vertical "slice" within this plane at the value of μ for which the sphere is defined. Furthermore, a particular spinup trajectory, which covers an entire range of μ, may be superimposed on this plane so that the behavior during spinup can be easily observed with respect to the equilibria. This is illustrated in the next chapter, when we examine the effects of different conditions on the outcome of spinup.

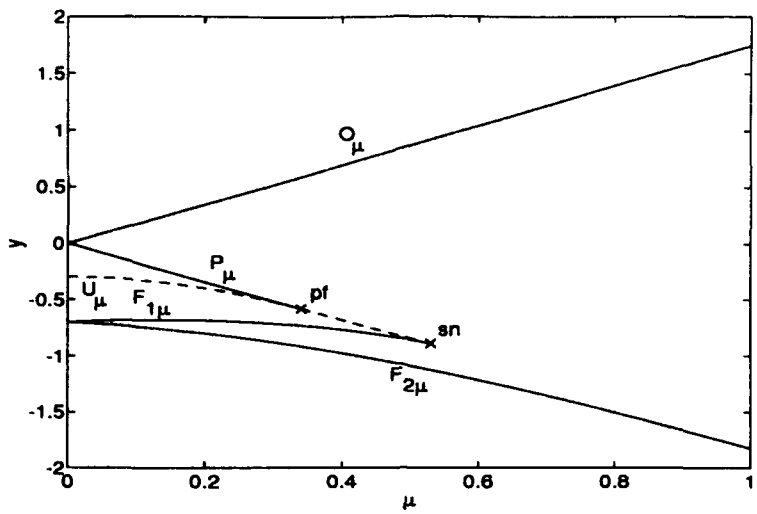

Figure 6. The μy Plane for the Oblate-Prolate Gyrostat. The points "pf" and "sn" denote the pitchfork and saddle-node bifurcations, respectively. $i_1 = 0.7, i_2 = 0.3, \alpha_1 = 0.5, \alpha_3 = 0.866$

4.2.1 Geometric Influence on the Shape of the μy Plane. The shape of the μy plane depends on the spacecraft geometry. An unbalanced gyrostat corresponds to one of three general types. These are termed *Oblate-Prolate*, *Oblate-Intermediate*, and *Intermediate-Prolate* and are classified by determining whether the plane containing the imbalance has the maximum and minimum, maximum and intermediate, or intermediate and minimum eigenvalues of **J**, respectively. The nomenclature used here are modified versions of their biaxial counterparts (7). In the pseudo-principal frame, the imbalance is located in the $\hat{p}_1\hat{p}_3$ plane. Therefore, this determination is made by comparing the magnitudes of the inertia-like quantities J_1 and J_3 to that of J_2. In this analysis we assume that $J_1 > J_3$ without loss of generality (the justification can be found in (5:§3.5)), and the results are summarized in Table 3.

Since the governing equations are in dimensionless form, these definitions would be more useful if they are written in terms of the dimensionless parameters. We

Classification	Requirement
Oblate-Prolate	$J_1 > J_2 > J_3$
Oblate-Intermediate	$J_1 > J_3 > J_2$
Intermediate-Prolate	$J_2 > J_1 > J_3$

Table 3. Classification of Spacecraft Geometry in Terms of the Inertia-Like Parameters

repeat the transformations below:

$$
\begin{aligned}
i_1 &= 1 - \frac{J_3}{J_1} \\
i_2 &= 1 - \frac{J_3}{J_2} \\
i_3 &= 1 - \frac{J_3}{J_3'}
\end{aligned}
$$

where $J_3' \equiv J_3 + I_s \alpha_3^2$. Clearly, the following relations must be true:

$$
\begin{aligned}
J_3 > J_n &\implies i_n < 0 \text{ (for } n = 1, 2) \\
J_3 < J_n &\implies i_n > 0.
\end{aligned}
$$

Because only i_1 and i_2 explicitly appear in the equations of motion, they alone define the shape of the μy plane. Also, since we assume $J_1 > J_3$ without loss of generality, the same must be true for $i_1 > 0$. These transformations change the criteria in Table 3 to those in Table 4. The alternative set of requirements for each case arises from an inherent symmetry of the spacecraft which exists only in $\mathcal{F}^p$, the details of which are also given in reference (5:§3.5). Figure 6 is an example of the Oblate-Prolate geometry. This form is the primary focus of this study, but examples of the other two are shown in Figures 7 and 8.

The μy plane also reveals the gyrostat's degree of asymmetry and degree of imbalance. The former can be qualitatively determined by the size of the gap between

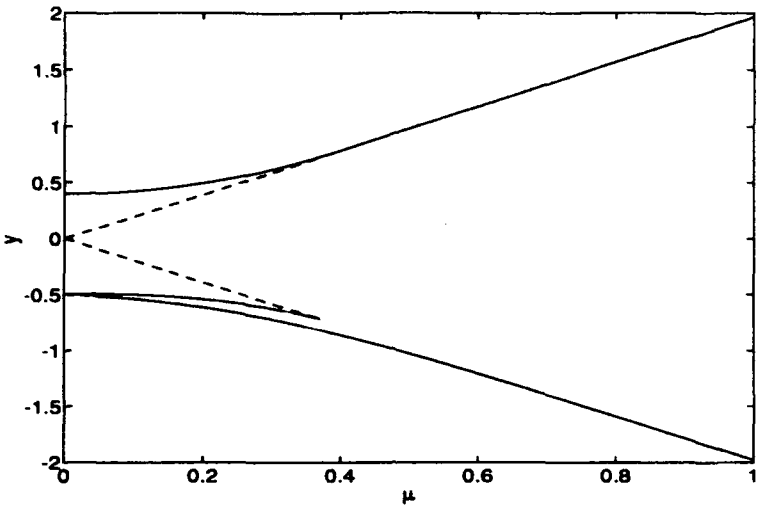

Figure 7. The μy Plane for the Oblate-Intermediate Gyrostat: $i_1 = 0.5, i_2 = -0.4, \alpha_1 = 0.2, \alpha_3 = 0.9798$

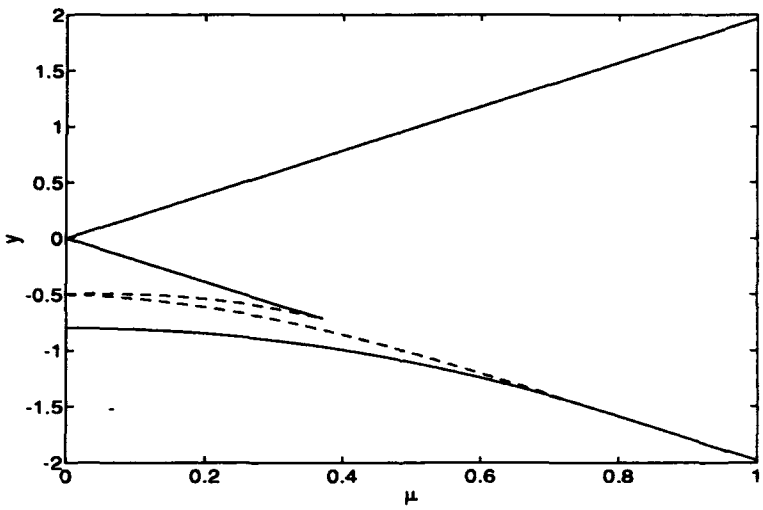

Figure 8. The μy Plane for the Intermediate-Prolate Gyrostat: $i_1 = 0.5, i_2 = 0.8, \alpha_1 = 0.2, \alpha_3 = 0.9798$

Classification	Requirement
Oblate-Prolate	$i_1 > i_2 > 0$ or $i_2 < i_1 < 0$
Oblate-Intermediate	$i_1 > 0 > i_2$ or $i_2 < 0 < i_1$
Intermediate-Prolate	$i_2 > i_1 > 0$ or $i_1 < i_2 < 0$

Table 4. Classification of Spacecraft Geometry in Terms of the Dimensionless Parameters

$\mathbf{U}_\mu$ and $\mathbf{F}_{1\mu}$. The closer they are to one another, the closer the gyrostat is to being symmetric. This can also be found quantitatively from the difference between i_1 and i_2; the closer it is to zero, the more symmetric the spacecraft. The model's degree of imbalance may be seen qualitatively from the plane as well. In this case it is based on the size of the gap between the two flat-spin trajectories; the smaller the gap, the smaller the imbalance. If both curves coincide, the spacecraft is balanced. This special case is the axial gyrostat, which is shown in Figure 9. The degree of imbalance may also be quantitatively determined by the dimensionless parameters α_1 and α_3. As $|\alpha_3|$ approaches unity (which implies that α_1 approaches 0), the closer is our model to the axial gyrostat.

4.2.2 Determination of the Equilibrium Trajectories. We now derive the evolution of the equilibrium trajectories in the μy bifurcation diagram. First we define the conditions for equilibrium in terms of the equations of motion. We then explain how these conditions are satisfied, resulting in the "coordinates" of the centers and saddles on the momentum sphere. This also enables us to determine their respective energies solely as functions of μ, leading to the μy plots of the equilibrium trajectories. Finally, when these trajectories have been established, we determine their stability.

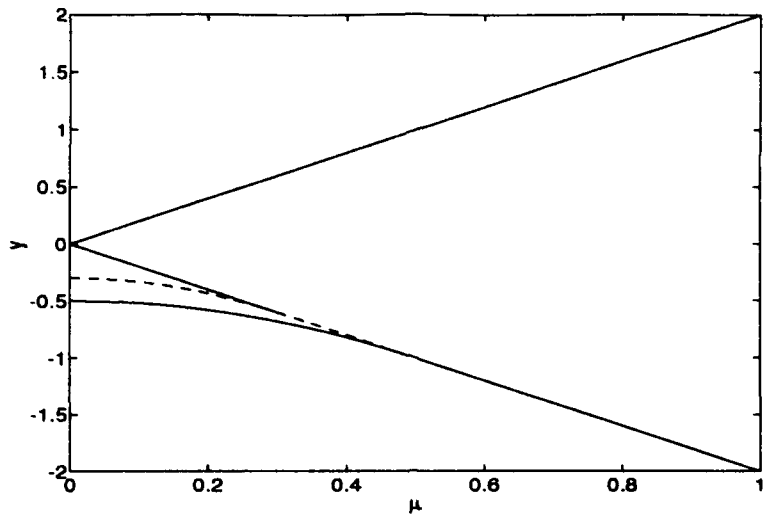

Figure 9. The μy Plane for the Axial Gyrostat: $i_1 = 0.5, i_2 = 0.3, \alpha_1 = 0, \alpha_3 = 1$

Once again we return to the equations governing the behavior of the spacecraft angular momentum:

$$\begin{aligned}
\dot{x}_1 &= (i_2 x_3 - \mu\alpha_3)x_2 \\
\dot{x}_2 &= -i_1 x_1 x_3 + \mu[\alpha_3 x_1 - \alpha_1(1 - i_1)x_3] \\
\dot{x}_3 &= [(i_1 - i_2)x_1 + (1 - i_1)\mu\alpha_1]x_2
\end{aligned}$$

When the system is in equilibrium, $(x_1, x_2, x_3) = (x_{1_{eq}}, x_{2_{eq}}, x_{3_{eq}})$, all of which are constant over time. Specifically, these values satisfy the following conditions:

$$\dot{x}_{1_{eq}} = (i_2 x_{3_{eq}} - \mu\alpha_3)x_{2_{eq}} = 0 \tag{72}$$

$$\dot{x}_{2_{eq}} = -i_1 x_{1_{eq}} x_{3_{eq}} + \mu[\alpha_3 x_{1_{eq}} - \alpha_1(1 - i_1)x_{3_{eq}}] = 0 \tag{73}$$

$$\dot{x}_{3_{eq}} = [(i_1 - i_2)x_{1_{eq}} + (1 - i_1)\mu\alpha_1]x_{2_{eq}} = 0. \tag{74}$$

They are also the coordinates defining the location of each center and saddle on a particular momentum sphere. The energy associated with these points comes from the energy equation

$$y_{eq} = 2\mu[(i_1 - 1)\alpha_1 x_{1_{eq}} - \alpha_3 x_{3_{eq}}] - (i_1 x_{1_{eq}}^2 + i_2 x_{2_{eq}}^2). \tag{75}$$

From our discussion on page 42, we noted that the positions of the equilibria shift over the momentum sphere as a function of μ. Clearly, their energies must also depend on this variable. Thus, if we are able to rewrite y_{eq} in terms of μ alone, the trajectories characterizing the μy plane can be found. For this reason, it is a bifurcation diagram since it shows the evolution of these equilibrium points *indirectly* via their associated energies.

To obtain this special relationship, we must find the expressions giving $x_{n_{eq}} = f_n(\mu)$ $(n = 1, 2, 3)$ and satisfying the conditions for equilibrium. There are two ways this can be done.

4.2.2.1 Case A. Obviously, one way to do this is to let $x_{2_{eq}} = 0$ so that (72) and (74) are identically satisfied. The other two equilibrium parameters must therefore simultaneously satisfy Equation (73) as well as conservation of angular momentum. They are found by decomposing this equation into a system of two quartic polynomials, one written in terms of $x_{1_{eq}}$ and the other in terms of $x_{3_{eq}}$. This lengthy algebraic manipulation results in

$$\begin{aligned} 0 &= i_1^2 x_1^4 + 2i_1(1 - i_1)\mu\alpha_1 x_1^3 + [(1 - i_1)^2\mu^2\alpha_1^2 + \mu^2\alpha_3^2 - i_1^2]x_1^2 \\ &\qquad -2i_1(1 - i_1)\mu\alpha_1 x_1 - (1 - i_1)^2\mu^2\alpha_1^2 \qquad (76) \\ 0 &= i_1^2 x_3^4 - 2i_1\mu\alpha_3 x_3^3 + [\mu^2\alpha_3^2 + (1 - i_1)^2\mu^2\alpha_1^2 - i_1^2]x_3^2 - 2i_1\mu\alpha_3 x_3 \\ &\qquad -\mu^2\alpha_3^2. \qquad (77) \end{aligned}$$

For a given geometry, the roots of these polynomials vary only with μ. The ($x_{1_{eq}}$, $x_{3_{eq}}$) roots are paired together such that (73) is satisfied. Thus, we are left with expressions of the following forms:

$$\begin{aligned} x_{1_{eq}} &= f_1(\mu) \\ x_{2_{eq}} &= 0 \\ x_{3_{eq}} &= f_3(\mu). \end{aligned}$$

4.2.2.2 Case B. When $\mu < \mu_{pf}$, there exist two additional equilibria for which $x_{2_{eq}}$ cannot be zero. As a result, in order to satisfy the conditions for equilibrium, Equations (72) and (74) must give, respectively:

$$x_{3_{eq}} = \frac{\mu\alpha_3}{i_2} \tag{78}$$

$$x_{1_{eq}} = \frac{\mu\alpha_1(i_1 - 1)}{i_1 - i_2}. \tag{79}$$

These automatically satisfy (73) as well. In this case the nonzero expression for $x_{2_{eq}}$ can be found from conservation of angular momentum:

$$x_{2_{eq}} = \pm\sqrt{1 - \left[\frac{\mu\alpha_1(i_1 - 1)}{i_1 - i_2}\right]^2 - \left[\frac{\mu\alpha_3}{i_2}\right]^2}. \tag{80}$$

Once again, for a given geometry, $x_{1_{eq}}$, $x_{2_{eq}}$, and $x_{3_{eq}}$ are functions of μ alone.

The results of either case are substituted directly into Equation (75), giving $y_{eq} = y(\mu)$. From this, it can be shown that both trajectories found in the latter case must be identical. Equations (78) and (79) show that they each have the same values of $x_{1_{eq}}$ and $x_{3_{eq}}$, and (80) implies that $x_{2_{eq}}$ must be positive for one and negative for the other. Because the $x_{2_{eq}}$ parameter is squared in (75), the sign difference is irrelevant when their energies are calculated. As a result, these paths are indistinguishable on the μy plane.

At this point we briefly digress in order to explain how μ_{pf} and μ_{sn} are determined. The first of these is important because it gives the value of μ at which $\mathbf{P}_\mu$ changes stability. Specifically, it occurs when Equations (76), (77), and (80) are simultaneously satisfied:

$$0 = \sqrt{1 - \left[\frac{\mu_{pf}\alpha_1(i_1 - 1)}{i_1 - i_2}\right]^2 - \left[\frac{\mu_{pf}\alpha_3}{i_2}\right]^2}$$

or equivalently,

$$1 = \mu_{pf}^2 \left\{ \left[\frac{\alpha_1(i_1 - 1)}{i_1 - i_2}\right]^2 + \left[\frac{\alpha_3}{i_2}\right]^2 \right\}.$$

Hence,

$$\mu_{pf} = \left\{ \left[\frac{\alpha_1(i_1 - 1)}{i_1 - i_2}\right]^2 + \left[\frac{\alpha_3}{i_2}\right]^2 \right\}^{-1/2}.$$

The other parameter, μ_{sn}, denotes the specific value of μ at which $\mathbf{P}_\mu$ becomes nonexistent. It is based on the spacecraft geometry and can only be found numerically.

4.2.3 Stability of the Equilibrium Trajectories. Now that we have shown how the equilibrium trajectories (denoted in this section as $\mathcal{E}$) in the μy plane evolve from the equations of motion, the next step is to determine their stability. Although we have shown this in our previous diagrams by the type of line used to represent these paths, we have not been able to justify this characteristic until now. By looking at the momentum sphere, it is easy to tell which equilibria are stable and which are not; centers and saddles are easy to distinguish because of their distinctive appearances. Therefore, one way to determine which trajectories in the μy plane are stable is to look at the corresponding equilibrium points on the sphere. Another way is to make use of *Poincaré stability criteria*, which are defined in texts on nonlinear oscillations such as Jordan and Smith (12:213-218).

In general, Poincaré stability is defined for autonomous systems of the form

$$\dot{\mathbf{z}} = \mathbf{Z}(\mathbf{z}).$$

Our set of governing equations, given by (50) – (54), is clearly a particular example of such a system. When $\varepsilon \neq 0$, their general solution forms perturbed, or nonequilibrium, trajectories in the μy plane. These paths are labeled here as $\mathcal{N}$ to distinguish them from the special case of $\mathcal{E}$. In simple terms, we can show that a particular trajectory $\mathcal{E}$ is Poincaré stable if an initial condition near (or directly on) this path stays arbitrarily close to it when the system is perturbed. In other words, when μ changes slowly, the nonequilibrium trajectory $\mathcal{N}$ follows $\mathcal{E}$ very closely for all time. If, on the other hand, $\mathcal{N}$ deviates significantly, then the particular equilibrium trajectory near which it originates corresponds to an unstable equilibrium point.

Figures 10 – 12 depict the application of these criteria to the μy plot in Figure 6. The heavy lines indicate actual numerically integrated trajectories $\mathcal{N}$ which start on the various equilibrium points at $\mu = 0$. Note that the integrated trajectories that start on a stable equilibrium point remain arbitrarily close to the solid lines as μ increases. On the other hand, those that travel near a dashed trajectory eventually diverge.

The μy plane is a valuable tool for analyzing spinup, as demonstrated in the following chapter. However, it too has shortcomings. Because it is a two-dimensional representation of the three-dimensional momentum spheres, there are certain important aspects which the μy plane cannot reveal. These are shown in Chapter 5 as well. In short, there are advantages and disadvantages of both representations. The μy plane lacks the "depth" of the momentum sphere, but the momentum sphere lacks the "breadth" of the μy plane. Both are useful tools in their own right, but they are most beneficial when used together.

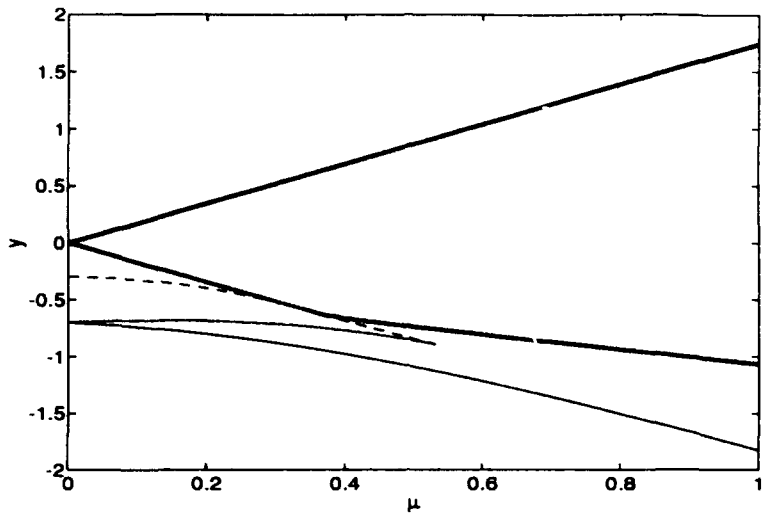

Figure 10. Application of Poincaré Stability Criteria Along the Dual-Spin Equilibrium Trajectories

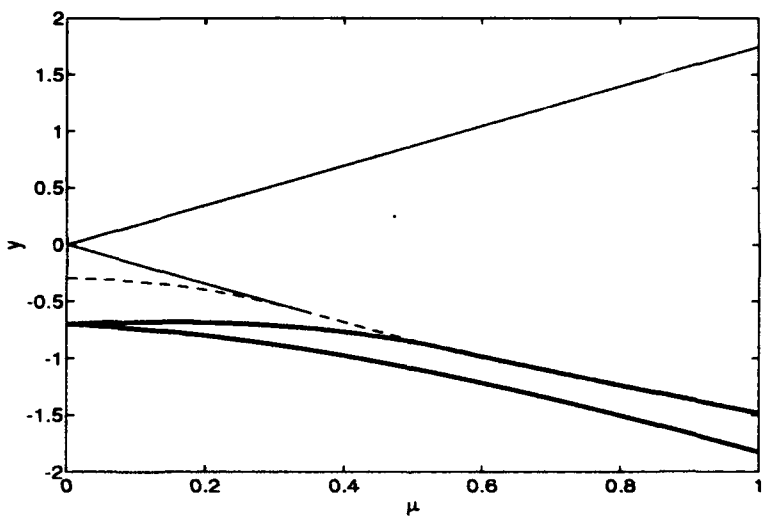

Figure 11. Application of Poincaré Stability Criteria Along the Flat Spin Equilibrium Trajectories

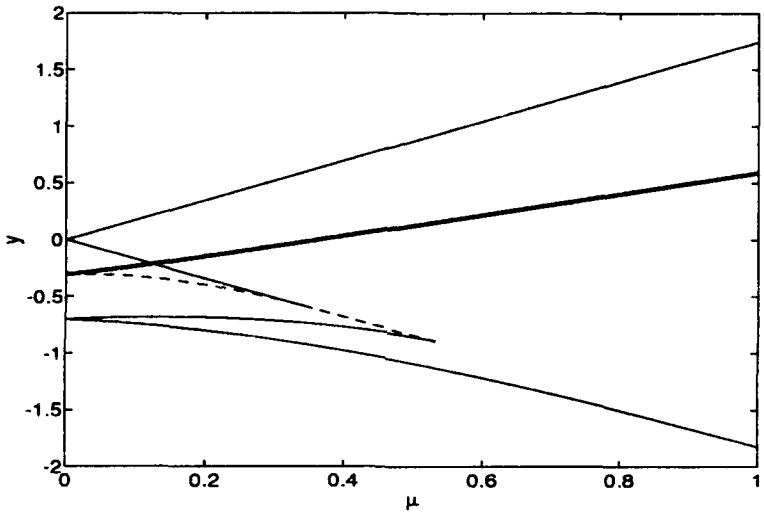

Figure 12. Application of Poincaré Stability Criteria Along the Unstable Equilibrium Trajectories

V. *Spinup*

In this chapter we discuss the phenomenon known as *precession phase lock (PPL)* or *resonance capture*. These terms describe the onset of unconstrained growth in the gyrostat's nutation angle during platform despin. It is a phenomenon which may occur in any gyrostat that is either asymmetric or dynamically unbalanced. Precession phase lock has been studied since the early 1970s, but its explanation continues to be debated. Kinsey *et al.* (14, 13:8) contend that, for sufficiently small motor torques, this occurs when the spin rate of the unbalanced body approaches the inertial free precession rate of the spacecraft. At this point, both the platform and the rotor inertial angular velocities decrease toward zero. When this occurs, the effect of the motor torque is diverted toward increasing the spacecraft's coning motion.

More recently, Hall (6) has offered an alternative explanation which can be clearly shown on the μy plane. However, this analysis is pertinent to the balanced asymmetric gyrostat, which is a very close approximation of Kinsey's model, but is not representative of the more general unbalanced system in this study. Reference (6) shows that nutation growth results when trajectories of the perturbed ($\varepsilon \neq 0$) system cross an instantaneous separatrix such that they oscillate about a stable flat-spin equilibrium point at the conclusion of spinup rather than about the desired dual-spin center. Capture, according to Hall, is a phenomenon related to the final energy state of the spacecraft.

In the following pages, Hall's analysis is applied directly to Kinsey's model. In doing so, we show that the size of the motor torque is not the only factor which influences the onset of precession phase lock. Finally, we develop an alternative method to reduce the *probability of capture* of the spacecraft if a stronger motor becomes infeasible. This involves selection of proper initial spinup conditions. From

the results of our analysis, a new, more generalized definition of resonance capture is offered which is a hybrid of both Kinsey's and Hall's points of view.

5.1 Kinsey's Model

Kinsey formulated the equations of motion by considering the platform and rotor separately. Unlike Hughes (11), after whose equations our own system is modelled, Kinsey defined the moment of inertia tensors of both bodies independently, each relative to the spacecraft center of mass. The platform is both axially symmetric and dynamically balanced in the body-fixed reference frame, and the rotor is axially symmetric but dynamically unbalanced. Their axis of relative rotation coincides with the platform's axis of symmetry. Hence, the body-fixed frame about which Kinsey chose to derive the governing equations are the principal axes of the platform. In our terminology, this is $\mathcal{F}^b$, the balanced-body frame.

Kinsey's equations of motion are expressed in terms of angular velocity rather than angular momentum. Because they are written in the balanced-body frame, these equations are considerably more complex than the ones developed in our study. Kinsey carried out the analysis in dimensionless form and showed that the behavior of the system during spinup depends on the magnitude of four parameters: the size of the rotor imbalance relative to the spacecraft transverse moments of inertia (ν), the size of the rotor axial moment of inertia relative to the spacecraft transverse moments of inertia (σ), the size of the platform axial moment of inertia relative to that of the rotor (J), and the magnitude of the despin motor torque (K). Throughout the analysis, Kinsey assumed that $\nu \ll 1$, thereby simplifying the dimensionless equations and allowing for the approximation of their solution using the method of averaging via a near-identity transformation. Despite the resulting simplifications, this approximation also leads to a major disadvantage in Kinsey's approach; it is not applicable to the more general unbalanced system (see page 13). Our analysis, on the other hand, is still valid in such a case. After a second round of scaling,

Kinsey's equations provide a means with which to estimate the final cone angle of the spacecraft during despin. This method is only applicable for final cone angles $< 30°$, but it gives reasonably accurate predictions (within 10%).

5.1.1 PPL According to Kinsey (13, 14) Kinsey defined resonance capture in terms of its effect on the inertial angular momenta of both the platform and rotor during spinup. If the motor torque is too small, then once the unbalanced body (in this case the rotor) reaches the spacecraft inertial free precession rate, the system starts to exhibit the undesirable effects of precession phase lock. The rotor velocity fails to maintain its steady increase. Instead, it actually decreases while the spacecraft's nutation angle grows. At the conclusion of this maneuver, the spacecraft tumbles in a flat-spin. During normal despin, however, the rotor velocity exceeds the inertial free precession rate and continues to grow until the spinup motor is deactivated. In this case, the increase in nutation is less appreciable. Both normal despin and precession phase lock are shown in Figure 13.

Kinsey's view of resonance capture does not offer a precise set of criteria that define its occurrence. He asserts that precession phase lock occurs "when the rotor rate ω_B is approximately equal to the free precession rate of the s/c" (14). Also, Kinsey seems to imply that a captured spacecraft has a final nutation angle of approximately 90° while smaller, albeit significant, cone angles render *escape*. Although this seems like good qualitative reasoning, it is nonetheless a generalization. To get more precise conditions, we approach this phenomenon using energy-based criteria similar to those developed in reference (6). In this reexamination, more rigorous conditions leading to capture are provided. Before proceeding, however, it is helpful to translate Kinsey's parameters into those used here.

5.1.2 Kinsey's Model Translated into the μy Plane. Kinsey's model is reexamined using the tools developed in the previous chapters. First, his dimensionless parameters are translated into those defined in this thesis. The dynamics of Kinsey's

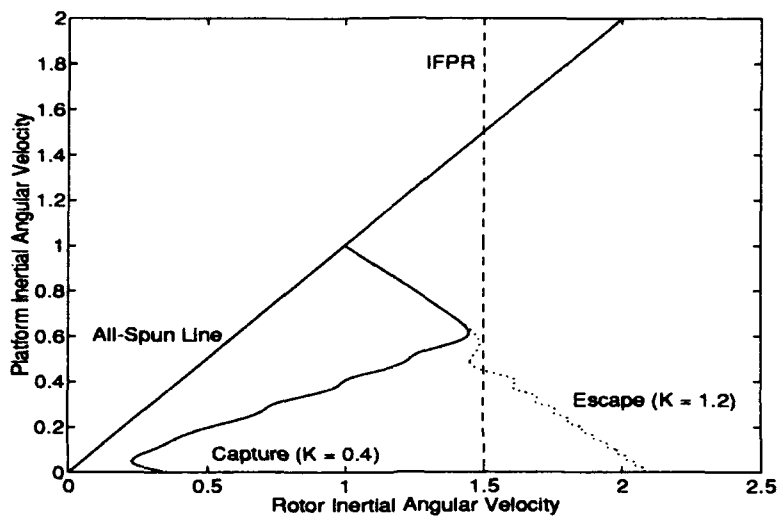

Figure 13. Capture and Escape as Defined by Kinsey. The spacecraft is initially in the all-spun configuration. For the smaller motor torque (K = 0.4), capture occurs when the rotor angular velocity approaches the inertial free precession rate (IFPR). Both the platform and rotor angular velocities approach zero. In normal despin ($K = 1.2$), the rotor rate continues to increase while the platform rate approaches zero (escape). Kinsey Parameters: $\nu = 0.005, \sigma = 0.667, J = 1.25$

Kinsey	Tsui
$\nu = 0.005$	$i_1 = 0.33313$
$\sigma = 0.667$	$i_2 = 0.33308$
$J = 1.25$	$i_3 = 0.55553$
$\bar{\omega}_1(0) = 0.00998$	$\alpha_1 = -0.01501$
$\bar{\omega}_2(0) = 0$	$\alpha_3 = -0.99989$
$\bar{\omega}_A(0) = 1$	$x_{1_0} = -0.02499$
$\bar{\omega}_B(0) = 1$	$x_{2_0} = 0$
	$x_{3_0} = -0.99969$

Table 5. Translation of Kinsey's Geometric Parameters and Initial Conditions

Kinsey K	Tsui ε
0.4	-2.1942×10^{-4}
0.6	-3.2913×10^{-4}
0.8	-4.3884×10^{-4}
1.0	-5.4854×10^{-4}
1.2	-6.5825×10^{-4}

Table 6. Translation of Kinsey's Dimensionless Motor Torques

model are then projected onto the μy plane, and two of the different spinup conditions he examined are shown using the energy-based technique for comparison. The equations and algorithm used to translate Kinsey's dimensionless parameters are explained in Appendix B. The translated geometric parameters and initial conditions are summarized in Table 5 and the motor torques are shown in Table 6.

The μy plane associated with these parameters is shown in Figure 14. Because $i_1 > i_2 > 0$, it is an Oblate-Prolate gyrostat. Of particular interest are the regions bounded within Boxes 1 and 2, which are shown in greater detail in Figures 15 and 16, respectively. The pitchfork bifurcation is shown in Box 1, and the saddle-node bifurcation is depicted in Box 2. They also reveal other interesting features of this particular gyrostat. From Figures 14 and 15, it is clear that for most of the spinup maneuver, there is only *one* possible stable flat spin equilibrium point, and that the saddles remain very close at all times to this particular center. This indicates that

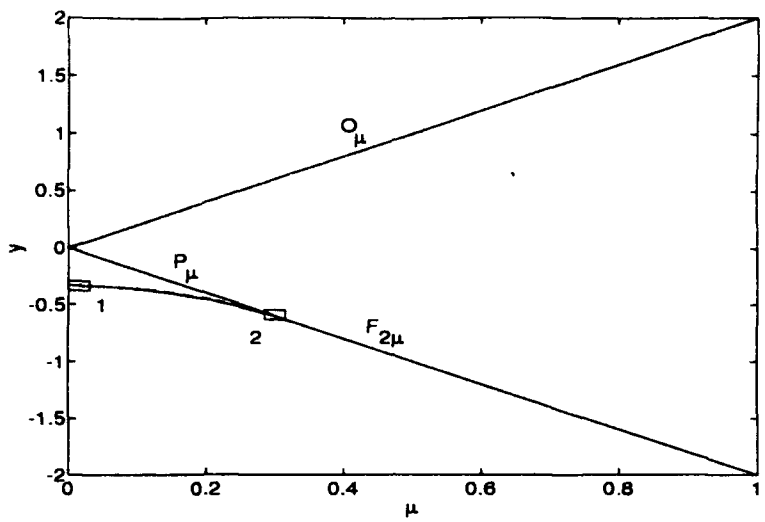

Figure 14. The μy Plane for Kinsey's Gyrostat

Kinsey's gyrostat is *very nearly* axisymmetric and balanced. Next, when Figure 16 is considered, it is apparent that *this particular Oblate-Prolate geometry is different from the example introduced in Figure 6.* In fact, it is not too difficult to see that Kinsey's gyrostat is qualitatively equivalent to the earlier example reflected over the horizontal axis. Now that his particular gyrostat has been transformed into the μy plane, we introduce the energy-based criteria for resonance capture and apply them to Kinsey's special case.

5.2 Redefinition of Resonance Capture

Rather than explain resonance capture in terms of the system angular momenta, we do so in terms of its energy. This analysis requires the projection of the spinup maneuver onto the μy plane. Capture is examined exclusively for the Oblate-Prolate geometry. As did Kinsey, we assume that spinup concludes when the balanced axisymmetric body has completely despun ($\mu = 0$). Our analysis is not limited to the initially all-spun gyrostat, but we include this in the discussion due

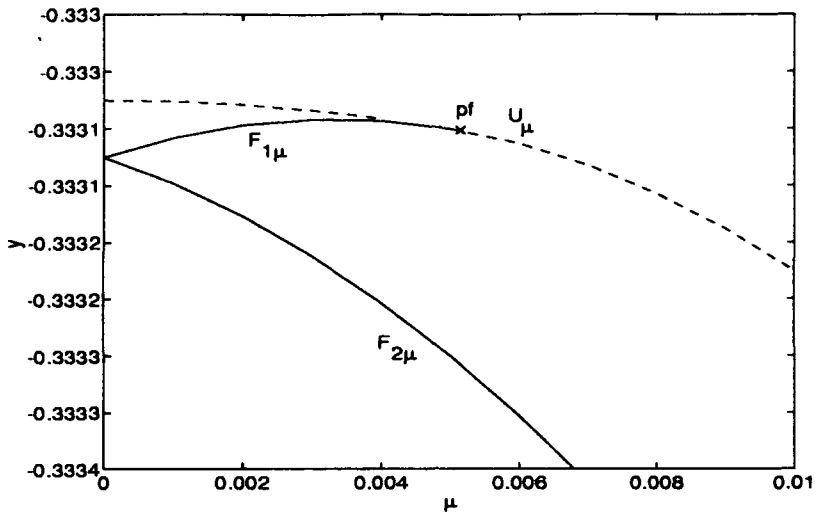

Figure 15. Closeup of the μy Plane for Kinsey's Gyrostat (Inset 1)

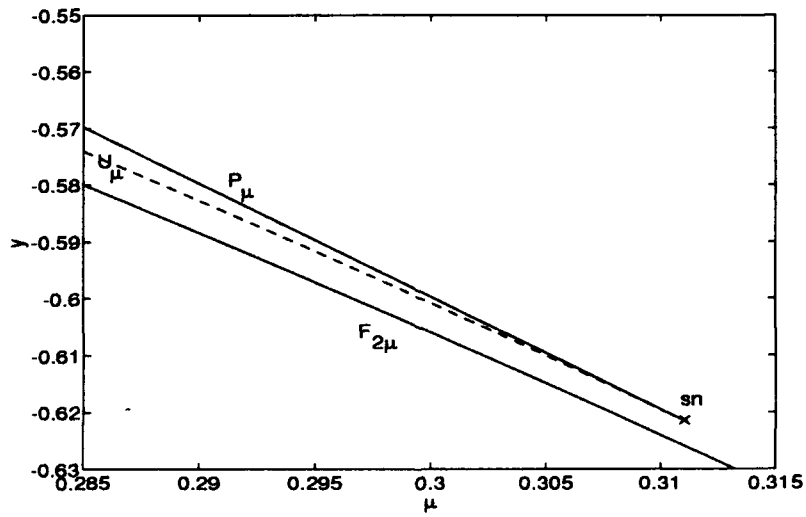

Figure 16. Closeup of the μy Plane for Kinsey's Gyrostat (Inset 2)

to its relevance to Kinsey's examples. In this condition, the gyrostat is essentially a single rigid body so that

$$\mu_0 = \frac{\alpha_1 x_1(1 - i_1) + \alpha_3 x_3}{\alpha_3^2/i_3 + \alpha_1^2(1 - i_1)}.$$

The derivation of this parameter is given in Appendix C.

There are three types of spinup conditions for the Oblate-Prolate gyrostat. These are ***oblate spinup***, ***prolate spinup***, and ***resonance capture***. The third condition has already been discussed and is the main topic of this chapter. Oblate and prolate spinup as defined herein refer to the condition in which the spacecraft concludes the maneuver oscillating about either the oblate ($\mathbf{O}_\mu$) or prolate ($\mathbf{P}_\mu$) equilibrium point, respectively. In the μy plane, their spinup trajectories follow those of their respective centers. Both of these spinup conditions, described here as ***dual-spin*** conditions, lead to escape. Although Hall (8, 5:60) used these two terms in the analysis of axial dual-spinners, their meaning has been slightly altered in this thesis and should not be confused with his previous definitions.

Reference (6) shows how capture of an axial gyrostat is represented on a series of momentum spheres. This can be easily extended to the spacecraft geometry studied in this thesis. If the final energy of the system (at $\mu = 0$) forms a closed curve about either of the transverse (flat-spin) equilibria, the system has been captured. If, on the other hand, this curve encircles either dual-spin center, it has escaped. One can think of the set of all constant energy curves which surround a particular center as lying within its ***domain***. These are isolated from one another by the separatrices. Moreover, because each closed curve within a given domain represents a specific rotational kinetic energy, we may specify the ***energy range*** of that domain. A schematic representation of this is shown in Figure 17, which depicts the four (numbered) domains at $\mu = 0$. The energy ranges of each are shown in the μy plane on top, which is a closeup of Figure 6 in the previous chapter. They are drawn at

different values of μ only for the sake of clarity; it is important to emphasize that at motor shut-off, all of these energies are defined at $\mu = 0$ so that these energy ranges actually overlap.

At the end of spinup, the value of the final system energy, y_f, must lie in one of the energy ranges defined at $\mu = 0$. Recall that the energy of the system is given by

$$y = 2\mu[(i_1 - 1)\alpha_1 x_1 - \alpha_3 x_3] - (i_1 x_1^2 + i_2 x_2^2)$$

so that

$$y_f = -(i_1 x_1^2 + i_2 x_2^2).$$

The equilibria are located at the following points on the momentum sphere with the associated final energies, $y_{f_{eq}}$, obtained by direct application of this relation:

Equilibrium Point	x_1	x_2	x_3	$y_{f_{eq}}$
Stable Flat Spin Equilibria	± 1	0	0	$-i_1$
Unstable Saddles	0	± 1	0	$-i_2$
Prolate Dual-Spin Equilibrium	0	0	$+1$	0
Oblate Dual-Spin Equilibrium	0	0	-1	0

We can now define the energy range of each domain in terms of the geometric parameters of the spacecraft:

$$\text{Dual-Spin Energy Range:} \quad -i_2 < y_f < 0$$

$$\text{Flat-Spin Energy Range:} \quad -i_1 < y_f < -i_2$$

With this result, the conditions for capture and escape are clear. From our previous discussion:

$$\begin{aligned} \text{Escape:} \quad & -i_2 < y_f < 0 \\ \text{Capture:} \quad & -i_1 < y_f < -i_2 \end{aligned} \tag{81}$$

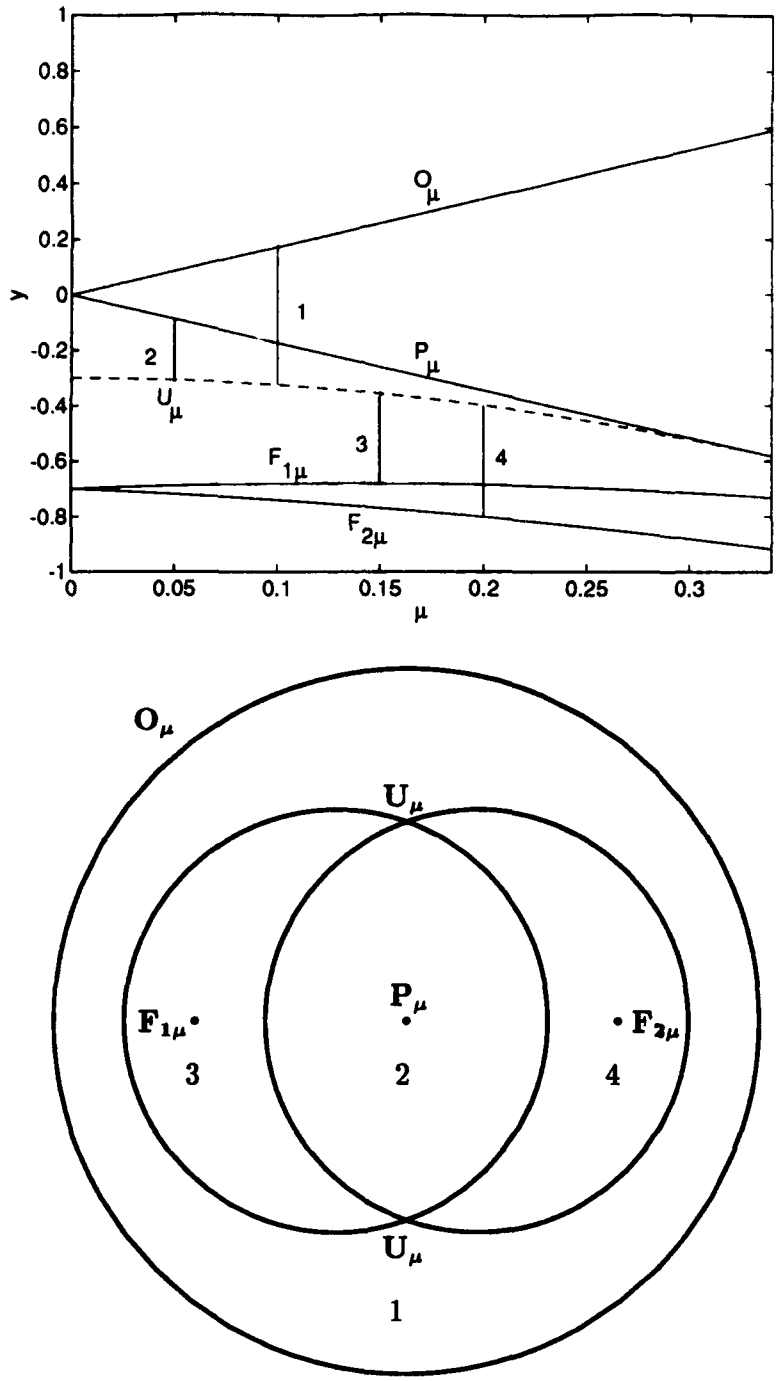

Figure 17. Momentum Sphere at the End of Spinup. The domains of all four stable centers are shown in the μy plane (top) and on a schematic of the momentum sphere (bottom). Note that the sphere is symmetric at $\mu = 0$.

A very simple expression for the criteria leading to the *possibility* of resonance capture for a slightly asymmetric, balanced gyrostat is developed in reference (6). In the present analysis, no simple expression can be found. The existence of the imbalance precludes the possibility of any set of simple rules. However, more general criteria analogous to those established in that study may be stated. First, resonance capture may occur if

$$\mu_0 > \mu_{sn} > \mu_{pf}$$
$$y_{\mathbf{F}_{2\mu}} < y_0 < y_{sn}. \tag{82}$$

These μy coordinates, illustrated in Figure 18, are defined as follows:

$\mu_0 \equiv$ initial value of μ which may lead to capture

$\mu_{sn} \equiv$ value of μ at which the saddle-node bifurcation occurs

$\mu_{pf} \equiv$ value of μ at which the pitchfork bifurcation occurs

$y_0 \equiv$ initial system energy which may lead to capture

$y_{sn} \equiv$ system energy at which the saddle-node bifurcation occurs

$y_{\mathbf{F}_{2\mu}} \equiv$ energy associated with $\mathbf{F}_{2\mu}$ at $\mu = \mu_0$.

Recall that μ_{pf} was determined analytically in the previous chapter. It is restated here:

$$\mu_{pf} = \left\{ \left[\frac{\alpha_1(i_1 - 1)}{i_1 - i_2} \right]^2 + \left[\frac{\alpha_3}{i_2} \right]^2 \right\}^{-1/2}. \tag{83}$$

On the other hand, μ_{sn} can only be found numerically from the geometric parameters of the spacecraft.

The second condition which leads to the possibility of capture is related to when significant nutation growth begins. In this case, it starts when $\mu \approx \mu_{sn}$. The first

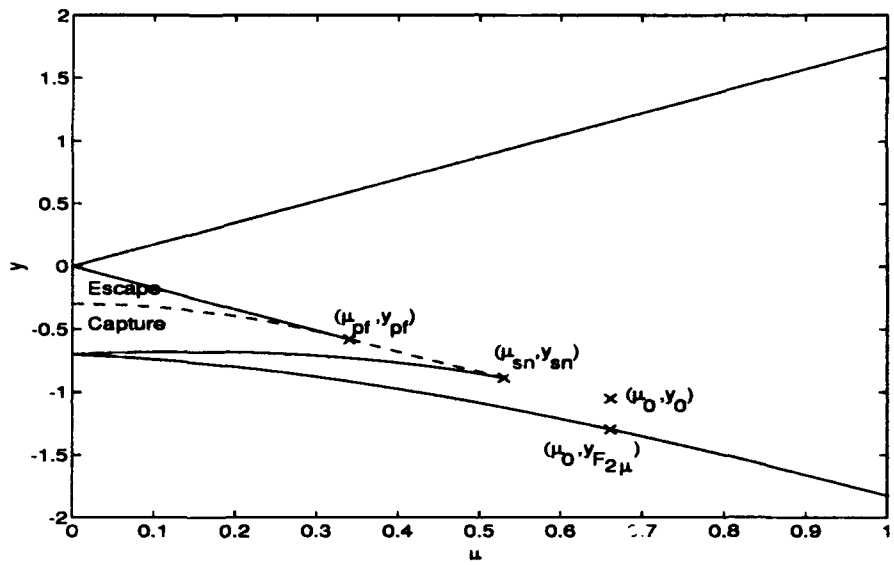

Figure 18. Conditions Which May Lead to Capture. At $\mu = 0$, trajectories terminating above the dotted line have escaped, and those below the dotted line are captured. These are projected onto the μy plane introduced in Figure 6.

condition expressed above is the more general analogy of Equation (10) in reference (6), and the second is the counterpart of Equation (11).

5.2.1 Effects of the Motor Torque ε. Given these conditions, we now illustrate capture and escape using the μy plane. As previous authors have done, we first show how the magnitude of the despin motor torque affects the likelihood of capture. It has been shown that for prolate spinup, higher-torque motors improve the chance for escape. The first example shows two gyrostats with identical geometric configurations, but different-sized motors.

For the original Oblate-Prolate example from the previous chapter, Figure 19 shows a captured and an escaped trajectory. Note that the all-spun initial condition, identical for both spacecraft, is denoted in the figure by "IC" ($t = 0$) and that the spinup maneuver concludes when $\mu = 0$, as previously defined. Hence, spinup in the μy plane proceeds *from right to left.* By comparing y_f in each spinup trajectory to the criteria for capture and escape given in Equations (81), we see that the higher motor torque does indeed prove to be advantageous. Figure 19 also shows how nutation angle η varies over time for both cases. This parameter is defined as the angle between the rotor spin axis and the angular momentum vector. Mathematically,

$$\eta = \cos^{-1}\left(\frac{\mathbf{m}^T\boldsymbol{\alpha}}{m}\right) = \cos^{-1}(x_1\alpha_1 + x_3\alpha_3).$$

It is clear that the nutation angle of the escaped spacecraft is smaller than that of the captured one. Also, the maneuver takes less time with the larger torque.

From this example, it is clear why Kinsey based the remedy for resonance capture on increasing the motor torque. Figures 20 and 21 show one of the captured and escaped trajectories along with their respective nutation angles analyzed in (13, 14). From the bottom of Figure 20, it is interesting to note that this "captured" trajectory is actually one that has barely escaped! Again, this becomes apparent when comparing y_f to the criteria in Equations (81). This example illustrates the

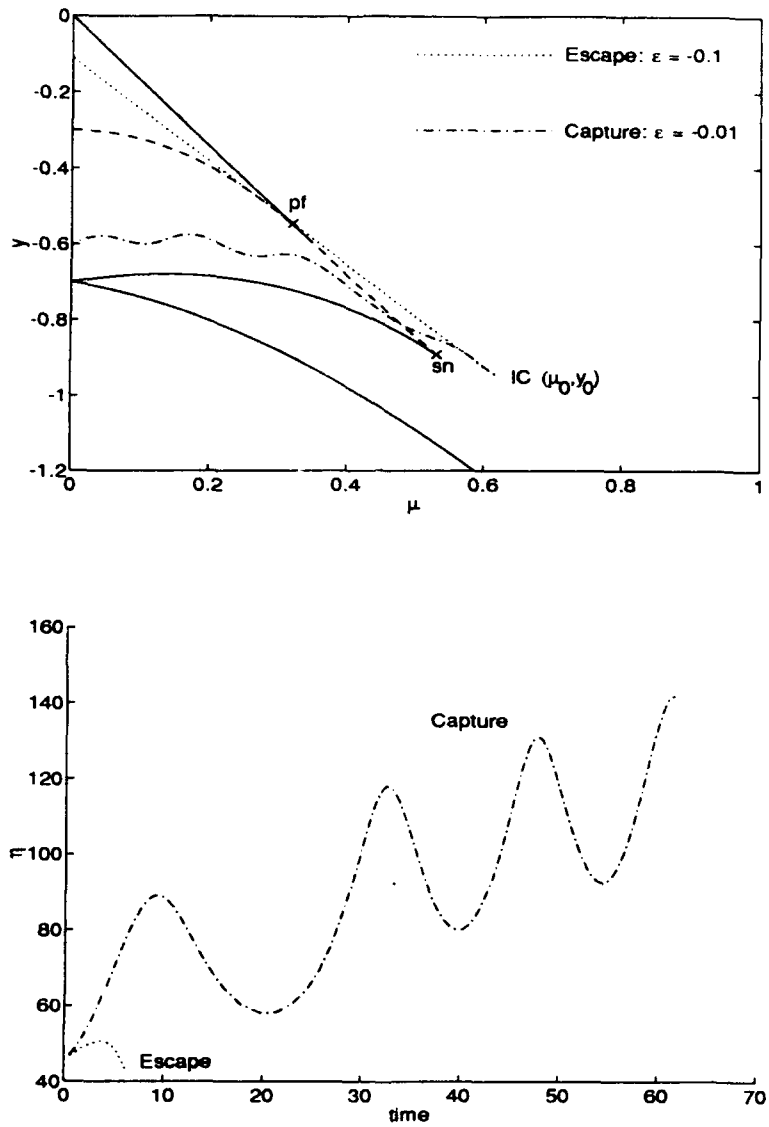

Figure 19. Capture and Escape of Two Geometrically Identical Spacecraft with Different Motor Torques. The nutation angle η is measured in degrees. IC: $\mu_0 = 0.6060, y_0 = -0.9434$. $i_1 = 0.7, i_2 = 0.3, i_3 = 0.8, \alpha_1 = 0.5, \alpha_3 = 0.866$

difference between Kinsey's and Hall's definitions of resonance capture. According to Hall, even though Kinsey's captured spacecraft has a cone angle near 90°, its final energy state is actually within the domain of the dual-spin center very close to the separatrix which segregates it from that of the flat-spin. The fundamental difference lies in the fact that Kinsey's interpretation is based on the spacecraft's *behavior* whereas Hall's is dependent upon quantitative criteria. From a practical standpoint, Kinsey's definition is more useful to the spacecraft designer although its drawback is its lack of definitive capture criteria. On the other hand, Hall's is easier to see mathematically. It is therefore necessary to redefine resonance capture to encompass both interpretations. To this end, we offer the following terminology:

> A dual-spin spacecraft is **effectively captured** when its final cone angle prevents the accomplishment of its intended mission; otherwise, it has escaped.
>
> A dual-spin spacecraft is **strictly captured** when the criteria for capture as stated in Equations (81) are satisfied; otherwise, is has escaped.

Clearly, Hall's definition is equivalent to the latter case. The former, on the other hand, is not an exact restatement of Kinsey's. It is more utilitarian and "open-ended" in the sense that its satisfaction depends on each specific case. In the remainder of this study, we continue to abide by Hall's interpretation.

Having illustrated resonance capture in the μy plane, it becomes necessary to highlight an important characteristic which distinguishes our spinup model from the one analyzed in reference (6). Although Hall's study shows that a trajectory of the perturbed system must cross an instantaneous separatrix of the unperturbed system for capture of the balanced asymmetric gyrostat, *this is not necessarily true for our particular model.* By looking at the μy plane of a typical Oblate-Prolate gyrostat (e.g. Figure 19), we see that the trajectories of the flat-spin equilibria ($\mathbf{F}_{1\mu}$ and $\mathbf{F}_{2\mu}$) form a "pocket" when $\mu < \mu_m$. Spinup trajectories which lie within this region have not crossed a dashed line in the μy plane, but they continue to oscillate about one of the flat-spin equilibria and are therefore captured. Taking this observation one step

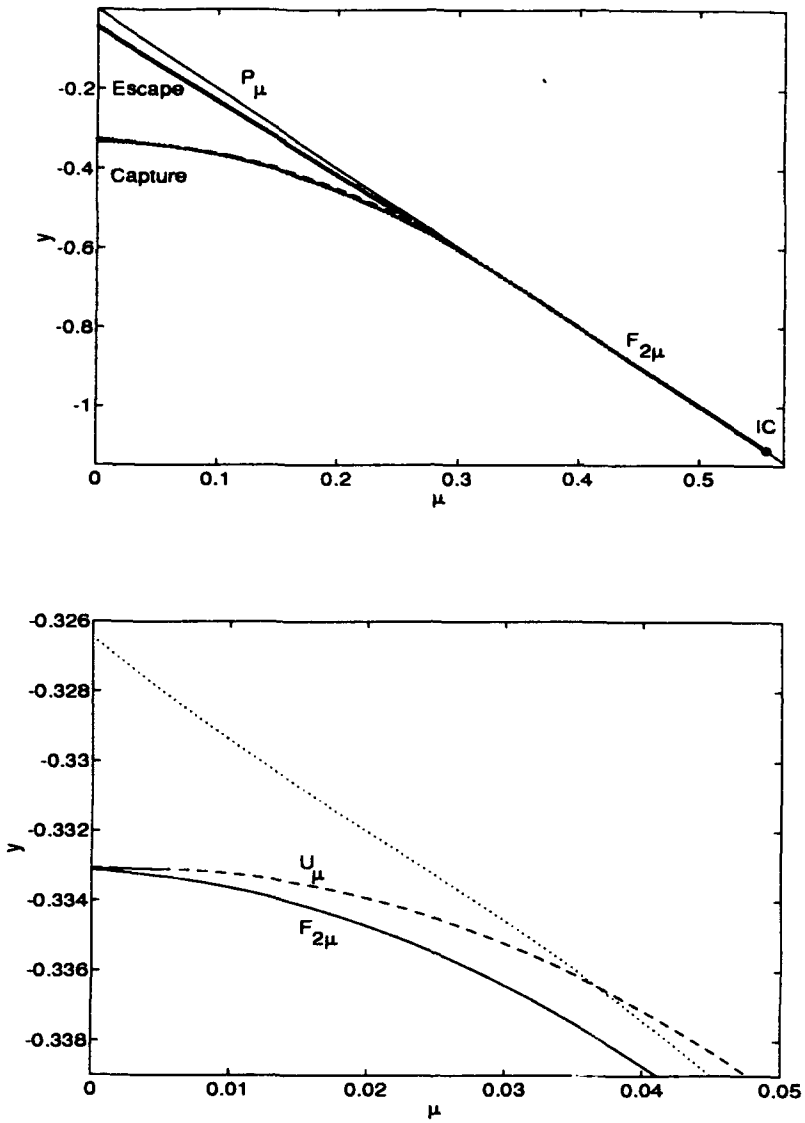

Figure 20. Capture and Escape of Two Identical Spacecraft Having Kinsey's Geometric Parameters and Different Motor Torques. Capture: $K = 0.4$. Escape: $K = 1.2$. These are shown by the dark lines in the upper plot. The lower plot is a closeup of the "captured" trajectory toward the conclusion of spinup.

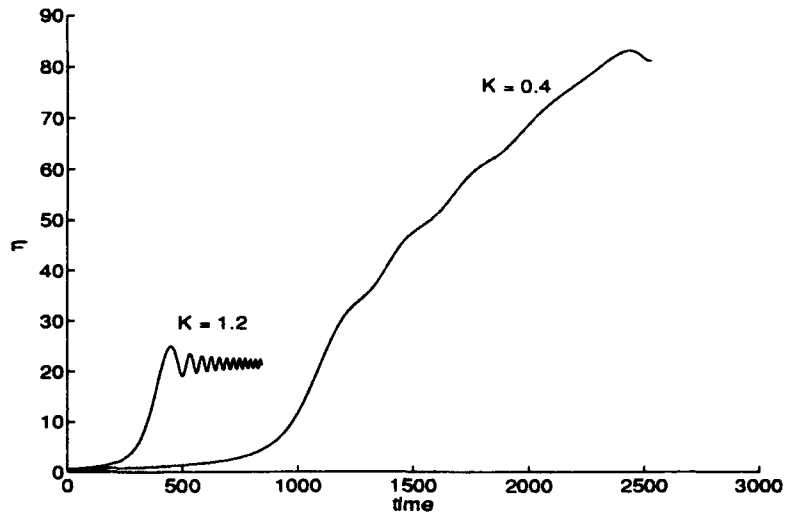

Figure 21. Nutation Angles for Capture and Escape of Kinsey's Gyrostat. η is expressed in degrees.

further, it can be shown that a separatrix-crossing will in fact result in *escape* for initial conditions at which $\mu > \mu_{pf}$. In these instances, prolate spinup begins near either of the flat-spin centers since $\mathbf{P}_\mu$ is either unstable or non-existent (see Figures 4, 5). The pitchfork bifurcation marks the transformation of $\mathbf{P}_\mu$ from a saddle to a center, so the trajectory which oscillates initially about either $\mathbf{F}_{1\mu}$ or $\mathbf{F}_{2\mu}$ must cross a separatrix to escape.

5.2.2 Effects of Initial Phase. We have seen that one way to avoid capture during spinup is to use a motor with a large torque. The cost of this alternative is the greater size and weight associated with a more powerful motor. Due to physical constraints, this may not be a viable solution. Reference (6) shows that a larger motor torque is not always necessary because the initial conditions (i.e. the initial position on the momentum sphere) also affect the likelihood of capture. These features *cannot* always be seen on the μy plane due to its limited two-dimensional scope. It is clear from this plane that, for a given motor torque, ε, at which capture

is known to occur, one may choose a different initial μy coordinate to avoid this problem (see Figure 22). This is not always necessary. We show here that for a given motor torque ε and initial conditions μ and y at which capture occurs, escape may still be possible (see Figure 23). This is achieved not with a larger spinup motor nor by selecting new μy initial conditions, but by finding a new starting point *having the same energy, but different initial* angular phase *on the momentum sphere.*

The angular phase, ϕ, is only defined when $\varepsilon = 0$ because it represents the position of the angular momentum vector on a given closed (constant) energy curve. Hall (5:§5.6.1) defined this parameter in terms of elliptic functions:

$$\phi_H = \frac{u}{4K}$$

where u is the time-like argument of the elliptic functions in the unperturbed solutions and $K = K(k)$ is an elliptic integral of the first kind. The subscript H is added here only to distinguish Hall's definition of ϕ from our own. We show below that both forms are actually equivalent. Recall from Chapter 3 the impracticality of obtaining explicit closed-form solutions to the unperturbed system. Although we are able to show that in theory such a solution can be found, actually doing so is quite cumbersome. For this reason, all results in this study are obtained from numerical integration of the equations of motion. The same is true for the determination of the phase. After we show how ϕ is defined for our analysis, we will prove that it is completely equivalent to ϕ_H.

Recall that μ defines a specific momentum sphere, y denotes a particular constant energy curve of the unperturbed motion, and (x_1, x_2, x_3) pinpoint the exact position of the system angular momentum on this curve. When $\varepsilon = 0$, kinetic energy is conserved so that the system angular momentum vector is constrained to "orbit" around this path. An example, projected onto the x_2x_3 plane, is shown in Figure 24. The period of this orbit, denoted here as t_f, is constant. Suppose we choose

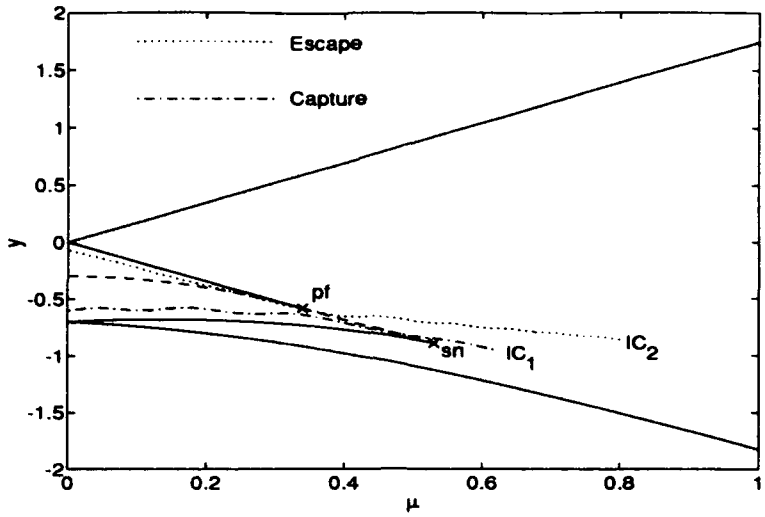

Figure 22. Capture and Escape Resulting From Two Different Initial Values of μ and y. In both cases, $\varepsilon = -0.01$. IC_1: $\mu_0 = 0.6060, y_0 = -0.9434$. IC_2: $\mu_0 = 0.8, y_0 = -0.8540$. $i_1 = 0.7, i_2 = 0.3, i_3 = 0.8, \alpha_1 = 0.5, \alpha_3 = 0.866$

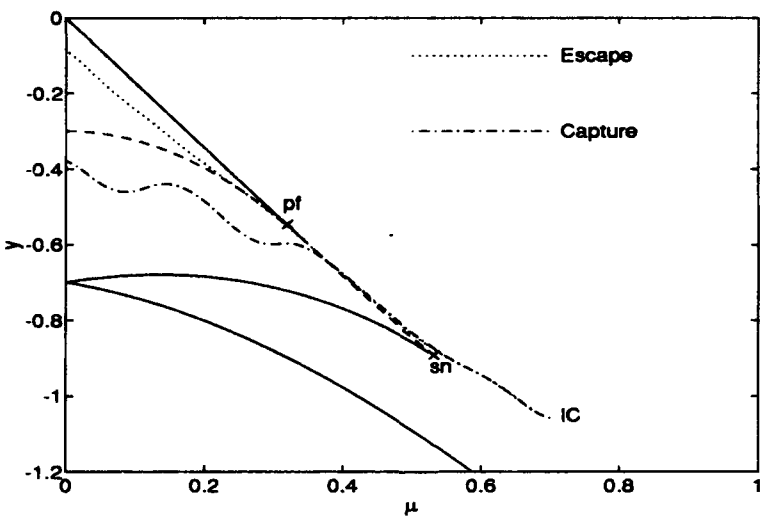

Figure 23. Capture and Escape Resulting From Two Different Initial Positions on the Momentum Sphere at the Same Values of μ and y. In both cases ($\varepsilon = -0.01$). IC: $\mu_0 = 0.7, y_0 = -1.0576$. $i_1 = 0.7, i_2 = 0.3, i_3 = 0.8, \alpha_1 = 0.5, \alpha_3 = 0.866$

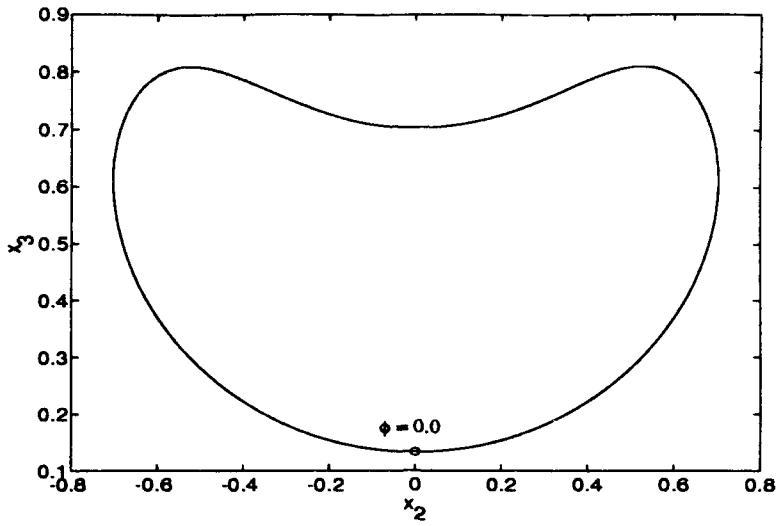

Figure 24. Constant Energy Curve Defined By $\mu = 0.7$ and $y = -1.0576$ Projected in the x_2x_3 Plane. $i_1 = 0.7, i_2 = 0.3, i_3 = 0.8, \alpha_1 = 0.5, \alpha_3 = 0.866, \varepsilon = 0$

a point on this curve to be the reference from which to define an initial time t_0. By doing so, the position of the angular momentum vector at any arbitrary time t, where $t_0 \leq t \leq t_f$, can be found. We define this position parameter as ϕ and its initial value at t_0 as ϕ_0. From this discussion, it is clear that ϕ must be a function of t. Specifically, ϕ is equal to t normalized with respect to the orbital period, i.e.

$$\phi = \frac{t}{t_f} + \phi_0. \tag{84}$$

If we let $t_0 = \phi_0 = 0$, then $0 \leq \phi \leq 1$.

Now we establish its equivalence to the angular phase defined in (5). In his study, the (unnormalized) parameter denoting the position of the angular momentum vector is given by $u = \lambda t + u_0$. Note that the period of the elliptic function solution is $4K$. Hence, $4K = \lambda t_f$. We now rearrange these expressions in terms of t and t_f,

respectively:

$$t = \frac{u}{\lambda}$$
$$t_f = \frac{4K}{\lambda}.$$

Since Hall's angular phase parameter is given as $\phi_H = u/4K$, it is clear that $\phi_H = t/t_f$. Hence, both definitions of ϕ are identical ($\phi \equiv \phi_H$). With the advent of this term, we have effectively reduced the number of variables which define the system angular momentum from four (x_1, x_2, x_3, μ) to three (ϕ, μ, y).

We now show how resonance capture can be avoided by varying the *phase of the initial condition*, $\phi(0)$, for a particular value of μ and y. Assume that the curve in Figure 24 is the set of all possible initial conditions for the system angular momentum vector where $\mu = 0.7$ and $y = -1.0576$. This trajectory lies within the domain of $\mathbf{F}_{2\mu}$ and represents the unperturbed state of the system just prior to spinup. As $\phi(0)$ undergoes a complete cycle, it follows the curve in a counter-clockwise manner starting and ending at the point denoted by o. Now, assume the motor torque is fixed at $\varepsilon = -0.01$ so that the system is slightly perturbed. In this case, the angular momentum vector is no longer constrained to this curve. Its path may take it away from $\mathbf{F}_{2\mu}$ into $\mathbf{P}_\mu$'s domain (escape), or it may continue to oscillate about $\mathbf{F}_{2\mu}$ (capture). The path that it follows will depend on the point on the initial closed curve at which it was situated the moment the spinup torque was applied.

In order to determine the effect of these points on the final outcome of spinup, the initial conditions defined by $\phi(0)$ are allowed to vary along this curve, and the final value of y during spinup is calculated at each initial condition. The resulting final energies plotted against their respective initial conditions are shown in Figure 25. Application of Equations (81) allows us to determine which final energy states, y_f, result in a captured spacecraft. Thus, escape occurs if the initial phase lies within the ranges for which $y_f > -i_2$. The parts of the constant energy curve corresponding

to these "safe zones" are shown in Figure 26. This analysis is also useful to show that, for prolate spinup, a larger motor torque promises greater opportunity for escape. This is illustrated in Figure 27.

It is important to note that only *one point* on the constant energy curve corresponds to the all-spun initial condition. Thus, if the all-spun spacecraft inevitably leads to resonance capture, the spinup maneuver may need to be initiated with a nonzero relative angular velocity between the rotor and platform ($\omega_s \neq 0$).

5.3 Probability of Capture

We can now extend this result into something which Henrard (9) defined as the probability of capture, denoted in this study as P_c. Here we find another advantage of the energy-based definition of capture: the determination of P_c is very straightforward because more precise, albeit less conservative criteria are given by Equations (81). Once the data used to create Figure 25 is available, we know from these criteria at which initial phases the system has been captured. P_c is then simply the sum of the ranges of $\phi(0)$ for which the final energy state $y_f < -i_2$. For example, the initial energy curve in Figure 26 has a probability of capture of $P_c = 0.9064$.

Knowing the probability of capture for a given initial condition would be of particular interest to the spacecraft designer, whose obvious goal would be to commence the spinup maneuver at an initial condition that is both feasible for the spacecraft and that has the least likelihood of resulting in capture. It therefore follows that, given all relevant parameters, the preceding analysis can be applied to find the most desirable initial condition. Up until now, the probability of capture has been found for a single constant energy curve on a particular momentum sphere (a particular value of μ). Our next step is to extend this analysis to all possible constant energy curves on a given sphere. This corresponds to finding P_c at different points along a particular vertical "slice" of the μy plane. Finally, this method is extended over the

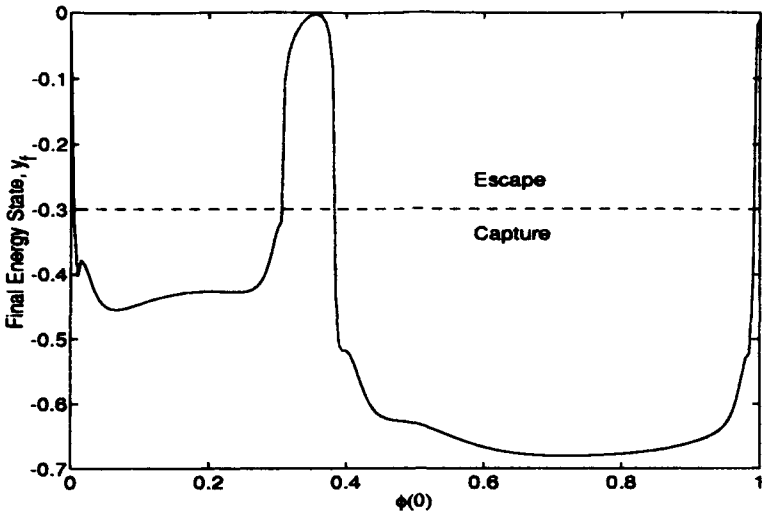

Figure 25. Capture and Escape for Initial Conditions Along the Constant Energy Curve Defined By $\mu = 0.7, y = -1.0576$, and $\varepsilon = -0.01$. $i_1 = 0.7, i_2 = 0.3, i_3 = 0.8, \alpha_1 = 0.5, \alpha_3 = 0.866$

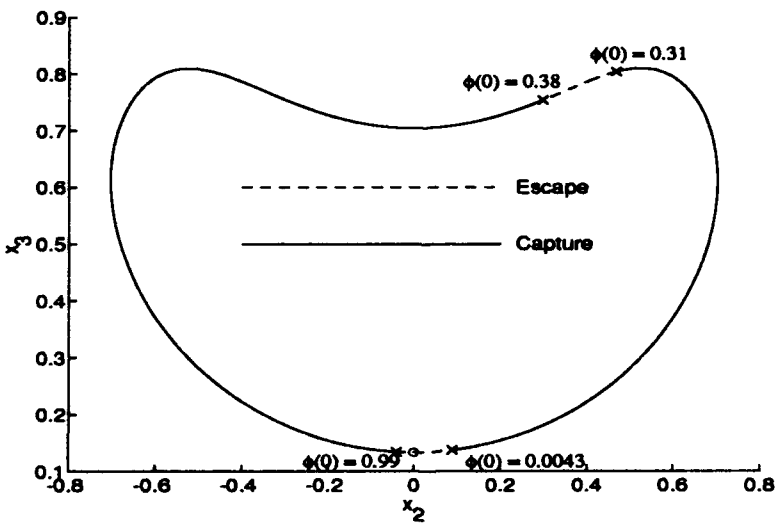

Figure 26. Sections of the Constant Energy Curve Corresponding to Capture and Escape. $\mu = 0.7, y = -1.0576, i_1 = 0.7, i_2 = 0.3, i_3 = 0.8, \alpha_1 = 0.5, \alpha_3 = 0.866, \varepsilon = -0.01$

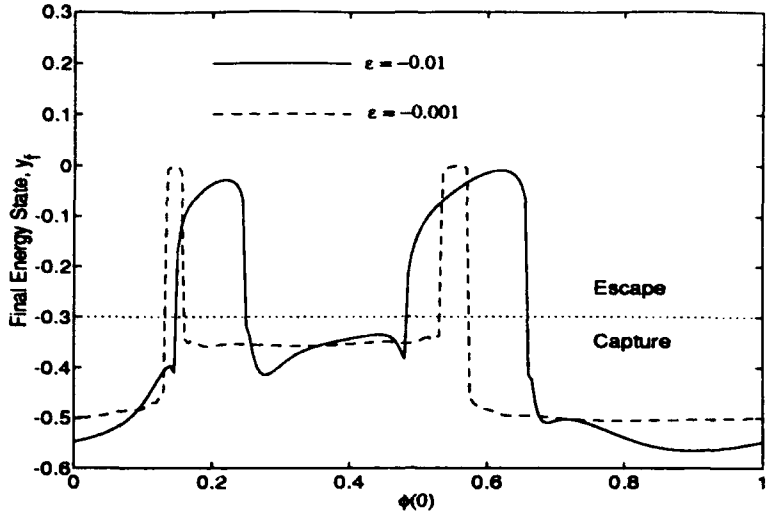

Figure 27. Capture and Escape for Initial Conditions Along the Constant Energy Curve Defined By $\mu = 0.7, y = -0.8638$, and the Given Torques. $i_1 = 0.7, i_2 = 0.3, i_3 = 0.8, \alpha_1 = 0.5, \alpha_3 = 0.866$

entire plot. In effect, we are determining the probabilities of capture for a "grid" of initial conditions on the μy plane.

5.3.1 Probabilities of Capture Across a Single Momentum Sphere. The Oblate-Prolate μy plane can be divided into three distinct regions depending on the number of equilibria in each. This is shown in Figures 28 – 31. Region A has six equilibria and four subregions (1 - 4), Region B has four equilibria and three subregions (5 - 7), and Region C has two equilibria and no subregions. Recall our previous discussion of the "domain" of a stable equilibrium point on the momentum sphere. Each subregion corresponds to one of these domains. Although each domain appears to overlap in the μy plane (tops of Figures 29 and 30), they are actually distinct when viewed on the surface of the momentum sphere (bottoms of same figures). Recall that the inability to view the phase angle ϕ was one limitation of

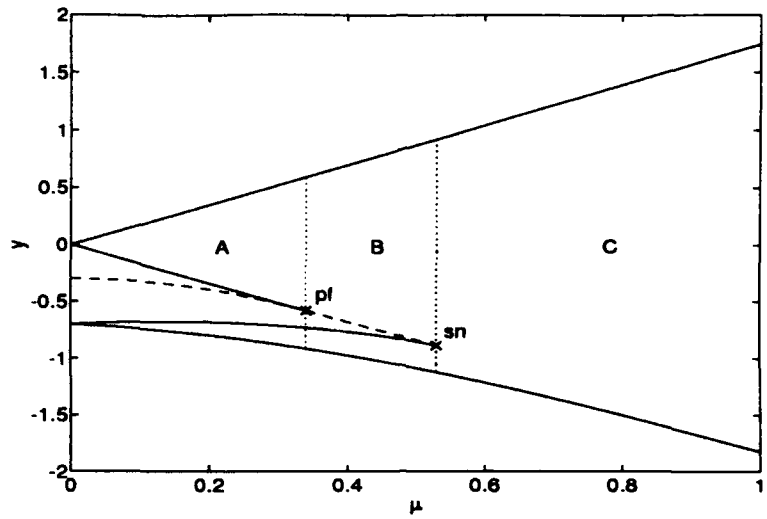

Figure 28. Three Distinct Regions of the μy Plane. $i_1 = 0.7, i_2 = 0.3, i_3 = 0.8, \alpha_1 = 0.5, \alpha_3 = 0.866$

the μy plane; here is another handicap. The determination of P_c in each region is discussed individually.

5.3.1.1 Region C. First we examine the probabilities of capture for initial conditions in Region C. P_c for a single point in this region has already been determined above. We now perform the same analysis at the same initial value of μ ($= 0.7$ in our example) but over the entire range of y_0. Recall that each initial energy is a closed curve on the surface of the sphere surrounding the stable equilibria. As can be seen from Figures 5 and 31, there are no separate domains in this region. Hence, y_0 can take any value between the energies associated with $\mathbf{O}_\mu$ and $\mathbf{P}_\mu$. By plotting P_c against this range of initial energies, we obtain Figure 32, which has some interesting properties. This Figure shows four distinct areas of interest, labelled by the corresponding Roman Numerals. Note that Area II has been divided into two subareas.

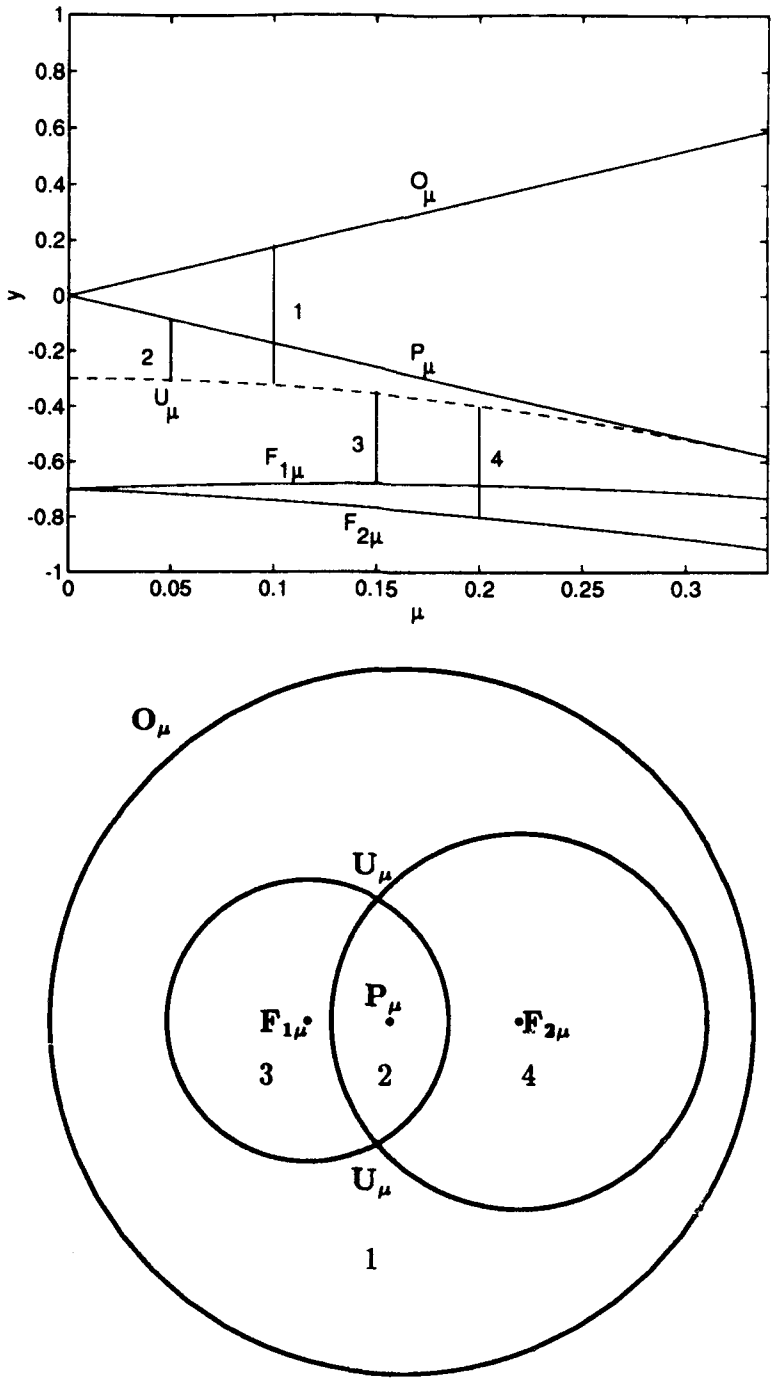

Figure 29. Region A. The domains of all four stable centers are shown in the μy plane (top) and on a schematic of a typical momentum sphere from this region (bottom).

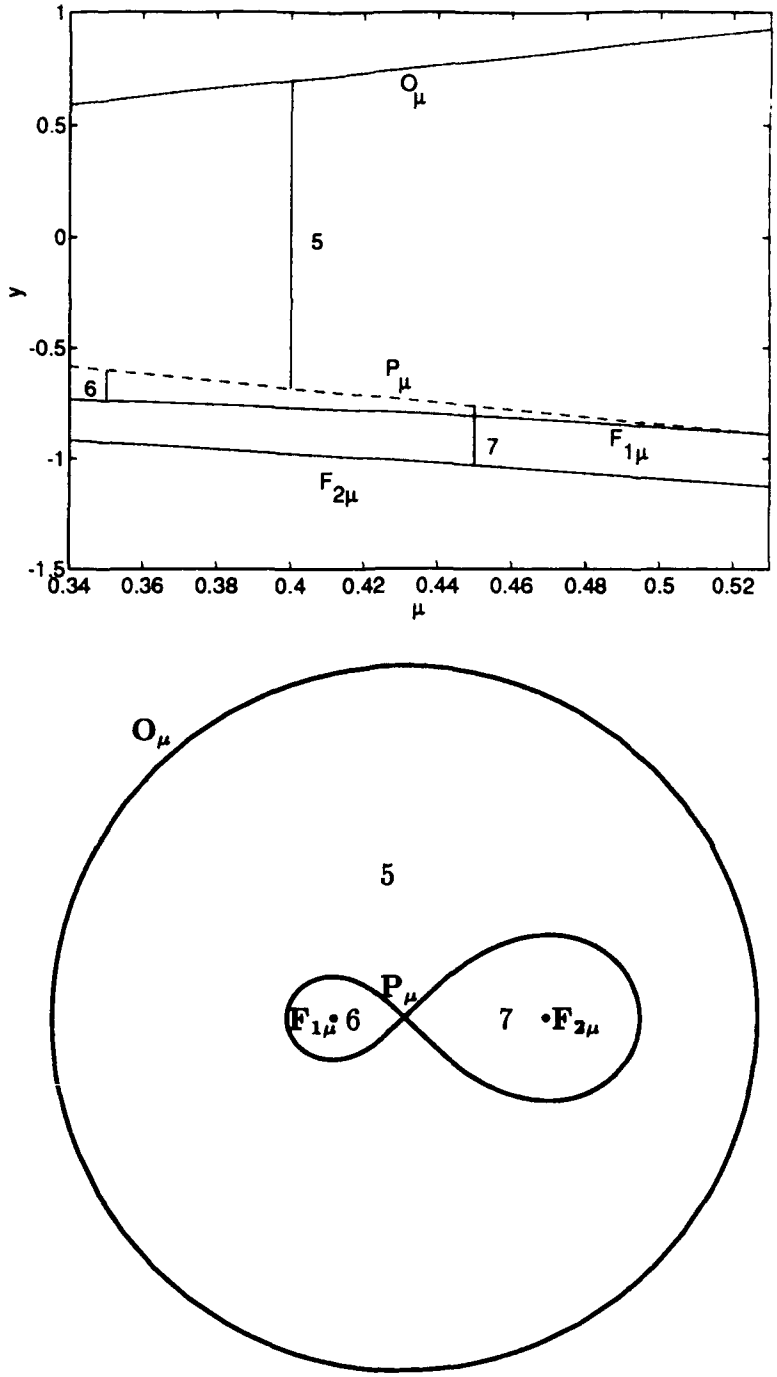

Figure 30. Region B. The domains of all three stable centers are shown in the μy plane (top) and on a schematic of a typical momentum sphere from this region (bottom).

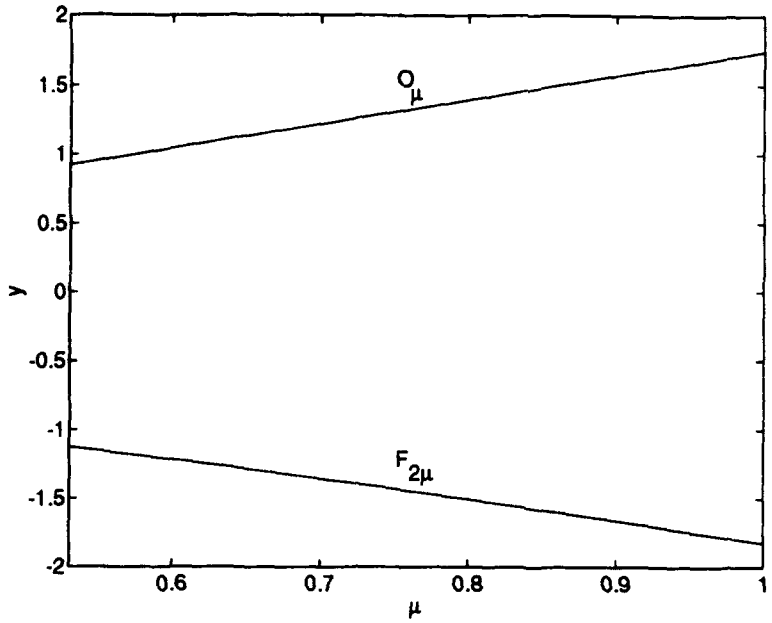

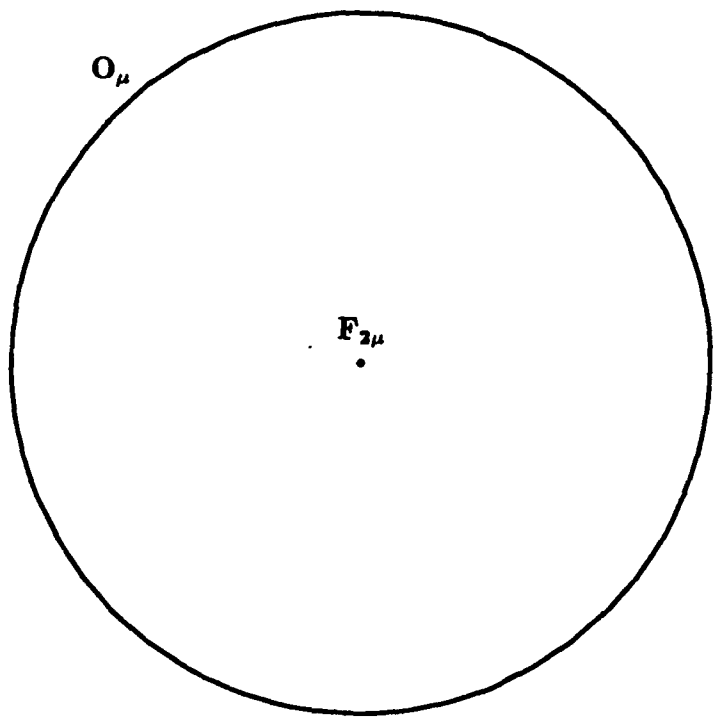

Figure 31. Region C. The domain of both stable centers is shown in the μy plane (top) and on a schematic of a typical momentum sphere from this region (bottom).

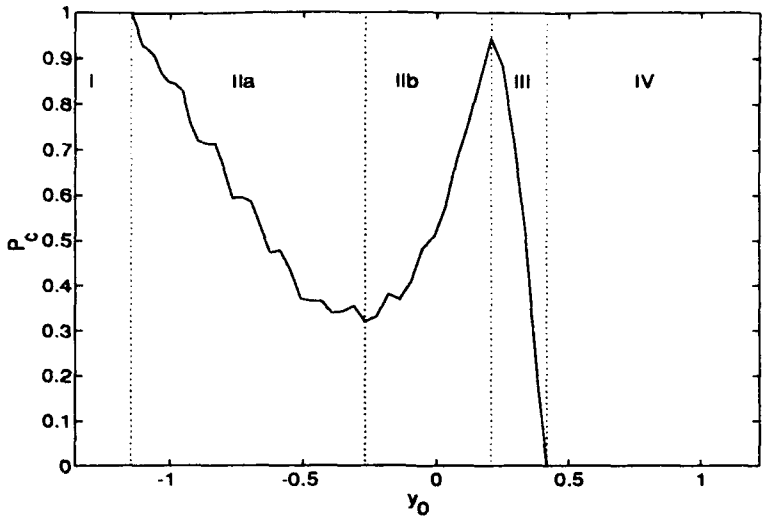

Figure 32. Probability of Capture Versus Initial Energy at $\mu_0 = 0.7$. $i_1 = 0.7, i_2 = 0.3, i_3 = 0.8, \alpha_1 = 0.5, \alpha_3 = 0.866, \varepsilon = -0.01$

Area I is a region of *guaranteed capture*. For a gyrostat having motor torque $\varepsilon = -0.01$, $\mu_0 = 0.7$, and initial energies within the range $-1.50 \leq y_0 \leq -1.15$, all initial conditions for spinup lead to capture. On the other hand, Area IV (denoted in this example by $0.42 \leq y_0 \leq 1.22$) contains all initial conditions for *guaranteed escape*. Here capture will never occur. Unlike the other two, Areas II and III have diverse probabilities. If spinup is initiated in either of these locations, capture may or may occur. In Area II, P_c is a rough parabolic function of y_0. Somewhere within, there exists an initial energy for which P_c is a local minimum (in this case at $y_0 = -0.27$).

As an interesting aside, we use this technique to compare the overall probabilities of capture for two identical spacecraft having different motor torques. By superimposing a plot for which $\varepsilon = -0.001$ onto Figure 32, the composite plot of Figure 33 results. From this picture, we can see that spacecraft which undergo prolate spinup (low values of y_0) have a better chance to escape if a larger motor is

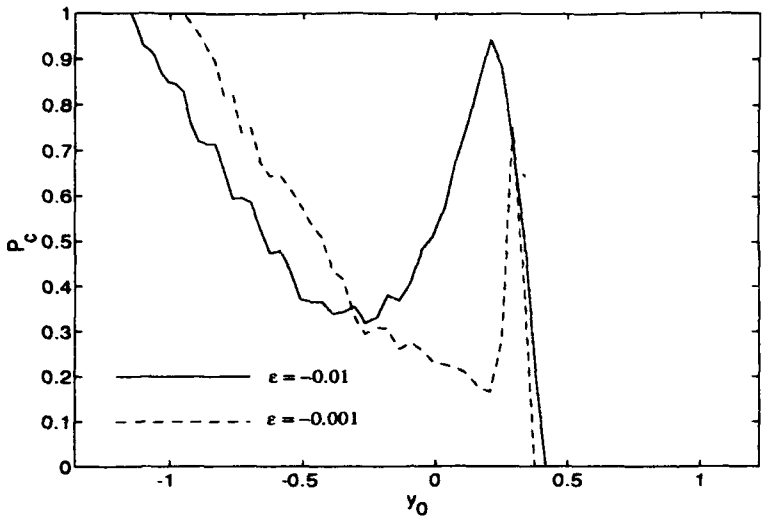

Figure 33. Probabilities of Capture of Two Identical Spacecraft Having Different Motor Torques. $\mu_0 = 0.7$. $i_1 = 0.7, i_2 = 0.3, i_3 = 0.8, \alpha_1 = 0.5, \alpha_3 = 0.866$

used. This has been documented throughout the literature as well as earlier in this chapter. If, however, oblate spinup is desired (higher values of y_0), *a smaller motor torque would best serve this purpose.*

5.3.1.2 Region B. Estimation of P_c for initial conditions in this region involves a little more work. Because there are three domains, we need to repeat this procedure three times. Our goal is to determine the probabilities of capture at initial conditions that lie within each domain, thereby obtaining for each case a plot similar to Figure 32. Note that in Region C, no separatrices delimit the domains of the oblate and prolate equilibrium points; hence, the entire region is a single domain. In Region B (as well as in A), all of the stable centers are bounded from one another by the separatrices (see Figures 3, 4, 29, and 30). The range of initial energy curves in each domain, when viewed on the momentum sphere, blankets the entire domain from the stable center up to and including the separatrix.

The probabilities of capture for initial conditions in each domain are shown in Figures 34 – 36. Note that P_c is unity throughout most of the flat-spin domains. Since these grow during spinup, trajectories which begin in orbit near the flat-spin centers will continue to circle these equilibria at motor shut-off. Initial conditions very close to the separatrices, however, may be ensnared by $\mathbf{P}_\mu$ whose domain is born when $\mu = \mu_{pf}$. This explains the sudden drop in P_c for initial conditions near the upper limit of y_0. Thus, for the most part, the flat-spin domains are analogous to Area I as previously described for Region C. On the other hand, the domain of the oblate center, $\mathbf{O}_\mu$, has the same characteristics of Areas II, III, and IV. This can be seen by comparing Figure 34 to Figure 32.

5.3.1.3 Region A. Region A has four domains. The same procedure is followed here as above to determine the probabilities of capture. The plots for each domain are shown in Figures 37 – 40. Again, we see that the domains of $\mathbf{F}_{1\mu}$ and $\mathbf{F}_{2\mu}$ predominately exhibit Area I behavior, but this time with IIa as well. Of greater interest are those of $\mathbf{O}_\mu$ and $\mathbf{P}_\mu$. Within the domain of $\mathbf{O}_\mu$, the region of negative slope characteristic of Area IIa is truncated, leaving only the rapid ascent and peak of IIb. The equally dramatic drop and the region of guaranteed escape which characterize Areas III and IV remain qualitatively unchanged. The spinup behavior for initial conditions within the domain of $\mathbf{P}_\mu$, heretofore nonexistent in the analyses of Regions B and C, is even more intriguing. In this domain, the probabilities of capture are zero throughout. The reason for this interesting phenomenon is quite simple. As do the flat-spin domains, this one grows with time. Hence, trajectories which start here are likely to remain in orbit about the prolate center.

5.3.2 Probabilities of Capture Throughout the μy Plane. Now that we have seen how the overall probabilities of capture vary on the three distinctive momentum spheres which characterize the Oblate-Prolate gyrostat, the results obtained above can be transcribed onto a single μy plane. The probabilities of capture for initial

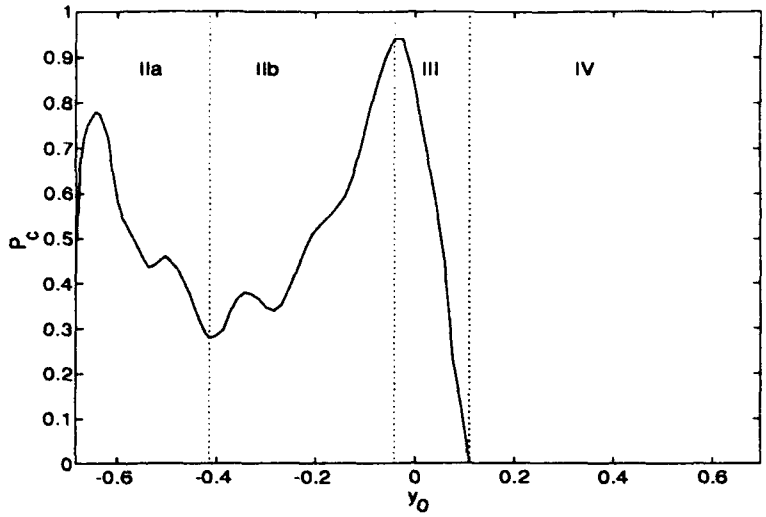

Figure 34. Probabilities of Capture in the Domain of $\mathbf{O}_\mu$ ($\varepsilon = -0.01$ and $\mu = 0.4$). $i_1 = 0.7, i_2 = 0.3, i_3 = 0.8, \alpha_1 = 0.5, \alpha_3 = 0.866$

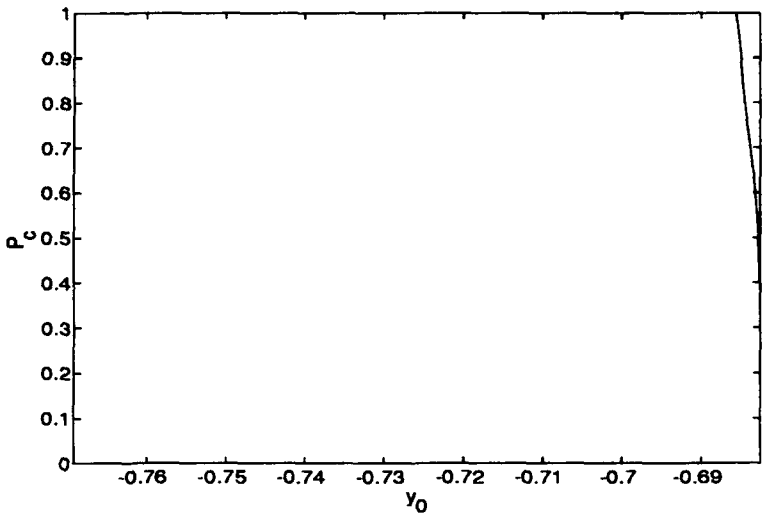

Figure 35. Probabilities of Capture in the Domain of $\mathbf{F}_{1\mu}$ ($\varepsilon = -0.01$ and $\mu = 0.4$). $i_1 = 0.7, i_2 = 0.3, i_3 = 0.8, \alpha_1 = 0.5, \alpha_3 = 0.866$

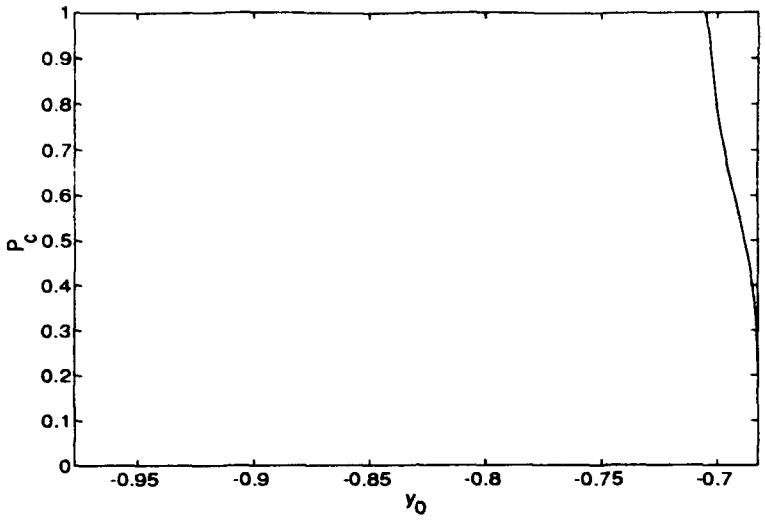

Figure 36. Probabilities of Capture in the Domain of $\mathbf{F}_{2\mu}$ ($\epsilon = -0.01$ and $\mu = 0.4$). $i_1 = 0.7, i_2 = 0.3, i_3 = 0.8, \alpha_1 = 0.5, \alpha_3 = 0.866$

conditions within any single stable equilibrium domain – as well as any *combination* of these domains – can be shown over the entire range of μ. The major areas which depict important trends in P_c, similar to those described in Figure 32, are marked on this plot to locate favorable and unfavorable initial conditions. It must be emphasized, however, that this is only useful if combinations of equilibria whose domains do not overlap on the μy plane are considered, such as $\mathbf{F}_{1\mu}$ – $\mathbf{P}_\mu$ or $\mathbf{F}_{2\mu}$ – $\mathbf{O}_\mu$. This latter example is shown in Figure 41. It depicts the probabilities of capture for initial conditions in either of their domains for all values of μ. Each major area has been labeled. These correspond to Areas I – IV, which have been previously described. For comparison, the μy plane of a different Oblate-Prolate dual-spinner is shown in Figure 42. This gyrostat is more asymmetric and better balanced than the one analyzed in detail above. Comparison of both plots provides us with a better idea of how spacecraft geometry affects the overall likelihood of capture.

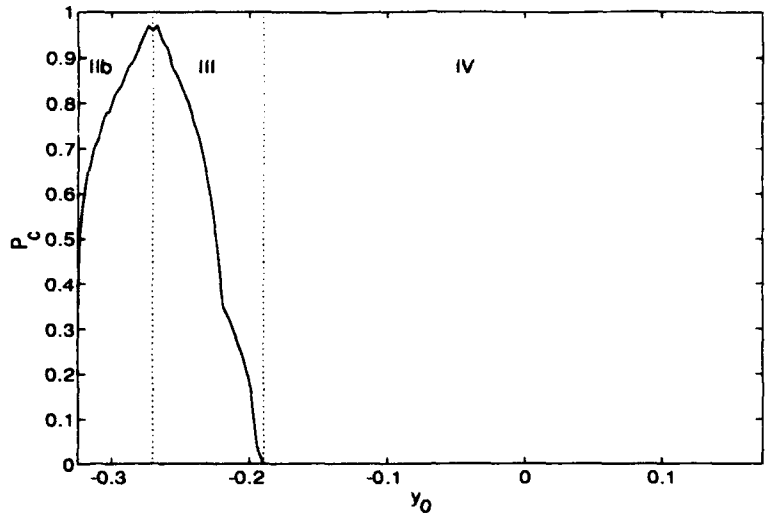

Figure 37. Probabilities of Capture in the Domain of $\mathbf{O}_\mu$ ($\varepsilon = -0.01$ and $\mu = 0.1$). $i_1 = 0.7, i_2 = 0.3, i_3 = 0.8, \alpha_1 = 0.5, \alpha_3 = 0.866$

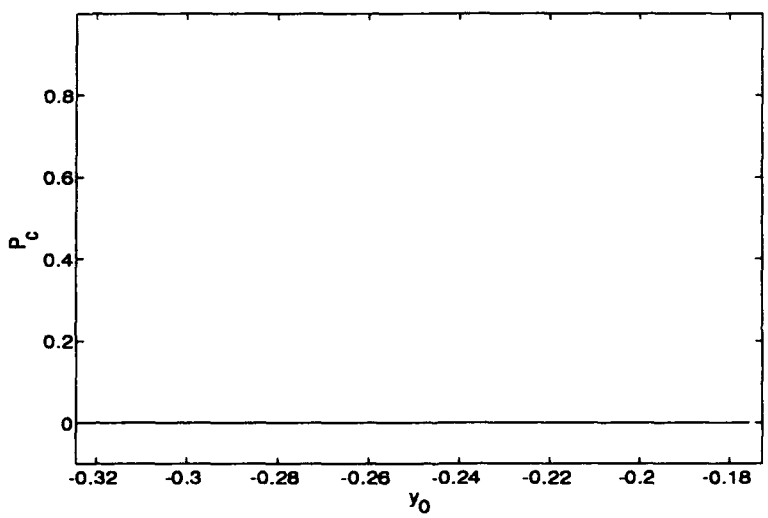

Figure 38. Probabilities of Capture in the Domain of $\mathbf{P}_\mu$ ($\varepsilon = -0.01$ and $\mu = 0.1$). $i_1 = 0.7, i_2 = 0.3, i_3 = 0.8, \alpha_1 = 0.5, \alpha_3 = 0.866$

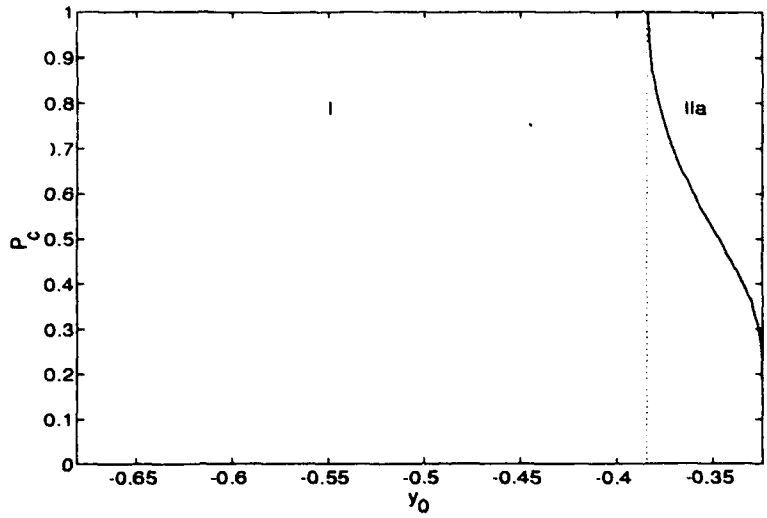

Figure 39. Probabilities of Capture in the Domain of $\mathbf{F}_{1\mu}$ ($\varepsilon = -0.01$ and $\mu = 0.1$). $i_1 = 0.7, i_2 = 0.3, i_3 = 0.8, \alpha_1 = 0.5, \alpha_3 = 0.866$

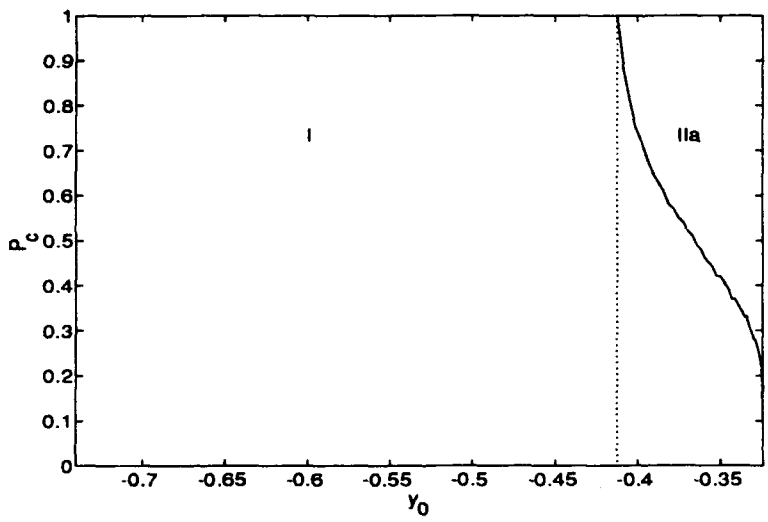

Figure 40. Probabilities of Capture in the Domain of $\mathbf{F}_{2\mu}$ ($\varepsilon = -0.01$ and $\mu = 0.1$). $i_1 = 0.7, i_2 = 0.3, i_3 = 0.8, \alpha_1 = 0.5, \alpha_3 = 0.866$

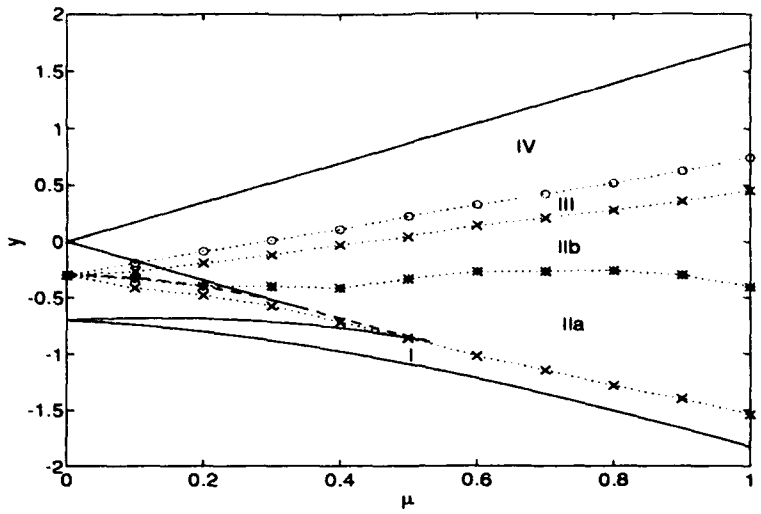

Figure 41. Probabilities of Capture for Initial Conditions Throughout the μy Plane ($\varepsilon = -0.01$). $i_1 = 0.7, i_2 = 0.3, i_3 = 0.8, \alpha_1 = 0.5, \alpha_3 = 0.866$

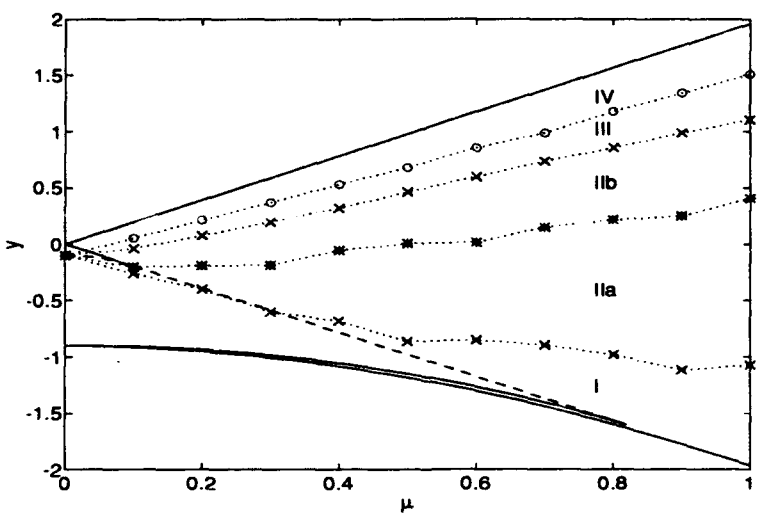

Figure 42. Probabilities of Capture in a Highly Asymmetric Gyrostat ($\varepsilon = -0.01$). $i_1 = 0.9, i_2 = 0.1, i_3 = 0.6, \alpha_1 = 0.2, \alpha_3 = 0.9798$

Diagrams similar to the ones in Figures 41 and 42 are useful tools for spacecraft designers. They can be considered "maps" from which the best initial spinup condition is chosen to avoid resonance capture. Area I must be avoided and Area IV is ideal. However, given the constraints of spacecraft geometry and available power, jockeying the satellite into Area IV prior to spinup may not be feasible. More realistically, the designer should strive towards initial conditions as close as possible to the boundary between Areas IIa and IIb. These maps provide qualitative estimates for P_c. If used in conjunction with plots similar to Figures 32 - 40, the likelihood of launching a successful spacecraft is maximized.

VI. Conclusion and Recommendations

In this final chapter we summarize our analytical procedure and results. We also offer recommendations for possible research to augment our findings.

6.1 Summary and Conclusions

In developing the governing equations for our model, we considered three different body-fixed reference frames in which to express them. We first discussed the principal frame of the axisymmetric, balanced body, $\mathcal{F}^b$. Kinsey derived his equations in this particular coordinate system, but because they were too complex, he introduced a further simplification. Kinsey ignored all high order terms of the rotor imbalance, i.e. terms of $\mathcal{O}(\nu^2)$, thereby limiting their applicability to systems having small products of inertia. Next, we examined the principal frame of the entire spacecraft, $\mathcal{F}^e$. By deriving our equations in terms of this frame, we found that they were also too complex. Rather than pursue the analysis using either of these systems, we chose to derive our governing equations in terms of the pseudo-principal frame, $\mathcal{F}^p$. In doing so, we obtained simple dimensionless expressions. This also permitted us to determine the system kinetic energy in terms of the angular momentum components, leading to the development of the μy plane. Despite the limitations of this two-dimensional plot, the μy plane is a convenient means from which spinup can be observed.

After finding these equations, we integrated them numerically to get a history of the behavior of the spacecraft during spinup. Our analysis centered on the Oblate-Prolate gyrostat. By applying Hall's energy-based criteria for resonance capture, we showed how different initial conditions lead to either capture or escape. We also found that the "captured" example used by Kinsey is actually one in which the spacecraft barely escapes. Because of the disparity in the definition of and conditions for capture established by Kinsey and Hall, we introduced new nomenclature to more

precisely differentiate between the two concepts. Kinsey defines a form of *effective capture*, which is based on the spacecraft's observed behavior. There is no precise set of conditions which signify its onset; it depends on the impact of the nutation angle on a given spacecraft's mission. On the other hand, Hall describes *strict capture*. His definition gives precise criteria for this to occur. These can easily be shown on the μy plane. Using this definition, we have shown that a spacecraft with a final nutation angle close to 90° can still escape.

Having established the criteria for resonance capture, we then showed how different conditions affect its likelihood. The examples given are those for which the final desired spin configuration is about the prolate dual-spin equilibrium point, $\mathbf{P}_\mu$. First, we saw that larger motor torques provide a better chance for escape than smaller ones. This fact has already been well-established. Next, we found that for a given motor torque, capture and escape also depend on the initial conditions. For a given μ and y, these are constrained to lie on a closed curve on the surface of the momentum sphere and are denoted by the angular phase $\phi(0)$. By varying this parameter, we determined the probability of capture for initial conditions along this curve. We then repeated this procedure throughout the domains of each stable center. In each case, we noted four distinct areas characterized by the behavior of P_c as it varies with the initial energy y_0. These areas are easily projected onto the μy plane, resulting in a simple map which shows spacecraft designers which initial conditions have the greatest and least probability of capture.

In addition to the development of this useful tool, two new results which have not been shown in previous works were found from our analysis. First, we saw that a separatrix crossing is not necessary for capture to occur in an unbalanced gyrostat. Instead, we found that this is actually required for escape. Second, we found that whereas a larger motor torque is favorable for prolate spinup, a smaller one is preferable for oblate spinup.

6.2 *Recommendations for Further Research*

1. The unbalanced dual-spin model studied in this thesis is slightly more general than the axial gyrostat since the rotor does not coincide with a principal axis of the spacecraft. Instead, it lies somewhere within a principal *plane*, i.e. a plane defined by any two of the three principal axes. This, however, is still a specific case of an even more general geometry – a gyrostat having an arbitrarily-aligned rotor. It would be interesting as well as useful to study this case because it is an even more realistic model. No real gyrostat is perfectly balanced or symmetric.

2. As mentioned above, knowing the probability of capture would be useful to spacecraft designers. The method we use to determine this probability can be described as "brute force" because we must numerically integrate from one hundred or more different initial conditions to get a reasonably accurate probability for a *single* μy coordinate. This is a demanding, resource-intensive procedure. Thus, we recommend that an adaptation of Henrard's (9) analytical method be developed for this specific purpose. By using this procedure, one would be able to obtain P_c at any initial point in the μy plane with fewer integrations. This can be extended throughout the entire plane with far fewer integrations for the same given "grid size" of initial points as in the present analysis.

3. Another topic of great interest is to develop methods to coax the spacecraft into a desirable initial spinup condition. The map developed in the previous chapter provides the designer with useful information, but requires that some means be found to reorient the deployed spacecraft into one of these favorable initial conditions prior to spinup. Because of geometric constraints, this cannot always be done at the initial deployment. Ideally, a way must be found which uses no thrusters. Instead, strategic pulsing of the spinup motor alone should accomplish this task. Scher and Farrenkopf (20) were able to determine similar means to escape from the dynamic trap states which occur either during or after completion of this maneuver.

4. It would be a great triumph if an exact analytical solution could be found for the unperturbed equations of motion, if at all possible.

5. An aid to improving the efficiency of this analysis is to translate the programs written for this study into a compiled language such as FORTRAN or C. All programs used herein have been written in *MATLAB*. Although *MATLAB* is an extremely powerful analytical tool, its subroutines are uncompiled and therefore run very slowly. These are listed in Appendix D.

Appendix A. Converting From $\mathcal{F}^e$ to $\mathcal{F}^p$

Since our model's inertia matrix can only be properly diagonalized in the form of an apparent gyrostat, as defined in (11:158), the equations of motion must be expressed relative to the pseudo-principal frame.

A.1 Direction Cosine Matrix, $\mathbf{Q}$

A.1.1 Description. $\mathbf{Q}$ "rotates" each parameter from $\mathcal{F}^e$ to $\mathcal{F}^p$. Its columns are the eigenvectors of the inertia-like matrix expressed in $\mathcal{F}^e$: $\mathbf{I}^e - I_s\mathbf{a}\mathbf{a}^T$.

A.1.2 Matrix Form. Since the rotor imbalance is in the $\hat{e}_1\hat{e}_3$ plane, $\hat{e}_2 \equiv \hat{p}_2$. Therefore, $\mathbf{Q}$ has the following form:

$$\mathbf{Q} = \begin{bmatrix} Q_{11} & 0 & Q_{13} \\ 0 & 1 & 0 \\ -Q_{13} & 0 & Q_{11} \end{bmatrix}.$$

A.2 Direction of the Rotor Spin Axis, $\boldsymbol{\alpha}$

A.2.1 Vector Form.

$$\begin{aligned} \boldsymbol{\alpha} &= \begin{bmatrix} \alpha_1 \\ 0 \\ \alpha_3 \end{bmatrix} \\ &= \mathbf{Q}\mathbf{a} \\ &= \begin{bmatrix} Q_{11}a_1 + Q_{13}a_3 \\ 0 \\ Q_{11}a_3 - Q_{13}a_1 \end{bmatrix}. \end{aligned}$$

A.2.2 Inverse Transformation.

$$
\begin{aligned}
\mathbf{a} &= \mathbf{Q}^T \boldsymbol{\alpha} \\
&= \begin{bmatrix} Q_{11}\alpha_1 - Q_{13}\alpha_3 \\ 0 \\ Q_{11}\alpha_3 + Q_{13}\alpha_1 \end{bmatrix}.
\end{aligned}
$$

A.3 Angular Velocity, $\boldsymbol{\nu}$

A.3.1 Vector Form.

$$
\begin{aligned}
\boldsymbol{\nu} &= \begin{bmatrix} \nu_1 \\ \nu_2 \\ \nu_3 \end{bmatrix} \\
&= \mathbf{Q}\boldsymbol{\omega}_R \\
&= \begin{bmatrix} Q_{11}\omega_1 + Q_{13}\omega_3 \\ \omega_2 \\ Q_{11}\omega_3 - Q_{13}\omega_1 \end{bmatrix}.
\end{aligned}
$$

A.3.2 Inverse Transformation.

$$
\begin{aligned}
\boldsymbol{\omega}_R &= \mathbf{Q}^T \boldsymbol{\nu} \\
&= \begin{bmatrix} Q_{11}\nu_1 - Q_{13}\nu_3 \\ \nu_2 \\ Q_{11}\nu_3 + Q_{13}\nu_1 \end{bmatrix}.
\end{aligned}
$$

A.4 *Angular Momentum,* m

A.4.1 *Vector Form.*

$$
\begin{aligned}
\mathbf{m} &= \begin{bmatrix} m_1 \\ m_2 \\ m_3 \end{bmatrix} \\
&= \mathbf{Qh} \\
&= \begin{bmatrix} Q_{11}h_1 + Q_{13}h_3 \\ h_2 \\ Q_{11}h_3 - Q_{13}h_1 \end{bmatrix}.
\end{aligned}
$$

A.4.2 *Inverse Transformation.*

$$
\begin{aligned}
\mathbf{h} &= \mathbf{Q}^T\mathbf{m} \\
&= \begin{bmatrix} Q_{11}m_1 - Q_{13}m_3 \\ m_2 \\ Q_{11}m_3 + Q_{13}m_1 \end{bmatrix}.
\end{aligned}
$$

A.5 *The Inertia-Like Matrix,* J

A.5.1 Description. J is a diagonal matrix whose components are the eigenvalues of $\mathbf{I}^e - I_s\mathbf{aa}^T$. These correspond to the respective eigenvectors of $\mathbf{I}^e - I_s\mathbf{aa}^T$ which make up the columns of $\mathbf{Q}$.

A.5.2 *Matrix Form.*

$$
\begin{aligned}
\mathbf{J} &= \begin{bmatrix} J_1 & 0 & 0 \\ 0 & J_2 & 0 \\ 0 & 0 & J_3 \end{bmatrix} \\
&= \mathbf{Q}[\mathbf{I}^e - I_s\mathbf{aa}^T]\mathbf{Q}^T
\end{aligned}
$$

$$
= \mathbf{Q} \begin{bmatrix} I_1 - I_s a_1^2 & 0 & -I_s a_1 a_3 \\ 0 & I_2 & 0 \\ -I_s a_1 a_3 & 0 & I_3 - I_s a_3^2 \end{bmatrix} \mathbf{Q}^T.
$$

A.5.3 Inverse Transformation.

$$
\begin{aligned}
\mathbf{I}^e &= \mathbf{Q}^T[\mathbf{J} + I_s \alpha \alpha^T]\mathbf{Q} \\
&= \mathbf{Q}^T \begin{bmatrix} J_1 + I_s \alpha_1^2 & 0 & I_s \alpha_1 \alpha_3 \\ 0 & J_2 & 0 \\ I_s \alpha_1 \alpha_3 & 0 & J_3 + I_s \alpha_3^2 \end{bmatrix} \mathbf{Q}. \qquad (85)
\end{aligned}
$$

Appendix B. Translation of Kinsey's Parameters (13)

Kinsey expressed his parameters in terms of the spacecraft's balanced-body frame, $\mathcal{F}^b$. In Chapter 5, we reexamine his model using the technique developed in this study. Thus, we must translate Kinsey's dimensionless parameters directly to those used here. This is done in three steps: first, they are returned to dimensional form by inverting the relationships defined in his thesis. Second, Kinsey's dimensional parameters are translated to ours and then rotated into the principal frame, $\mathcal{F}^e$. Finally, they are rotated into $\mathcal{F}^p$ and then nondimensionalized as described in Chapter 2 and Appendix A. Since this last step is explained in detail in the aforementioned sections, we devote this space only to the first two.

B.1 Definitions

For the sake of convenience, we summarize below all of Kinsey's relevant parameters.

B.1.1 Kinsey's Dimensional Parameters. Kinsey's dimensional parameters are defined as follows:

$$
\begin{aligned}
I_{11}^A &\equiv \text{platform moment of inertia about } \hat{b}_1 \\
I_{33}^A &\equiv \text{platform moment of inertia about } \hat{b}_3 \\
I_{11}^B &\equiv \text{rotor moment of inertia about } \hat{b}_1 \\
I_{33}^B &\equiv \text{rotor moment of inertia about } \hat{b}_3 \\
I_{13}^B &\equiv \text{rotor dynamic imbalance in the plane of } \hat{b}_1\hat{b}_3 \\
I_1 &\equiv I_{11}^A + I_{11}^B \\
N &\equiv \text{spinup motor torque} \\
\omega_{1_K} &\equiv \text{platform/rotor angular velocity about } \hat{b}_1 \\
\omega_{2_K} &\equiv \text{platform/rotor angular velocity about } \hat{b}_2
\end{aligned}
$$

$$\omega_A \equiv \text{platform angular velocity about } \hat{b}_3$$

$$\omega_B \equiv \text{rotor angular velocity about } \hat{b}_3.$$

The initial values of the angular velocity components are expressed as $\omega_{1_K}(0)$, $\omega_{2_K}(0)$, etc. The subscript K is added here to distinguish Kinsey's parameters from our own.

B.1.2 Kinsey's Dimensionless Geometric Parameters. The physical interpretations of these parameters are given on page 59. In terms of the dimensional parameters shown above, they are defined as:

$$\nu = \frac{I_{13}^B}{I_1} \tag{86}$$

$$\sigma = \frac{I_{33}^B}{I_1} \tag{87}$$

$$J = \frac{I_{33}^A}{\sigma I_1} \tag{88}$$

$$K = \frac{N}{\omega_A^2(0)}\left(\frac{1}{I_{33}^A} + \frac{1}{I_{33}^B}\right) \tag{89}$$

B.1.3 Kinsey's Dimensionless Angular Velocity Components. The angular velocity components are scaled by the initial value of ω_A. They are as follows:

$$\bar{\omega}_1 = \frac{\omega_{1_K}}{\omega_A(0)} \tag{90}$$

$$\bar{\omega}_2 = \frac{\omega_{2_K}}{\omega_A(0)} \tag{91}$$

$$\bar{\omega}_A = \frac{\omega_A}{\omega_A(0)} \tag{92}$$

$$\bar{\omega}_B = \frac{\omega_B}{\omega_A(0)} \tag{93}$$

B.1.4 Kinsey's Dimensionless Initial Conditions. Kinsey assumes that the spinup maneuver starts from the all-spun condition. The initial spin axis is nearly

coincident with $\hat{b}_3$. His dimensionless initial conditions are

$$
\begin{aligned}
\bar{\omega}_1(0) &= \frac{[1-\sigma(1+J)] + \sqrt{[1-\sigma(1+J)]^2 + 4\nu^2}}{2\nu} \\
\bar{\omega}_2(0) &= 0 \\
\bar{\omega}_A(0) &= 1 \\
\bar{\omega}_B(0) &= 1.
\end{aligned}
$$

B.2 Step 1: Redimensionalizing Kinsey's Equations

From Equations (86) – (88) it is clear that the inertia parameters are scaled by I_1. Furthermore, the motor torque K as well as the angular velocity components are scaled by $\omega_A(0)$. Since neither of these scale parameters are explicitly given, they must be assumed. As a result, infinite sets of dimensional values can be found, but the elements of each are in the same proportions. Recall from the second chapter that this is one of the advantages of nondimensionalization; it allows one to analyze the behavior of not just one, but a whole class of similar models having identical behavior. Thus, without loss of generality, we assume in this thesis that $\omega_A(0) = I_1 = 1$. The redimensionalized parameters, using Equations (86) – (89) and (90) – (93), are obtained from

$$
\begin{aligned}
I_{33}^A &= \sigma J I_1 \\
I_{13}^B &= \nu I_1 \\
I_{33}^B &= \sigma I_1 \\
N &= \nu K \omega_A^2(0) \left(\frac{I_{33}^A I_{33}^B}{I_{33}^A + I_{33}^B} \right) \\
\omega_{1_K}(0) &= \bar{\omega}_1(0)\omega_A(0) \\
\omega_{2_K}(0) &= \bar{\omega}_2(0)\omega_A(0) \\
\omega_B(0) &= \bar{\omega}_B(0)\omega_A(0).
\end{aligned}
$$

B.3 Step 2: Parameter Translation and Rotation to $\mathcal{F}^e$

B.3.1 Spacecraft Moment of Inertia Tensor, **I**. The inertia tensor of Kinsey's model expressed in $\mathcal{F}^b$ is:

$$\mathbf{I}^b = \begin{bmatrix} I_1 & 0 & I_{13}^B \\ 0 & I_1 & 0 \\ I_{13}^B & 0 & I_{33}^A + I_{33}^B \end{bmatrix}. \tag{94}$$

In the principal frame this becomes:

$$\mathbf{I}^e = \begin{bmatrix} I_1^e & 0 & 0 \\ 0 & I_2^e & 0 \\ 0 & 0 & I_3^e \end{bmatrix}.$$

Since the $\hat{b}_2$ axis is common to both coordinate frames, the direction cosine matrix **R** which transforms expressions from $\mathcal{F}^b$ to $\mathcal{F}^e$ looks like the following:

$$\mathbf{R} = \begin{bmatrix} R_{11} & 0 & R_{13} \\ 0 & 1 & 0 \\ -R_{13} & 0 & R_{11} \end{bmatrix}.$$

The columns of **R** are the eigenvectors of $\mathbf{I}^b$. They correspond to the respective eigenvalues of $\mathbf{I}^b$ which make up the diagonal elements of $\mathbf{I}^e$. We now have the relationship between Kinsey's inertia parameters and our own. To express it in the principal frame, the following transformation is used:

$$\mathbf{I}^e = \mathbf{R}\mathbf{I}^b\mathbf{R}^T.$$

Furthermore, the moment of inertia of the platform about the relative spin axis, defined herein as I_s, is simply

$$I_s = I_{33}^A. \tag{95}$$

B.3.2 Rotor Inertial Angular Velocity, ω_R. The rotor inertial angular velocity vector in the balanced-body frame is written as:

$$\omega_R^b = \begin{bmatrix} \omega_{1_K} \\ \omega_{2_K} \\ \omega_B \end{bmatrix}. \tag{96}$$

B.3.3 Direction of the Rotor's Axis of Symmetry, **a**. From Figure 1 in Chapter 2, it is clear that $\mathbf{a} \equiv \hat{b}_3$. Thus, with respect to $\mathcal{F}^b$,

$$\mathbf{a}^b = \begin{bmatrix} 0 \\ 0 \\ 1 \end{bmatrix}. \tag{97}$$

Premultiplying this by **R** gives an expression for **a** in terms of the principal frame, or:

$$\mathbf{a}^e = \begin{bmatrix} R_{13} \\ 0 \\ R_{11} \end{bmatrix}.$$

B.3.4 Relative Velocity Between the Platform and Rotor, ω_s. Our expression for ω_s can also be written in terms of Kinsey's parameters. It is simply

$$\omega_s = \omega_A - \omega_B \tag{98}$$

B.3.5 Angular Momentum Vector, **h**. Knowing these inertia and velocity parameters allows us to immediately determine the spacecraft's angular momentum vector in $\mathcal{F}^b$. This is given as $\mathbf{h}^b = \mathbf{I}^b\omega_R^b + I_s\omega_s\mathbf{a}^b$. Substitution of Equations (94) –

(98) into this expression gives:

$$\mathbf{h}^b = \begin{bmatrix} I_1\omega_1 + I_{13}^B\omega_B \\ I_1\omega_2 \\ I_{33}^A\omega_A + I_{33}^B\omega_B + I_{13}^B\omega_1 \end{bmatrix}.$$

Its $\mathcal{F}^e$ counterpart is obtained from

$$\mathbf{h}^e = \mathbf{R}\mathbf{h}^b.$$

B.3.6 Motor Torque, g_a. The motor torque, g_a, expressed in terms of Kinsey's parameters is simply

$$g_a = -N.$$

Appendix C. The All-Spun Initial Condition

A gyrostat is said to be "all-spun" when there is no relative rotation between the platform and rotor ($\omega_s = 0$). Thus, to the inertially-fixed observer, it appears to rotate as a single body. The relation corresponding to this initial condition is derived below.

Equation (8) gives an expression for the component of the platform's inertial angular velocity along its symmetry axis. It is repeated here.

$$h_a = I_s \mathbf{a}^T \boldsymbol{\omega}_R + I_s \omega_s$$

The all-spun condition is thus

$$h_{a_0} = I_s \mathbf{a}^T \boldsymbol{\omega}_R,$$

and with the help of Equations (17) and (18), this result can be rewritten in $\mathcal{F}^P$ as follows:

$$h_{a_0} = I_s \boldsymbol{\alpha}^T \boldsymbol{\nu}.$$

Into this expression, Equation (20) is substituted. This produces

$$h_{a_0} = I_s \boldsymbol{\alpha}^T \mathbf{J}^{-1} \mathbf{m} - h_a I_s \boldsymbol{\alpha}^T \mathbf{J}^{-1} \boldsymbol{\alpha}.$$

Substitution of the respective representations of each matrix followed by algebraic manipulation reduce this to

$$h_{a_0} \left[1 + I_s \left(\frac{\alpha_1^2}{J_1} + \frac{\alpha_3^2}{J_3} \right) \right] = I_s \left(\frac{\alpha_1 m_1}{J_1} + \frac{\alpha_3 m_3}{J_3} \right).$$

Dividing both sides of this equation by m gives

$$\mu_0 \left[1 + I_s \left(\frac{\alpha_1^2}{J_1} + \frac{\alpha_3^2}{J_3} \right) \right] = I_s \left(\frac{\alpha_1 x_1}{J_1} + \frac{\alpha_3 x_3}{J_3} \right)$$

into which $J_1 = J_3/(1 - i_1)$ is substituted. This, in turn, leaves

$$\mu_0 \left[1 + I_s \left(\frac{\alpha_1^2(1 - i_1)}{J_3} + \frac{\alpha_3^2}{J_3} \right) \right] = \frac{I_s}{J_3} \left[\alpha_1 x_1 (1 - i_1) + \alpha_3 x_3 \right]$$

which we then multiply through by J_3/I_s to get:

$$\mu_0 \left[\frac{J_3}{I_s} + \alpha_1^2(1 - i_1) + \alpha_3^2 \right] = \alpha_1 x_1 (1 - i_1) + \alpha_3 x_3.$$

Finally, recall from Chapter 2 that $J_3 = J_3' - I_s \alpha_3^2$, so that we are left with

$$\mu_0 = \frac{\alpha_1 x_1 (1 - i_1) + \alpha_3 x_3}{\alpha_3^2 / i_3 + \alpha_1^2 (1 - i_1)}.$$

This is the all-spun initial condition. Note that $\dot{\mu}_0 \neq 0$.

Appendix D. Computer Code

All of the relevant computer programs used in this analysis are listed below. This set of code is written in *MATLAB* and is provided as a reference for the interested reader.

D.1 CAPPROB.M

```
% PROGRAM: capprob.m

% GENERAL DESCRIPTION: This is a collection of subroutines which
% determine the probabilities of capture for a given value of mu.
% Given the dimensionless spacecraft parameters, a series of
% initial curves of constant energy on the unperturbed momentum
% sphere are generated. Every point along these curves are initial
% conditions for numerical integration of the perturbed equations
% of motion. The final energy associated with each initial
% condition is calculated. From this information, plots of final
% energy, yf, versus initial angular phase, phi, may be drawn for
% each initial point. The probabilities of capture are also
% computed.

% CAUTION: This program takes about 12 hours to run.

%%%%%%%%%%%%%%%%%%%%%%%%%%%%%%%%%%%%

% The dimensionless parameters for a particular spacecraft are
% defined in this section. Their definitions are self-evident
% from the variable names. When new parameters are used, they
% are changed directly within this program in this section.

% REMINDER: When changing parameters, make these changes to
% the functions 'notorqeom.m', 'phaseint.m', and 'eom.m' also.

clear

i1 = 0.7;
i2 = 0.3;
i3 = 0.8;
```

```
alpha1 = 0.5;
alpha3 = sqrt(1 - alpha1^2);
epsilon = -0.01;
mu = 0.1;

%%%%%%%%%%%%%%%%%%%%%%%%%%%%%%%%%%%%

% Single points on each initial constant energy curve (x10, x20,
% x30) as well as their associated energies (y0) are found
% using ONLY ONE of the following functions: 'initialcond.m' or
% 'initialcondx2not0.m'. The former is used when considering a
% sphere for which mu is less than the value of mu at which the
% pitchfork bifurcation occurs. In this case, the statement
% ''x20 = zeros(size(x10))'' MUST ALSO BE USED. The latter function
% is used when mu is greater than the value of mu at which the
% pitchfork bifurcation occurs. DO NOT USE the statment
% ''x20 = zeros(size(x10))'' in this case. Comment out the
% statement(s) that do not apply, as shown below.

% [x10, x30, y0] = initialcond(i1,i2,i3,alpha1,alpha3,mu);
% x20 = zeros(size(x10));
[x10, x20, x30, y0] = initialcondx2not0(i1,i2,i3,alpha1,alpha3,mu);

% These initial values are stored for future use.

save x1ics x10 /ascii /double;
save x2ics x20 /ascii /double;
save x3ics x30 /ascii /double;
save y0ics y0 /ascii /double;

%%%%%%%%%%%%%%%%%%%%%%%%%%%%%%%%%%%%

% Determine the probability of capture (Pc) for each initial curve
% of constant energy. 'findprob.m' also determines the
% final energy, yf, for a given initial phase angle, phi. This
% information is saved in files called 'yfeps01' and 'phieps01'.
% These output files are explained in more detail within the
% subroutine 'findprob.m'.

[Pc] = findprob(x10,x20,x30,y0,i1,i2,i3,alpha1,alpha3,mu);

%%%%%%%%%%%%%%%%%%%%%%%%%%%%%%%%%%%%
```

```
% Plot the probability of capture versus the initial energy.  Note
% that because of the way the subroutines work, ONLY elements
% 2 - 100 of y0 and Pc are relevant.

plot(y0(2:100),Pc(2:100))
xlabel('Initial Energy at Mu = 0.1')
ylabel('Probability of Capture')
print -deps y0vsPc
```

D.2 EOM.M

```
function xdot = eom(t,x)

% GENERAL DESCRIPTION:  This program stores the equations of motion
% used for numerical integration.

i1 = .7;
i2 = .3;
a1 = 0.5; %  alpha1
a3 = sqrt(1 - a1^2); %  alpha3
epsilon = -0.01;

% Legend

% x(1) = x1
% x(2) = x2
% x(3) = x3
% x(4) = mu
% x(5) = y

xdot(1) = x(2)*(i2*x(3) - x(4)*a3);
xdot(2) = -i1*x(1)*x(3) + x(4)*(a3*x(1) - a1*x(3)*(1 - i1));
xdot(3) = x(2)*(x(1)*(i1 - i2) + x(4)*a1*(1 - i1));
xdot(4) = epsilon;
xdot(5) = 2*epsilon*(x(1)*a1*(i1 - 1) - x(3)*a3);
```

D.3 FILTERCOMP.M

```
function [RE,rstart,rend,cstart,cend] = filtercomp(X)

% GENERAL DESCRIPTION: This subroutine picks real and complex
% subvectors out of a single given vector made up of real and
% complex segments.

current = 0;
numreal = 0;
numcomp = 0;
RE = zeros(200,200);
CO = zeros(200,200);

for index = 1:length(X)
   if imag(X(index)) == 0
      if current ~= 1
         current = 1;
         numreal = numreal + 1;
         rstart(numreal) = index;
         if numcomp > 0
            cend(numcomp) = index - 1;
         end
      end
   else
      if current ~= 2
         current = 2;
         numcomp = numcomp + 1;
         cstart(numcomp) = index;
         if numreal > 0
            rend(numreal) = index - 1;
         end
      end
   end
end
if current == 1
   rend(numreal) = index;
else
   cend(numcomp) = index;
end
if numreal > 0
   for index = 1:numreal
```

```
      RE(index,rstart(index):rend(index)) = ...
         ...X(rstart(index):rend(index));
   end
else
   RE = zeros(200,200);
end
if numcomp > 0
   for index = 1:numcomp
      CO(index,cstart(index):cend(index)) = ...
         ...X(cstart(index):cend(index));
   end
else
   CO = zeros(200,200);
end
```

D.4 FINDPROB.M

```
function [Pc] = findprob(x10,x20,x30,y0,i1,i2,i3,a1,a3,mas)

% GENERAL DESCRIPTION: This subroutine takes each initial energy y0
% determined in 'capprob.m' and generates 101 coordinates for
% points all along this curve. It also determines the angular
% phase, phi of each point and calculates the associated final
% energy state at the conclusion of spinup, yf. Finally, the
% probability of capture for each initial energy curve is
% calculated.

%%%%%%%%%%%%%%%%%%%%%%%%%%%%%%%%%%%%%%%%

% This section determines phi and yf along each curve defined in y0.
% They are saved on disk as variables 'phieps01' and 'yfeps01'
% respectively. The variable 'repeat' denotes the ith curve of
% interest (i.e. the ith element of y0) and the variable 'count'
% denotes the jth point on each curve. Hence, the elements of
% 'phieps01' and 'yfeps01' give values of phi and y for he jth point
% along the ith energy curve in y0. NOTE: THIS SUBROUTINE IS
% WRITTEN IN SUCH A WAY THAT THE FIRST COLUMN IN EACH MATRIX IS
% USELESS DATA.
```

```
      RE(index,rstart(index):rend(index)) = ...
         ...X(rstart(index):rend(index));
   end
else
   RE = zeros(200,200);
end
if numcomp > 0
   for index = 1:numcomp
      CO(index,cstart(index):cend(index)) = ...
         ...X(cstart(index):cend(index));
   end
else
   CO = zeros(200,200);
end
```

D.4 FINDPROB.M

```
function [Pc] = findprob(x10,x20,x30,y0,i1,i2,i3,a1,a3,mas)

% GENERAL DESCRIPTION: This subroutine takes each initial energy y0
% determined in 'capprob.m' and generates 101 coordinates for
% points all along this curve. It also determines the angular
% phase, phi of each point and calculates the associated final
% energy state at the conclusion of spinup, yf. Finally, the
% probability of capture for each initial energy curve is
% calculated.

%%%%%%%%%%%%%%%%%%%%%%%%%%%%%%%%%%%%%%

% This section determines phi and yf along each curve defined in y0.
% They are saved on disk as variables 'phieps01' and 'yfeps01'
% respectively. The variable 'repeat' denotes the ith curve of
% interest (i.e. the ith element of y0) and the variable 'count'
% denotes the jth point on each curve. Hence, the elements of
% 'phieps01' and 'yfeps01' give values of phi and y for he jth point
% along the ith energy curve in y0. NOTE: THIS SUBROUTINE IS
% WRITTEN IN SUCH A WAY THAT THE FIRST COLUMN IN EACH MATRIX IS
% USELESS DATA.
```

```
clg

for repeat = 2:length(y0)-1

%  Repeat this process for each initial condition

   x1 = x10(repeat);
   x2 = x20(repeat);
   x3 = x30(repeat);
   yic = y0(repeat);
   t0 = 0;
   icvec = [x1 x2 x3 mas yic];
   [t,x] = myode45('notorqeom',0,icvec,10^(-10));
   x1 = x(:,1);
   x2 = x(:,2);
   x3 = x(:,3);

   step = length(t)/200;
   count = 0;
   for i = 1:step:length(t)
      count = count + 1;
      [phi(count,repeat),yf(count,repeat)] = phaseint...
         ...(i1,i2,i3,a1,t(i)/t(length(t)),x1(i),x2(i),...
         ...x3(i),mas,yic);
   end

%  Now add the remaining point if the last value is not tf due
%  to remainder in the division of length(t)/200.

   if i ~= length(t)
      i = length(t);
      count = count+1;
      [phi(count,repeat),yf(count,repeat)] = phaseint...
         ...(i1,i2,i3,a1,t(i)/t(length(t)),x1(i),x2(i),...
         ...x3(i),mas,yic);
   end

%%%%%%%%%%%%%%%%%%%%%%%%%%%%%%%%%%%%%%%%

%  The probability of capture associated with each column of 'phieps'
%  and 'yfeps' is now calculated.  All of these values are saved to
%  the hard disk for future reference.
```

```
    [Pc(repeat)] = probcap(phi(:,repeat), yf(:,repeat), -i2);

    save phieps01 phi /ascii /double
    save yfeps01 yf /ascii /double
    save Probcaptureeps01 Pc /ascii /double

end
```

D.5 IFPR.M

```
function [lambda, wplat, wrotor] =...
   ...ifpr(i1,i2,i3,x1,x2,x3,mu,alpha1,alpha3)

% GENERAL DESCRIPTION: This subroutine determines the inertial
% free precession rate of the spacecraft (lambda). It uses the
% numerically integrated values generated by the program
% 'integrate.m'. This function also determines the inertial
% angular velocities of the rotor (wrotor) and platform (wplat).
% Finally, it returns the values of Kinsey's dimensionless
% parameters.

% Get the J's, assuming that J3 = 1

J3 = 0.66692494184302;
J1 = J3/(1 - i1);
J2 = J3/(1 - i2);
Is = J3/alpha3^2 * (1/(1 - i3) - 1)

J = [J1 0 0; 0 J2 0; 0 0 J3]

% Get the m's, assuming that m = 1.50087471873876

m = 1.50087471873876;
m1 = m * x1;
m2 = m * x2;
m3 = m * x3;
ha = m * mu;
alpha = [alpha1 0 alpha3]'
```

```
mvector = [m1 m2 m3]';

%  Determine the principal moments of inertia and the rotation
%  matrix QT

W = J1 + Is * alpha1^2;
X = J2;
Y = J3 + Is * alpha3^2;
Z = Is * alpha1 * alpha3;


QT11 = -1/sqrt(1 + (Y - W - sqrt((W - Y)^2 + 4 * Z^2))^2/(4*Z^2));
QT31 = (Y - W - sqrt((W - Y)^2 + 4 * Z^2))/(2 * Z *...
   ...sqrt(1 + (Y - W - sqrt((W - Y)^2 + 4 * Z^2))^2/(4 * Z^2)));
QT13 = 1/sqrt(1 + (Y - W + sqrt((W - Y)^2 + 4 * Z^2))^2/(4*Z^2));
QT33 = -(Y - W + sqrt((W - Y)^2 + 4 * Z^2))/(2 * Z *...
   ...sqrt(1 + (Y - W + sqrt((W - Y)^2 + 4 * Z^2))^2/(4 * Z^2)));

QT = [QT11 0 QT13; 0 1 0; QT31 0 QT33]

I1 = (W + Y - sqrt((W - Y)^2 + 4 * Z^2))/2;
I2 = X;
I3 = (W + Y + sqrt((W - Y)^2 + 4 * Z^2))/2;

I = [I1 0 0; 0 I2 0; 0 0 I3]

a = QT * alpha %  Unit vector a
h = QT * mvector; %  Angular momentum in the principal frame

%  Angular velocity in the principal frame.

wM = (I - Is*a*a')\(h - [ha'*a(1); zeros(1,length(ha)); ha'*a(3)]);

%  Relative angular velocity between the platform and rotor.

ws = (ha' - Is*(a'*wM))/Is;

%  Determine the rotation matrix into the body frame.

RT = [a(3) 0 -a(1); 0 1 0; a(1) 0 a(3)];
```

```
% Determine the inertia parameters in the body frame.

Ib = RT * I * RT';

% Angular velocity vector in the body frame.

wK = RT * wM;

% Determine the inertial free precession rate (Kinsey's method).

lambda = (Is*wK(3,1) + (Ib(3,3)-Is)*(wK(3,1)+ws(1)))/Ib(1,1);

wplat = ha/Is;
wrotor = wplat-ws';

% Kinsey's dimensionless parameters.

sigma = (Ib(3,3)-Is)/Ib(1,1)
nu = Ib(1,3)/Ib(1,1)
Jkins = Is/(Ib(3,3)-Is)        % This parameter is actually 'J'
K = -(m^2*eps/J3)/wK(3,1)^2*(1/Is + 1/(Ib(3,3)-Is))/nu
```

D.6 INITIALCOND.M

```
function [x10, x30, y0] = initialcond(i1,i2,i3,a1,a3,m)

% GENERAL DESCRIPTION: This subroutine determines initial
% conditions in the mu y plane at a given value of m (mu).
% It is applicable only in cases where mu is greater than the
% value of mu at which the pitchfork bifurcation occurs.

% I found these values by running 'modeq.m', then examining the
% roots of R1 and R3 (a very tedious procedure).

x1ic = -0.025025933586;
x1fc = 0.006255577732;
x3ic = -0.999686802278;
x3fc = 0.999980433682;
```

```
totaldeltapsi = acos(x1ic*x1fc+x3ic*x3fc);

deltapsi = totaldeltapsi/100;

psi0 = atan2(x3ic,x1ic);
psif = psi0 + totaldeltapsi;
psi = psi0;
x2 = 0;

for n=1:101
   x1 = cos(psi);
   x3 = sin(psi);
   y = 2*m*(a1*(i1-1)*x1 - a3*x3) - (i1*x1^2+i2*x2^2);
   x10 = [x10;x1];
   x30 = [x30;x3];
   y0 = [y0;y];
   psi = psi - deltapsi;
end
```

D.7 INITIALCONDX2NOT0.M

```
function [x10, x20, x30, y0] = initialcondx2not0(i1,i2,i3,a1,a3,mu);

% GENERAL DESCRIPTION: This subroutine determines initial
% conditions in the mu y plane at a given value of mu which is
% less than that for which the pitchfork bifurcation occurs.

x1ic = -0.0375;
x1fc = -0.019068969268;
stepx1 = (x1fc - x1ic)/100;

x3ic = 0.28867513459481;
x3fc = -0.999818170675;
stepx3 = (x3fc - x3ic)/100;

x2ic = real(sqrt(1 - x1ic^2 - x3ic^(2)));
x2fc = real(sqrt(1 - x1fc^2 - x3fc^(2)));

yic = real(2*mu*(a1*(i1-1)*x1ic - a3*x3ic) - (i1*x1ic^2+i2*x2ic^2));
```

```
yfc = real(2*mu*(a1*(i1-1)*x1fc - a3*x3fc) - (i1*x1fc^2+i2*x2fc^2));

x3 = x3ic;
for x1 = x1ic:stepx1:x1fc
   x2 = real(sqrt(1 - x1^2 - x3^(2)));
   y = real(2*mu*(a1*(i1-1)*x1 - a3*x3) - (i1*x1^2+i2*x2^2));
   if y < yic | y > yfc
      x2 = real(-sqrt(1 - x1^2 - x3^(2)));
      y = real(2*mu*(a1*(i1-1)*x1 - a3*x3) - (i1*x1^2+i2*x2^2));
   end

   x10 = [x10;x1];
   x20 = [x20;x2];
   x30 = [x30;x3];
   y0 = [y0;y];
   x3 = x3+stepx3;
end
```

D.8 INTEGRATE.M

```
% PROGRAM: integrate.m

% GENERAL DESCRIPTION: This program numerically integrates the
% equations of motion. It must be used in conjunction with
% 'eom.m' and 'ode45.m'. The latter subroutine is a built-in MATLAB
% function.

%%%%%%%%%%%%%%%%%%%%%%%%%%%%%%%%%%%

% The dimensionless parameters are defined below.

clear
hold on

t0 = 0; % Initial time for integration
i1 = .7;
i2 = .3;
i3 = .8;
```

```
a1 = .5; %  alpha1
a3 = sqrt(1 - a1^2); %  alpha3
eps = .001; %  Motor torque epsilon

%  Initial values for the dimensionless angular momentum coordinates
%  x1, x2, and x3.

x1 = 0;
x2 = 1;
x3 = 0;

%  All-spun initial condition.

mas = (x1*a1*(1 - i1) + x3*a3)/((a3^2)/i3 + a1^2 * (1 - i1));
y = 2*mas * (x1*a1*(i1 - 1) - x3*a3) - (i1*x1^2 + i2*x2^2);

%  Time at which spinup concludes.

tf = ceil((1 - mas)/eps);

%%%%%%%%%%%%%%%%%%%%%%%%%%%%%%%%%%%

%  Numerically integrate the equations of motion.

x0 = [x1 x2 x3 mas y];
[t,x] = ode45('eom',t0,tf,x0);

%%%%%%%%%%%%%%%%%%%%%%%%%%%%%%%%%%%

%  The following sections operate independently.  Those which are not
%  of interest may be commented out.

%%%%%%%%%%%%%%%%%%%%%%%%%%%%%%%%%%%

%  Plot the spinup trajectory onto the mu y plane.
%  Normally, this subroutine is called afterm 'modeq.m' is run
%  so that the integrated trajectory can be superimposed onto
%  the mu y plane.

plot(x(:,4),x(:,5))
break
```

```
%%%%%%%%%%%%%%%%%%%%%%%%%%%%%%%%%%%%

% Plot the nutation angle versus time.

plot(t,acos(x(:,1)*a1+x(:,3)*a3)*180/3.141592654)
break

%%%%%%%%%%%%%%%%%%%%%%%%%%%%%%%%%%%%

% Plot the inertial angular velocity of the rotor versus that of the
% platform. For comparison, the inertial free precession rate
% (applicable only for balanced or nearly balanced gyrostats) is
% determined by the function 'ifpr.m' and then plotted as well.

line = [0:.01:2];

[lambda, wplat, wrotor] = ifpr(i1,i2,i3,x(:,1),x(:,2),x(:,3),...
   ...x(:,4),a1,a3);
plot(wrotor,wplat)
hold on
plot(lambda*ones(size(line)),line,'--r')
plot(line,line)
xlabel('Rotor Inertial Angular Velocity')
ylabel('Platform Inertial Angular Velocity')
```

D.9 KINSEY.M

```
% PROGRAM: kinsey.m

% GENERAL DESCRIPTION: This program uses the method outlined in
% Appendix B to convert Kinsey's dimensionless parameters to our
% own.

% These are his dimensionless parameters (given).

nu = 0.005;
sigma = 0.667;
J = 1.25;
K = 1.2;
```

```
wA0 = 1;
wbar10 = ((1-sigma*(1+J))+sqrt((1-sigma*(1+J))^(2)+4*nu^(2)))/...
   ...(2*nu);
wbar20 = 0;
wbarB0 = 1;
wbarA0 = 1;

% Redimensionalize his parameters.

I1 = 1;
IA33 = sigma*J*I1;
IB13 = nu*I1;
IB33 = sigma*I1;
N=nu*K*wA0^(2)*(IA33*IB33)/(IA33+IB33);
w10 = wbar10*wA0;
w20 = wbar20*wA0;
wB0 = wbarB0*wA0;
hB1 = I1*w10+IB13*wB0;
hB2 = I1*w20;
hB3 = IA33*wA0+IB33*wB0+IB13*w10;

Ib = [I1 0 IB13; 0 I1 0; IB13 0 IA33+IB33]
hB = [hB1; hB2; hB3];

% Determine the rotation matrix Reb from the body frame to the
% principal frame. Then, rotate all of the parameters.

[R,Ip] = eig(Ib,'nobalance');
R = [R(:,2) R(:,1) R(:,3)];
Reb = R'
Ip = [Ip(2,2) 0 0; 0 Ip(1,1) 0; 0 0 Ip(3,3)];
Isp = IA33;
a = [Reb(1,3); 0; Reb(3,3)];

hE = Reb*hB;

% Determine the rotation matrix Qpe to from the principal frame
% to the pseudo-principal frame. Then, rotate each parameter.

Jugly = Ip-Isp*a*a'
```

```
[Q,J] = eig(Jugly,'nobalance');
Q = [Q(:,2) Q(:,1) Q(:,3)];
Qpe = Q'
J = [J(2,2) 0 0; 0 J(1,1) 0; 0 0 J(3,3)]
Qpe'*J*Qpe

alpha = Qpe*a
J3prime = J(3,3)+Isp*alpha(3)^2;

m = Qpe*hE;

% Nondimensionalize the parameters using our technique.

mmag = sqrt(m(1)^2+m(2)^2+m(3)^2)
i1 = 1-J(3,3)/J(1,1)
i2 = 1-J(3,3)/J(2,2)
i3 = 1-J(3,3)/J3prime
x1 = m(1)/mmag
x2 = m(2)/mmag
x3 = m(3)/mmag
epsilon = -(J(3,3)*N)/mmag^2
```

D.10 MODEQ.M

```
% FUNCTION: modeq.m

% GENERAL DESCRIPTION: This program uses the procedure outlined in
% Chapter 4 to plot the mu y plane. Unfortunately, there are some
% things which must be done manually. These are explained in the
% relevant sections below.

%%%%%%%%%%%%%%%%%%%%%%%%%%%%%%%%%%%%

clear
clg

% The dimensionless parameters are defined here. These parameters
% denote an Oblate-Prolate spacecraft.
```

```
i1 = .7;
i2 = .3;
i3 = .8;
a1 = .5; %  alpha1
a3 = sqrt(1 - a1^2); %  alpha3

m = [0:0.01:1]; %  Range of mu

%%%%%%%%%%%%%%%%%%%%%%%%%%%%%%%%%%%

%  Case I:  x2 is not equal to 0.

for j = 1:length(m)
   x1(j) = m(j)*a1*(i1 - 1)/(i1 - i2);
   x3(j) = m(j)*a3/i2;
   x2(j) = sqrt(1 - x1(j)^2 - x3(j)^2);
end

%  Any complex elements in x2 are filtered out and subsequently
%  ignored.

[RE,rstart,rend,cstart,cend] = filtercomp(x2);

for subvector = 1:length(rstart)
   for j = rstart(subvector):rend(subvector)
      y(j) = 2*m(j)*(x1(j)*a1*(i1 - 1) - x3(j)*a3) -...
         ...(x1(j)^2*i1 + x2(j)^2*i2);
   end

%  We know that this trajectory is unstable for the Oblate-
%  Prolate gyrostat.  Hence, we plot it here as a dotted line.

   plot(m(rstart(subvector):rend(subvector)),y,'--r')
   axis([0 1 -2 2])
   hold on
end
storage = y; %  Store this vector for future reference.

%%%%%%%%%%%%%%%%%%%%%%%%%%%%%%%%%%%

%  Case II:  x2 = 0.
```

```
clear y

for j = 1:length(m)

   c4 = i1^2;
   c3 = 2*i1*(1 - i1)*m(j)*a1;
   c2 = ((1 - i1)*m(j)*a1)^2 + (m(j)*a3)^2 - i1^2;
   c1 = -c3;
   c0 = -((1 - i1)*m(j)*a1)^2;

   eq1 = [c4 c3 c2 c1 c0];

   x2 = 0;
   X1 = sort(roots(eq1)');

   [RE,rstart,rend,cstart,cend] = filtercomp(X1);

   for subvector = 1:length(rstart)
      R1(j,rstart(subvector):rend(subvector)) = ...
      ...RE(subvector,rstart(subvector):rend(subvector));
   end

   for r = 1:4
      if R1(j,r) == 0
         if m(j) == 0
            R3(j,r) = 1;
         end
         else
            R3(j,r) = (m(j)*a3*R1(j,r))/(i1*R1(j,r) +...
               ...(1 - i1)*m(j)*a1);
         end
      end

   for subvector = 1:length(rstart)
      for q = rstart(subvector):rend(subvector)
         y(j,q) = 2*m(j)*(R1(j,q)*a1*(i1 - 1) - R3(j,q)*a3) -...
            ...(R1(j,q)^2*i1 + x2^2*i2);
      end
   end

   for subvector = 1:length(cstart)
      for q = cstart(subvector):cend(subvector)
```

```
        y(j,q) = i;
      end
   end
end

%%%%%%%%%%%%%%%%%%%%%%%%%%%%%%%%%%%%

% One of the big disadvantages of this program is that the routine
% above will not properly sort the four sets of x1 and x3
% coordinates (stored in the matrices R1 and R3, respectively).
% The rows correspond to the four possible x1 and x3 coordinates
% which locate the four equilibria at a given mu. The columns
% correspond to different values of mu. Sometimes parts of each
% column are swapped with corresponding parts of the other columns
% [e.g. R1(4:100,2) is swapped with R1(4:400,4)]. This can be
% fixed not by altering either of these matrices, but by altering
% the FINAL ENERGY MATRIX y, (defined at the end). The program
% has a built-in feature that prints this four-column matrix. The
% rows are numbered by a fifth column at the left-hand side.
% Scroll through the columns and see where there are breaks in
% the trends of the figures. Most of the time these breaks are
% obvious. These column sections must then be reassigned to the
% proper columns. Fortunately, this is a very simple process
% (it takes a little practice). The commands facilitating this
% procedure are shown in this section.

w = zeros(length(y(:,1))); % Temporary storage vector for
% swapped column sections.

% Once the reversed column sections are identified, store the first
% one in 'w'. This is denoted by statement 'A'. Then, replace the
% original section of 'y' with the correct one ('B'). Finally, take
% the temporarily stored value in 'w' and insert it into the section
% of 'y' where it belongs ('C'). Usually this only needs to be done
% twice, hence the two sets column changes shown.

w(75:101,2) = y(75:101,2); % Step A
y(75:101,2) = y(75:101,4); % Step B
y(75:101,4) = w(75:101,2); % Step C

w(55:101,1) = y(55:101,1); % Step A
y(55:101,1) = y(55:101,3); % Step B
```

```
y(55:101,3) = w(55:101,1); %  Step C

%%%%%%%%%%%%%%%%%%%%%%%%%%%%%%%%%%%%

%  Plot the trajectories determined from above.  Here is another
%  major disadvantage of the program.  The type of line to be plotted
%  (solid or dashed) must be determined manually.  Assuming the user
%  knows which trajectories are stable and which are not, the plot
%  statements must be altered to plot the appropriate line type.
%  There are four trajectories ( n = 1, 2, 3, 4), so the stability
%  along each trajectory must be determined.

%  Plot the first trajectory

n = 1;

[ZRE,zrstart,zrend,zcstart,zcend] = filtercomp(y(:,n)');
for subvector = 1:length(zrstart)
   z(n,zrstart(subvector):zrend(subvector)) =...
      ...ZRE(subvector,zrstart(subvector):zrend(subvector));
   plot(m(zrstart(subvector):zrend(subvector)),...
      ...z(n,zrstart(subvector):zrend(subvector)))
end

hold on

%  Plot the second trajectory

n = 2;

[ZRE,zrstart,zrend,zcstart,zcend] = filtercomp(y(:,n)');
for subvector = 1:length(zrstart)
   z(n,zrstart(subvector):zrend(subvector)) =...
      ...ZRE(subvector,zrstart(subvector):zrend(subvector));
   plot(m(1:35),z(n,1:35))
   plot(m(35:54),z(n,35:54),'--r')
end

hold on

%  Plot the third trajectory
```

```
n = 3;

[ZRE,zrstart,zrend,zcstart,zcend] = filtercomp(y(:,n)');
for subvector = 1:length(zrstart)
   z(n,zrstart(subvector):zrend(subvector)) =...
      ...ZRE(subvector,zrstart(subvector):zrend(subvector));
   plot(m(zrstart(subvector):zrend(subvector)),...
      ...z(n,zrstart(subvector):zrend(subvector)))
end

hold on

%  Plot the fourth trajectory

n = 4;

[ZRE,zrstart,zrend,zcstart,zcend] = filtercomp(y(:,n)');
for subvector = 1:length(zrstart)
   z(n,zrstart(subvector):zrend(subvector)) =...
      ...ZRE(subvector,zrstart(subvector):zrend(subvector));
   plot(m(zrstart(subvector):zrend(subvector)),...
      ...z(n,zrstart(subvector):zrend(subvector)))
end

%%%%%%%%%%%%%%%%%%%%%%%%%%%%%%%%%%%%

%  This section prints out the columns of 'y', renamed here as 'z'.
%  The columns of 'z' (and 'y') correspond to the energy of each
%  equilibrium point at a particular value of mu. The rows of 'z'
%  are defined at different values of mu.  The only difference
%  between 'y' and 'z' (which is of no concern to the user, unless
%  he wishes to modify the program) is that 'y' has complex elements
%  which are filtered out and subsequently ignored (set = 0) in 'z'.

number=1:length(y(:,1));
[number' z'] %  Print out the columns of z (y) to
%  facilitate the manual column correction
%  described above.
```

D.11 MYODE45.M

```
function [tout, yout] = myode45(ypfun, t0, y0, tol, trace)

%  THIS MODIFIED VERSION OF 'ODE45.M' IS PRINTED HERE WITH THE
%  WRITTEN CONSENT OF THE MATHWORKS, INC.

%  GENERAL DESCRIPTION:  This is a modified version of 'ode45.m.'
%  This program determines the 3-D (x1, x2, x3) coordinates of, and
%  the corresponding time for, each point along a given CLOSED
%  curve of constant energy on a momentum sphere.  Unlike the
%  original program from which it is derived, 'myode45.m' does not
%  require the user to include 'tfinal' as part of the input
%  arguments.  This parameter is actually determined by the
%  subroutine itself.  'myode45.m' integrates the equations of
%  motion until it determines that the trajectory has returned to
%  its origin, thereby closing the curve.  THE REMAINDER OF THE
%  INTRODUCTORY COMMENTS PERTAIN TO THE ORIGINAL 'ODE45.M' PROGRAM.

%ODE45 Solve differential equations, higher order method.
% ODE45 integrates a system of ordinary differential equations using
% 4th and 5th order Runge-Kutta formulas.
% [T,Y] = ODE45('yprime', T0, Tfinal, Y0) integrates the system of
% ordinary differential equations described by the M-file YPRIME.M,
% over the interval T0 to Tfinal, with initial conditions Y0.
% [T, Y] = ODE45(F, T0, Tfinal, Y0, TOL, 1) uses tolerance TOL
% and displays status while the integration proceeds.
%
% INPUT:
% F     - String containing name of user-supplied problem
%                 description.
%         Call: yprime = fun(t,y) where F = 'fun'.
%         t      - Time (scalar).
%         y      - Solution column-vector.
%         yprime - Returned derivative column-vector;
%                  yprime(i) = dy(i)/dt.
% t0    - Initial value of t.
% tfinal- Final value of t.
% y0    - Initial value column-vector.
% tol   - The desired accuracy. (Default: tol = 1.e-6).
% trace - If nonzero, each step is printed. (Default: trace = 0).
%
```

```
% OUTPUT:
% T  - Returned integration time points (column-vector).
% Y  - Returned solution, one solution column-vector per tout-value.
%
% The result can be displayed by: plot(tout, yout).
%
% See also ODE23, ODEDEMO.

% C.B. Moler, 3-25-87, 8-26-91, 9-08-92.
% Copyright (c) 1984-92 by The MathWorks, Inc.

% The Fehlberg coefficients:
alpha = [1/4  3/8  12/13  1  1/2]';
beta  = [ [    1      0      0     0      0    0]/4
          [    3      9      0     0      0    0]/32
          [ 1932  -7200   7296     0      0    0]/2197
          [ 8341 -32832  29440  -845      0    0]/4104
          [-6080  41040 -28352  9295  -5643    0]/20520 ]';
gamma = [ [902880  0  3953664  3855735  -1371249  277020]/7618050
          [ -2090  0    22528    21970    -15048  -27360]/752400 ]';
pow = 1/5;
if nargin < 5, tol = 1.e-6; end
if nargin < 6, trace = 0; end

% Initialization

t = t0;
hmax = 0.01;
h = hmax/8;
y = y0(:);
f = zeros(length(y),6);
chunk = 128;
tout = zeros(chunk,1);
yout = zeros(chunk,length(y));
k = 1;
tout(k) = t;
yout(k,:) = y.';
distance = 100;
theta = 0;
flag = 0;
initiald = 0;
thetamax = 0;
```

```
if trace
   clc, t, h, y
end

% The main loop

while distance >= 4*initiald | theta <3

   % Compute the slopes
   temp = feval(ypfun,t,y);
   f(:,1) = temp(:);
   for j = 1:5
      temp = feval(ypfun, t+alpha(j)*h, y+h*f*beta(:,j));
      f(:,j+1) = temp(:);
   end

   % Estimate the error and the acceptable error

   delta = norm(h*f*gamma(:,2),'inf');
   tau = tol*max(norm(y,'inf'),1.0);

   % Update the solution only if the error is acceptable

   if delta <= tau
      t = t + h;
      y = y + h*f*gamma(:,1);
      k = k+1;
      if k > length(tout)
         tout = [tout; zeros(chunk,1)];
         yout = [yout; zeros(chunk,length(y))];
      end
      tout(k) = t;
      yout(k,:) = y.';


      distance = sqrt((y(2)-y0(2))^2+(y(3)-y0(3))^2);
      if flag == 0
         initiald = distance;
         refangle = atan2(y(3) - y0(3),y(2) - y0(2));
      end
      newangle = atan2(y(3) - y0(3),y(2) - y0(2));
```

```
      theta = abs(newangle - refangle);
      if theta > thetamax & thetamax < 3
         thetamax = theta;
      elseif theta < thetamax & thetamax >= 3
         theta = theta + 2*3.141592654;
      end
      flag = 1;


   end
   if trace
      home, t, h, y
   end

   % Update the step size

   if delta ~= 0.0
      h = min(hmax, 0.8*h*(tau/delta)^pow);
   end
end


tout = tout(1:k);
yout = yout(1:k,:);
```

D.12 NOTORQEOM.M

```
function xdot = eom(t,x)

%  GENERAL DESCRIPTION:  This program stores the equations of motion
%  used by 'myode45.m' to generate the closed curves of constant
%  energy.

i1 = .7;
i2 = .3;
a1 = 0.5; %  alpha1
a3 = sqrt(1 - a1^2); %  alpha3
epsilon = 0;
```

```
% Legend

% x(1) = x1
% x(2) = x2
% x(3) = x3
% x(4) = mu

xdot(1) = x(2)*(i2*x(3) - x(4)*a3);
xdot(2) = -i1*x(1)*x(3) + x(4)*(a3*x(1) - a1*x(3)*(1 - i1));
xdot(3) = x(2)*(x(1)*(i1 - i2) + x(4)*a1*(1 - i1));
xdot(4) = epsilon;
```

D.13 PHASEINT.M

```
function [phi,yf] = phaseint(i1,i2,i3,a1,phiin,X1,X2,X3,X4,X5)

% GENERAL DESCRIPTION: This program is a simplified version of
% 'integrate.m'. It determines the angular phase phi and the final
% energy yf of each initial condition along the closed constant
% energy curves.

t0 = 0;
a3 = sqrt(1 - a1^2);
eps = -.01;

% Initial conditions

x1 = X1;
x2 = X2;
x3 = X3;
mas = X4;
y = X5;

tf = -mas/eps;

x0 = [x1 x2 x3 mas y];
[t,x] = ode45('eom',t0,tf,x0);

phi = phiin;
```

```
yf = x(length(x(:,5)),5);
```

D.14 PROBCAP.M

```
function [Pc] = probcap(phi, yf, yfcrit)

% GENERAL DESCRIPTION: This function determines the probability
% of capture given the phi and yf data AT EACH INITIAL CONDITION.

% Note that phi is a vector, each element of which corresponds
% to the initial phase that gets the corresponding final value
% in yf. yfcrit is the value of y above which it escapes and
% below which it is captured.

% This function works similar to filtercomp.m.

Pc = 0;

current = 0;    % Flag which denotes whether the computer is
                % currently cycling through a negative block (1)
                % or a positive block(2)
numpos = 0;     % Denotes number of positive blocks
                % (escaped segments in yf)
numneg = 0;     % Denotes number of negative blocks
                % (captured segments in yf)

for index = 1:length(yf)
   if yf(index) - yfcrit < 0
      if current ~= 1
         current = 1;
         numneg = numneg + 1;
         negstart(numneg) = index;
         if numpos > 0
            posend(numpos) = index - 1;
         end
      end
   else
      if current ~= 2
         current = 2;
```

```
            numpos = numpos + 1;
            posstart(numpos) = index;
            if numneg > 0
               negend(numneg) = index - 1;
            end
         end
      end
end
if current == 1
   negend(numneg) = index;
else
   posend(numpos) = index;
end
if numneg > 0
   for index = 1:numneg
      Pc = Pc + phi(negend(index)) - phi(negstart(index));
   end
end
```

D.15 SPHERE.M

```
% PROGRAM: sphere.m

% GENERAL DESCRIPTION: This quick-and-dirty momentum sphere-
% generating program requires that 'capprob.m' be run first
% and that the data files 'x1icsmu7,' 'x2icsmu7,' and 'x3icsmu7'
% be created. These three files contain the data for a single
% point on each of a series of constant energy curves on the
% momentum sphere. Each point serves as a ''seed'' from which
% 'myode45.m' generates the entire curve on which it lies. This
% program draws the momentum sphere at a given value of mu.

load x1icsmu7
load x2icsmu7
load x3icsmu7

skip = 1

% 'skip' determines the step size between each
```

```
% constant energy curve. 'x1icsmu7,' 'x2icsmu7,'
% and 'x3icsmu7' contain data for 100 of these
% curves in each domain. Because it is difficult
% to observe the topology of the sphere with
% this many curves, 'skip' is used to pick out
% only a few of these to be plotted.

while skip <= length(x1icsmu7)

   x0 = [x1icsmu7(skip) x2icsmu7(skip) x3icsmu7(skip) 0.7];

% 'x0' contains the initial conditions to be
% fed to 'myode45.m.' The last element is mu.

   [T,X] = myode45('notorqeom',0,x0,10^(-7));
   plot3(X(:,1),X(:,2),X(:,3))
   axis('square')
   hold on
   if skip+10>length(x1icsmu7) & skip ~= length(x1icsmu7)
      skip = length(x1icsmu7)
   else
      skip = skip + 10
   end
pause(1)
end
```

Bibliography

1. Adams, G.J. "Dual-Spin Spacecraft Dynamics During Platform Spinup." *Journal of Guidance and Control*, 3(1):29-36, Jan-Feb 1980.

2. Byrd, Paul F. and Morris D. Friedman. *Handbook of Elliptic Integrals for Engineers and Physicists*, Springer-Verlag, Berlin, Second Edition, 1971.

3. Cochran, John E., Ping-Huei Shu, and Stephen D. Rew. "Attitude Motion of Asymmetric Dual-Spin Spacecraft." *Journal of Guidance, Control and Dynamics*, 5(1):37-42, Jan-Feb 1982.

4. Guckenheimer, John and Philip Holmes. *Nonlinear Oscillations, Dynamical Systems, and Bifurcations of Vector Fields*, Volume 42 of *Applied Mathematical Sciences*. Springer-Verlag, New York, 1983.

5. Hall, Christopher D. *An Investigation of Spinup Dynamics of Axial Gyrostats Using Elliptic Integrals and the Method of Averaging*, PhD thesis, Department of Theoretical and Applied Mechanics, Cornell University, Ithaca, New York, 1992.

6. Hall, Christopher D. "Resonance Capture in Axial Gyrostats." *Spaceflight Dynamics 1993, Vol. 84, Advances in Astronautical Sciences*, pages 1133-1148, 1993.

7. Hall, Christopher D. "Spinup Dynamics of Biaxial Gyrostats." *Space Flight Mechanics 1993, Vol. 82, Advances in Astronautical Sciences*. pages 211-222, 1993.

8. Hall, Christopher D. and Richard H. Rand. "Spinup Dynamics of Axial Dual-Spin Spacecraft." *Journal of Guidance, Control and Dynamics*, 17(1):30-37, 1994.

9. Henrard, J. "Capture Into Resonance: An Extension of the Use of Adiabatic Invariants." *Celestial Mechanics*, 27:3-22, 1982.

10. Hubert, Carl Henry. *An Attitude Acquisition Technique for Dual-Spin Spacecraft*. PhD thesis, Department of Theoretical and Applied Mechanics, Cornell University, Ithaca, New York, 1980.

11. Hughes, Peter C. *Spacecraft Attitude Dynamics*. John Wiley & Sons, Inc., New York, 1986.

12. Jordan, D.W. and P. Smith. *Nonlinear Ordinary Differential Equations (Second Edition)*. Oxford University Press, New York, 1987.

13. Kinsey, Robert J. *Despin of a Dual-Spin Spacecraft with Limited Torque: Passage Through Precession Phase Lock Resonance*. UCLA PhD Dissertation, University of California, Los Angeles, 1991.

14. Kinsey, Robert J., D.L. Mingori, and R.H. Rand. "Spinup Through Resonance of Rotating Unbalanced Systems with Limited Torque." In *Proceedings of the 1990 AIAA/AAS Astrodynamics Conference, Part 2*, pages 805-813, Aug 1990. AIAA Paper 90-2966.

15. Likins, Peter W. *Elements of Engineering Mechanics*. McGraw-Hill, New York, 1973.

16. Likins, Peter W. "Spacecraft Attitude Dynamics and Control – A Personal Perspective on Early Developments." *Journal of Guidance, Control and Dynamics*, 9(2):129-134, March-April 1986.

17. Masaitis, Č. "On the Motion of Two Linked Bodies." *Archive for Rational Mechanics and Analysis*, 8(1):23-35, July 1961.

18. The Mathworks, Inc. *MATLAB for Sun Workstations: User's Guide*. The Mathworks, Inc., South Natick, Massachusetts, January 31, 1990.

19. Meirovitch, Leonard. *Methods of Analytical Dynamics*. McGraw-Hill Book Company, New York, 1970.

20. Scher, M.P. and R.L Farrenkopf. "Dynamic Trap States of Dual-Spin Spacecraft." *AIAA Journal*, 12(12):1721-1724, Dec 1974.

21. Wiesel, William E. *Spaceflight Dynamics*. McGraw-Hill, New York, 1989.

22. Wittenburg, Jens. "Beiträge zur dynamik von gyrostaten." In *Convegno Internazaionale sul Tema: Metodi Valutativi Nella Fisica-Matematica, Roma, 15-19 dicembre 1972*, Problemi Attuali di Scienza e di Cultura, Quaderno N. 217, pages 217-354. Accademia Nazionale dei Lincei, 1975.

23. Wolfram, Stephen. *Mathematica: A System for Doing Mathematics by Computer*. Addison-Wesley Publishing Company, Inc., New York, 1988.

Vita

First Lieutenant Raymond Tsui was born in Montréal, Québec, Canada on 12 May 1968. He graduated in 1986 from Fallsburg Central High School in Fallsburg, New York, and attended Cornell University. Lieutenant Tsui graduated in May 1990 with a degree in Mechanical Engineering and was commissioned through ROTC. He was initially assigned to the 2854th Civil Engineering Squadron (later redesignated as the 654th CES), Tinker Air Force Base, Oklahoma, where he worked in both the Infrastructure Design and Simplified Acquisition for Base Engineering Requirements (SABER) Sections as a Mechanical Engineer. He was also the squadron's Individual Mobilization Augmentee (IMA) Monitor. In May 1992, Lieutenant Tsui was reassigned to the Air Force Institute of Technology (AFIT) where he is currently working on a Master of Science Degree in Astronautical Engineering. Following his graduation, he will be reassigned to the 45th Civil Engineering Squadron at Cape Canaveral Air Force Station, Florida.

Permanent address: 950 Lake Shore Drive West
Rock Hill, New York 12775

REPORT DOCUMENTATION PAGE

Form Approved
OMB No. [illegible]

1. AGENCY USE ONLY (Leave blank)	2. REPORT DATE	3. REPORT TYPE AND DATES COVERED
	March 1994	Master's Thesis

4. TITLE AND SUBTITLE

RESONANCE CAPTURE IN UNBALANCED DUAL-SPIN SPACECRAFT

5. FUNDING NUMBERS

6. AUTHOR(S)

Raymond Tsui, First Lieutenant, USAF

7. PERFORMING ORGANIZATION NAME(S) AND ADDRESS(ES)

Air Force Institute of Technology, WPAFB OH 45433-6583

8. PERFORMING ORGANIZATION REPORT NUMBER

AFIT/GA/ENY/94M-3

9. SPONSORING/MONITORING AGENCY NAME(S) AND ADDRESS(ES)

Dr Arje Nachman
AFOSR/NM
Bolling AFB DC 20332-6448

10. SPONSORING/MONITORING AGENCY REPORT NUMBER

11. SUPPLEMENTARY NOTES

12a. DISTRIBUTION/AVAILABILITY STATEMENT

Approved for public release; distribution unlimited

12b. DISTRIBUTION CODE

13. ABSTRACT *(Maximum 200 words)*

This study examines the spinup dynamics of dual-spin spacecraft having an imbalanced rotor. Of particular interest is a phenomenon called "resonance capture" during which the spinup motor torque induces uncontrolled growth of nutation. A captured spacecraft tumbles end-over-end, while an escaped spacecraft experiences little nutation growth. The conditions which lead to both states are analyzed. A set of criteria based on the spacecraft's kinetic energy at the end of spinup is used to determine whether or not it has been captured. To calculate the final energies against which these criteria are compared, a set of nondimensional equations of motion are numerically integrated. Using computer simulations, the magnitude of the motor torque is shown to affect the probability of capture. For prolate spinup, larger torques are desirable, whereas for oblate spinup, smaller torques are preferred. This probability is also influenced by the initial spin configuration and is determined here as a function of the initial energies. For a given motor torque, some initial energies lead to guaranteed capture and others to guaranteed escape. This information is combined to form a "map" which allows designers to find the best initial spinup conditions for a given spacecraft.

14. SUBJECT TERMS

Dynamics, Nonlinear Analysis, Nonlinear Systems, Satellite Attitude, Spacecraft, Spin Resonance

15. NUMBER OF PAGES

151

16. PRICE CODE

17. SECURITY CLASSIFICATION OF REPORT	18. SECURITY CLASSIFICATION OF THIS PAGE	19. SECURITY CLASSIFICATION OF ABSTRACT	20. LIMITATION OF ABSTRACT
Unclassified	Unclassified	Unclassified	UL